博士論文

InGaN/AlN nanostructure light emitting diodes for long wavelength broad band emission

InGaN/AlN ナノ構造発光ダイオードによる長波長広帯域発光

マテウ　マニシュ

InGaN/AlN nanostructure light emitting diodes for long wavelength broad band emission

InGaN/AlN ナノ構造発光ダイオードによる長波長広帯域発光

A dissertation submitted to the Graduate School of Engineering
The University of Tokyo
in partial fulfillment of the requirements for the degree of
Doctor of Philosophy

マテウ　マニシュ

Mathew Manish

Under the supervision of

Professor Dr. Yoshiaki Nakano

Dedicated to my dear parents, my beloved wife and my wonderful kids

Acknowledgement

Working at The University of Tokyo (UT) has been an incredibly rewarding experience. I believe UT to be a unique university having state of the art facility and environment to perform research in the field of semiconductors. I had the opportunity to work and exchange ideas and information with people from different departments.

First of all, I would like to thank Prof. Yoshiaki Nakano for giving me the opportunity to work in his research group and for his constant guidance and support. I have learned a lot about several aspects of research from him and profited greatly from his insight. I am deeply indebted to Associate Professor Masakazu Sugiyama, who was kind enough to listen patiently to my numerous queries about physics and for taking the time to answer all of them. During the time I spend here, they patiently offered me valuable advice and always guided me in the right direction. I have learned a lot from them, without their help I could not have finished my dissertation successfully.

I would also like to thank Professor Katsushi Fujii, Professor Yoshitaka Okada and Associate Professor Takuo Tanemura for their valuable comments and suggestions that helped me to rethink into the mechanism of nanostructures.

I could not have finished my work without great friendly assistance from many people, including Assistant Professor Hassanet Sodabanlu, Assistant Professor Yunpeng Wang, Assistant Professor Kentarou Watanabe and Assistant Professor Masanori Kubota. I would specially like to thank Dr. Hassanet Sodabanlu for his suggestions and comments during my experimental work. I also want to thank my fellow PhD students and staff Mr. Cai Liu, Mr. Hongbo Wang, Ms. Kayo Koike and Mr. Akihiro Nakamura for their support in the regular running of the experimental setups and suggestions during my experiments. I would also like to thank Mr Jon for giving his suggestions during my experiments that helped me to look at my results in different perspectives. My work would have not been complete without the help and support of all the members of Nakano-Sugiyama-Tanemura Laboratory.

I am also thankful to Dr. Roman Talalaev, CEO, STR group inc, for the insightful discussions and suggestions for my work.

I would also like to give my sincere thanks to the Ministry of Education, Culture, Sports, Science and Technology, Japanese Government via Embassy of Japan in India and ministry of human recourse department (MHRD) India, who offered me such a great opportunity and supported my life expense during my study in Japan

Last but not the least, I would like to thank my parents, wife, daughter and son for their constant support and encouragement throughout my PhD.

Abstract

III-Nitrides light emitting diodes (LEDs) are extensively being used in solid state lighting (SSL), televisions, smart-phones, tablets and automotive applications. They offer benefits of small size, long life time, low heat output, no mercury content, less energy consumption and durability. Most of LEDs having application in SSL use yellow / red phosphor to convert blue/ ultraviolet LED into white light, but the use of phosphor lowers the overall luminous efficacy. Another problem with these LEDs is the uniform application of phosphor during the manufacturing process. Since band gap energies of InGaN vary from InN (0.6 eV) to GaN (3.4 eV), which covers the full visible spectral range would be helpful in manufacturing phosphor free LEDs. However, high internal quantum efficiency (IQE) is achieved only in the blue spectral range while high IQE in green, yellow or red spectrum region is not been achieved so far. This is often known as "green gap". Long wavelength InGaN LEDs requires high indium contents, which causes degradation of material quality due to lattice mismatch between InGaN and GaN.

To achieve monolithic white LED the first thing required is a broad emission in the green gap region. In this work we used the concept of tensile and compressive strain for achieving high indium composition in InGaN. We were able to achieve broadband emission due to effect of strain in nanostructures. In this study we focused on nanoisland and nanodisk LEDs. Nanoisland LEDs were grown by inserting a thin AlN between InGaN/GaN interfaces of blue MQW. For nanodisk LEDs, AlN was used as a barrier rather than conventional GaN. Both the LED structures were grown on sapphire substrate using MOVPE. Nanodisks were formed due to the crack formation in the first AlN layer. The succeeding InGaN/AlN layers introduced the branching of nanodisk from the initial cracks of AlN layer. Observation of electroluminescence (EL) showed broad spectrum emission of 100 nm with the peak wavelength of 586 nm. Large blue shift in wavelength was observed in the nanodisk was due to weakening of quantum confined stark effect (QCSE) at high injection current.

To improve the quality of InGaN/AlN nanodisk we inserted a monolayer of GaN between InGaN, AlN interfaces of the nanodisk. GaN having a lattice constant between InGaN and AlN acts a strain neutral layer thus helping in improving the quality of the nanodisks. Nanodisk LEDs with strain neutral layer exhibited 30% more IQE compared to nanodisk without strain neutral layer. This LED had a peak wavelength of 541 nm.

The effect of AlN growth temperature on nanodisk was studied in detail. The growth of InGaN/ AlN nanodisk light emitting diode (LED) structures were investigated under different AlN growth temperatures while keeping the InGaN temperature constant. AlN grown at the lower temperature had a rough surface and the increase in the temperature resulted in smoother planer surfaces. Rough AlN surface helped in the formation of nanodisk structures resulting in higher indium incorporation in InGaN. The fabricated LEDs had the wavelength emission range from 569 nm to 422 nm. Increasing the growth temperature of AlN resulted in blue shift in wavelength. Though AlN exhibits high resistance properties, the resistance in the LEDs with low-temperature AlN was less compared to LEDs with high temperature AlN. Low temperature AlN LEDs had three dimensional (3D) structures which resulted in the formation of nanodisks. Current can be injected to the nanodisks via the gap among AlN islands, while the samples having high temperature AlN had two dimensional (2D) structures and current injection to the InGaN layer suffers from high resistance due to the AlN barrier.

Further the thickness of AlN and InGaN were analyzed on s InGaN/GaN LED structure. The standard LED structure had a InGaN growth time of 1 min. We first increased the InGaN growth time from 1 min to 2 min, 3 min and 4 min. We found that there was no much change in wavelength and on increasing the growth time to 3 min and 4 min damaged the crystal quality which resulted in weak emission. On inserting an AlN beneath first interface of GaN and InGaN im multiquantum well resulted in red shift in wavelength.Thus we concluded that AlN and InGaN thickness plays a crucial role for emission in green gap region.

The final approach was to get the monolithic white LEDs by using the concept developed above. We used three approaches for monolithic white LEDs. In the first approach, AlN nanoislands were inserted into GaN and InGaN interface of conventional InGaN/GaN multi quantum wells (MQWs) LED structure. The fabricated LED emitted broad long wavelength emission in the yellow region along with a low intensity blue emission at low injection current of 10 mA. At high injection current of 70 mA, blue emission dominated over yellow emission. The combination of blue and yellow luminescence resulted in the emission of white light. Second approach was to place single nanodisks on conventional blue LEDs. The combination of nanodisk and MQWs resulted in white LEDs. The third approach was to use combination of MQW, nano disk and single QW

to generate bimodal emission. We succeeded in achieving monolithic white LED without any use of phosphor.

Table of Contents

1 Introduction

Light is one of the important necessities for life. We would have not survived on this planet if there was no light. Lighting has been an integral part of human civilization as recorded from history. Discovery of fire was the first artificial source of lighting. Prehistoric people used primitive lamps to illuminate surroundings. These lamps were made from naturally occurring materials such as rocks, shells, horns and stones, were filled with grease and fiber. Later glass and pottery lamps replaced the old lamps. With the development of electricity luminosity of artificial lighting improved enough to be used indoors. They became widely used and extended the time that people could stay up, among other developments. When we don't have natural light then we need artificial light. Today artificial lighting plays a crucial role in our modern lifestyle.

This chapter will first introduce about brief history of lighting followed by introduction to GaN material and their related alloys in section 1.1 and 1.2 respectively. Section 1.3 focuses on InGaN light emitting diodes (LEDs), their current trend and their limitations. The motivation for the nanostructure based broadband emission will be described in section 1.4.

1.1 A brief history of Lighting

The history of electric light started some 135 years back when Thomas Edison invented incandescent light bulb by passing a low current through a metallic filament wire in a vacuum environment. These bulb emitted light in the visible spectrum. Though these bulbs emitted visible light but 95% electricity was wasted by infrared light. Later in 1937 the first fluorescent tube was made by General Electric (GE). Fluorescent tubes consist of a glass tube filled with inert gas like argon and small amount of mercury. Ultraviolet (UV) light is generated by passing an electric current between electrodes at each end of the tube, which excites electron in mercury vapor. When the excited electron relaxes it emits UV light. The UV light excited the phosphor coating at the inner surface of the glass tube to emit visible light.

Fluroscent tubes have much longer lifetimes (7,500-30,000h) than incandescent light bulbs (100 h). The quality of white light emitted from these tubes depends on the phosphors

used. The efficacy of a fluorescent tube (60–100 lm/W) is much higher than that of an incandescent light bulb (15 lm/W), and the efficiency is typically 25%, compared to 5% for an incandescent bulb. These advantages, combined with reasonable costs, led to fluorescent tubes rapidly replacing incandescent lighting in the workplace, especially in offices and public buildings. Today, fluorescent tubes dominate lighting in the workplace [1].

After fluorescent tubes, then came the era of compact fluorescent lamps (CFLs). The first commercial CFL were available in early 1980s. These CFLs had two, four or six small fluorescent tubes, which can be straight or coiled. They have a lifetime of 15,000h and an efficiency of 20%. CFLs have longer lifetime if it is turned on for a long time but its life time drastically reduces if it is turned on/off frequently. Hence, the lifetime of CFL is sensitive to its use.

LEDs emitting red light were first demonstrated by Holonyak and Bevacqua in 1962 [2]. LED is an optoelectronic device which generates light via electroluminescence (EL). It consists of a p-n junction, through which electric current is sent to generate electrons and holes. A portion of energy is released as photons during recombination of these electrons and holes. The center wavelength and thus the emission color of an LED are largely determined by the bandgap energy of semiconductor material. By early 1990s high brightness red, orange, yellow and green LEDs started replacing the conventional traffic lights. These LEDs had a low power consumption compared to incandescent bulb, fluorescent tube and CFLs. They were extensively used in display and electronic circuits. The first bright blue LED was announced by Nakamura in 1993 [3]. Blue LED was made from indium gallium nitride (InGaN) on gallium nitride (GaN) template. If a blue LED is covered with phosphor, then it will emit white light in the same way as UV light emit white light in fluorescent tubes. These LEDs can last up to 100,000h unlike CFL and incandescent bulb which have shorter life-time. This breakthrough in lighting technology using LEDs has helped in reducing the power consumption. Since GaN and InGaN are the important material for getting high efficiency white LEDs, so we will look into the basic properties of III-nitride materials in the next section.

1.2 Gallium nitride material and related alloys

In the recent years III-nitride semiconductors are being extensively used in both commercial and strategic applications. It is being used in projectors, signaling, solid state lighting (SSL), automotive lighting, data storage in high density DVD standards, mobile

phones, televisions (TVs) etc for commercial use. For strategic point of view it is being used in radar, electronic warfare, navigation and communication system etc. All the applications based on III-N semiconductors are changing our lifestyle. SSL is the emerging and promising technology to replace the inefficient traditional lamp based lighting system.

1.2.1 Crystal structure

The group III- nitrides can crystallize either in hexagonal wurtzite (Wz) or zinc blende (ZB) structures. Both of these structures can be epitaxially grown, however under ambient conditions, the most thermodynamically stable structure for III-nitrides is wurtzite with a hexagonal symmetry. Most of the nitride semiconductors are grown in the c-plane of the Wz crystal. Wz structure has a hexagonal unit cell and thus two lattice constants, *c* and *a*. The lattice constant *c* defines the spacing of two identical hexagonal lattice planes and *a* describes the distance of atoms in the hexagonal plane. The crystal structure GaN is shown in Figure 1.1. GaN crystal exhibit two different sequences of atomic layering in the two opposing directions parallel to certain crystallographic axis, and consequently crystallographic polarity along the axes can be observed [5]. For binary A-B compounds with Wz structure, the sequence of the atomic layers of the constituents A and B is reversed along the [0001] and $[000\bar{1}]$ directions. The corresponding (0001) and $(000\bar{1})$ faces are the A-face and B-face, respectively. In the case of heteroepitexial growth of thin films by thin films of a noncentrosymmetric compound, the polarity of the material cannot be predicted in a straightforward way, and must be determined by experiments. This is the case for GaN epitaxial layers and GaN-based heterostructures with the most common growth direction normal to the {0001} basal plane, where the atoms are arranged in bilayers. These bilayers consist of two closely spaced hexagonal layers, one formed by cations and the other formed by anions, leading to polar faces. Thus, in the case of GaN, a basal surface should be either Ga- or N-faced. By Ga-faced we mean Ga on the top position of the {0001} bilayer, corresponding to the [0001] polarity. The other group III-N semiconductors, InN, AlN and their ternary and quaternary compounds have the same crystalline structure, in which group-III atoms occupy the sublattice shown with Ga atoms in figure. 1.1. Lattice constants a, c and u for GaN, InN, AlN are given in table 1.1 [6]

The deviation of the GaN unit cell from the ideal hexagonal wurtzite geometry and the strong ionic character of the III-N bond leads to polarization properties of wurtzite III-N semiconductors. The total polarization in the crystal in the absence of external fields is the sum of spontaneous and piezoelectric polarizations. Spontaneous polarization is caused by the deviation of the unit cell from the ideal hexagonal structure. Due to the crystal symmetry

the polarization is aligned along the [0001] direction, with the positive direction pointing parallel to the [0001]-axis. In Ga-polar GaN films the spontaneous field points towards the surface plane of the film [7].

The polarities of GaN vary according to different growth methods. When GaN is grown on (0001) sapphire substrate by molecular beam epitaxy (MBE) are N-polar surface while Ga-polar surface is obtained when the growth is done with metalorganic vapour phase epitaxy (MOVPE) [8-9]. All the samples studied in this work are grown by MOVPE thus having Ga-polar.

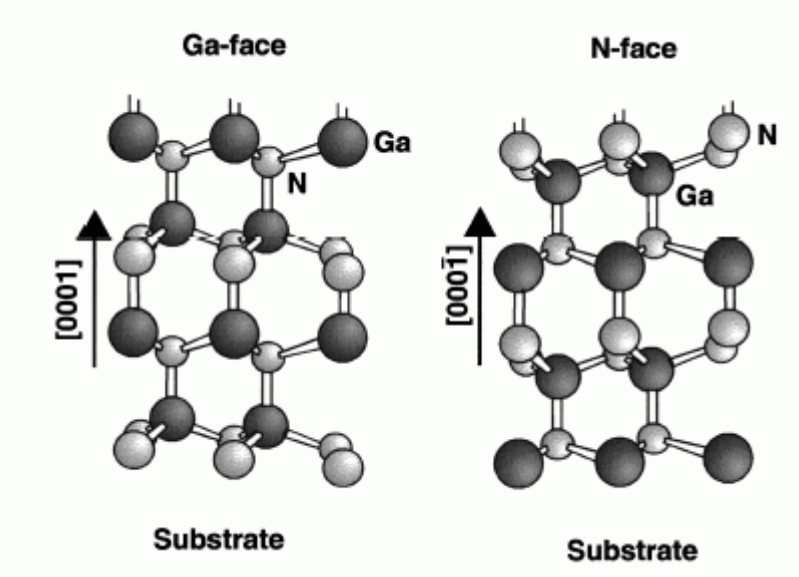

Figure 1.1 Hexagonal Wz crystal structure of GaN with Ga-face and N-face [5].

Table 1.1 Lattice constants a, c and u for GaN, InN and AlN [6]

Lattice constant	**GaN**	**AlN**	**InN**
a (A^o)	3.189	3.111	3.534
c (A^o)	5.185	4.978	5.718
U	0.377	0.379	0.382

The spontaneous polarization constant p_{sp} and piezoelectric constant (e_{31} and e_{33}) of GaN, AlN and InN is shown in table 1.2.

Table 1.2 Spontaneous and piezoelectric constants for GaN, AlN and InN

Parameter **(C/m^2)**	**GaN**	**AlN**	**InN**
p_{sp}	-0.029	-0.081	-0.032
e_{31}	-0.49	-0.60	-0.57
e_{33}	0.73	1.46	0.97

The piezoelectric polarization is caused by strain induced deformation of lattice parameters a, c and u. In hexagonal wurtzite lattice the piezoelectric polarization p_{pe} along the [0001]-axis depends on two independent piezoelectric coefficients e_{31} and e_{33} as

$$\delta p_{pe} = e_{33}\frac{c-c0}{c0} + 2\, e_{31}\frac{a-a0}{a0} \quad (1.1)$$

where $a0$ and $c0$ are the equilibrium values of the lattice parameters [7]. Eq.1.1 omits the polarization caused by shear strain, as it is not present in epitaxial structures. Starting from Eq. 1.1 it can be shown that in epitaxial III-N layers under tensile strain, the polarization is always negative, and in layers under compressive strain the polarization is positive. The electric field is connected to the polarization p by the relative dielectric constant ϵ_r (x) of the material according to

$$E = -\frac{p}{\epsilon r(x)\epsilon 0} \quad (1.2)$$

1.2.2 Band gap

The major advantage of the III-N material system is that by alloying GaN with InN and AlN the band gap of the ternary or quaternary alloy can be tuned in a controllable fashion. Figure 1.2 shows the band gap versus the lattice parameter a of the III-N materials. The band gap of III-N alloys can be varied continuously from 6.2 eV (AlN) to 0.7 eV (InN). It covers the spectral range from deep UV to infrared. However, as the In or Al content of InGaN and AlGaN film is increased the growth of high quality material becomes more

difficult due to the different optimum growth conditions of In and Al containing III-N alloys [10]. The difficulty of growth currently limits the possible wavelength range of GaN-based emitters from near UV to green.

In ternary and quaternary compounds the change of the band gap energy with composition can be described by linear interpolation with the inclusion of a bowing parameter b. The bowing parameter represents the magnitude of the second order correction to the linear dependence. For quaternary $In_xAl_yGa_{1-x-y}N$ alloy the energy band gap can be written as [11]

$$E_g(x, y) = xE_{g,InN} + yE_{g,AlN} + (1 - x - y)E_{g,GaN} - b_{Al}\, y\,(1 - y) - b_{In}\, x(1 - x). \qquad (1.3)$$

Here b_{Al} and b_{In} are the bowing parameters related to Al and In composition, respectively. The bowing of $Al_y Ga_{1-y} N$ can be modeled with a static bowing parameter b_{Al} [12, 13]. In-containing alloys are more complex to model, because the bowing parameter b_{In} is believed to depend strongly on the In and Al content [11, 14]. Commonly used values for b_{Al} and b_{In} in hexagonal III-N alloys are listed in Table 1.3.

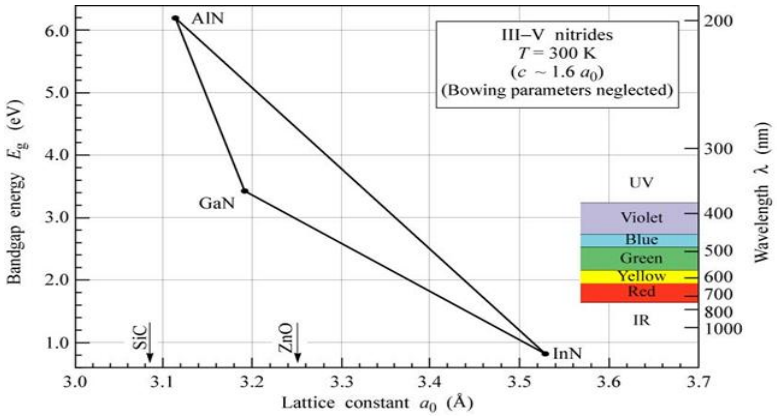

Figure 1.2 Bandgap vs lattice constant for III-V nitride semiconductor.

Table 1.3 Band bowing parameters b_{In} and b_{Al} for AlGaN, InGaN, InAlN and InGaN alloys. The b values marked as * depend on composition.

$Al_xGa_{1-x}N$

Al content (*x*)	**b_{Al} (eV)**	**Ref.**
0≤ x <0.45	0.69±0.45	[13]
0≤ x ≤1	1	[12]

$In_xGa_{1-x}N$

In content (*x*)	**b_{In} (eV)**	**Ref.**
0 ≤ x <0. 5	1.4	[15]
0 ≤ x 0.12	3.5	[16]
0≤ x ≤1	3.5-0.9*	[11]

$In_xAl_{1-x}N$

In content (*x*)	**b_{In} (eV)**	**Ref.**
0≤ x <0.85	6 - 1*	[11]
0.25 ≤ x	3	[17]

$In_xAl_y Ga_{1-x-y}N$

In content (*x*)	**Al content (*y*)**	**b_{In} (eV)**	**Ref.**
0.1 ≤ x <0.2	*y <0.2*	3*	[11]
0.03	*0.2 ≤ y*	17*	[11]

1.3 InGaN LEDs

Electricity generation is the main source of energy related greenhouse gas emissions and lighting uses one-fifth of its output. Worldwide demand for lighting is increasing rapidly. The average North American consumes over 100 Mlmh each year of lighting, whereas the average person in India uses only 3 Mlmh. In addition, the world population is increasing rapidly, from 5 billion in 1987 to 7 billion today, an increase of 40% in the past 27 years. A conservative estimate is that the global demand for artificial lighting will be 80% higher by 2030 [1,18]. If we do not move to more efficient lighting, then by 2030, lighting will be responsible for emitting more than twice the CO_2 of all of today's cars and nine times the emissions of all of today's aircraft.

Solid-state lighting (SSL) using LEDs is poised to reduce this value by at least 50%, so that lighting will then use less than one-tenth of all electricity generated. LED lighting will provide reductions of at least 10% in fuel consumption and carbon dioxide emissions from power stations within the next 5–10 years. Even greater reductions are likely on a 10–20 year timescale [1].

There are mainly three popular approaches to achieve white light LEDs using InGaN for SSL [19]. The first approach is to use blue LED with yellow phosphor. These type of LEDs have very high efficacy (luminous flux or visible light output power per unit electrical power) but low color rendering index (CRI) values due to lack of green and red components. The phosphor conversion process also limits the overall luminous efficacy. CRI is referred to as the ability of a light source to show or "render" the true colors of an object. The second approach is to use ultraviolet LED with blue and yellow phosphor or red, green and blue phosphors. These LEDs have very low efficacy but very high CRI values. The third approach is to combine red, green and blue LEDs. These LEDs have a medium efficacy but high CRI values. All the three approaches are depicted in figure 1.3.

Most of the commercial white LEDs available in the market are combination of blue LED covered with phosphor. White LEDs offer a huge variety of benefits compared to conventional lighting technology. Some of the favorable characteristics of LED sources over their traditional counterpart include directionality, size, rigid, dimming, color tuning, extended lifetime etc. The internal quantum efficiency (IQE) of today's best LEDs is at least 75% and may even be approaching 80% [22].

In addition to the energy savings and positive environmental effects promised by solid-state lighting, solid-state sources in particular, LED-based sources offer what was

inconceivable with conventional sources: controllability of their spectral, spatial, temporal, and polarization properties as well as their color temperature. Technologies currently emerging are expected to enable tremendous benefits in lighting, automobiles, transportation, communication, imaging, agriculture, and medicine [20].

Figure 1.3 Three dominant ways to produce white LEDs [19]

Ass mentioned above it is difficult to get high efficacy and high CRI values simultaneously with the current LEDs used in SSL. Other then efficacy and CRI values LEDs have some more disadvantages. The first disadvantage is the uniform application of phosphor in manufacturing process. It is difficult to apply phosphor uniformly on blue LEDs. Another disadvantage is the limited range of available color properties based on phosphor availability. Application of phosphor also increases the overall cost of LEDs. In order to solve these issues regarding phosphor it is important to look for an alternative material that can replace phosphor.

1.4 Motivation of this work

As discussed in the previous section there are issues related luminous efficacy, phosphor coating and CRI in the commercial white LEDs available in the market. To solve these issues we have to look into some of the alternative material which would help in replacing phosphor. The second aspect that we have to keep in mind while replacing phosphor is the overall cost of LED should not be high. The selected material should be such that it can be grown in the same reactor with the same technology of blue LEDs without increasing the complexity of the process and easy for the industry to adapt to it.

Again going back to figure 1.2 we can observe that InN, GaN having a bandgap of 0.7 eV and 3.4 eV respectively. If we use an alloy of InGaN then it can cover the whole

visible range of spectrum form ultraviolet to red spectral range. Though it looks easy to add more indium in InGaN to achieve longer wavelength to replace phosphor but it is very difficult to add more indium in InGaN. Figure 1.4 shows the graph between external quantum efficiency (EQE) vs peak wavelength. From the graph we can observe that EQE is highest at 55% for blue LEDs and as we move towards green region the EQE drastically reduces to below 20 %. There is no efficient material emitting from 530 to 570 nm which is termed as "green gap". Usually high indium in InGaN can be achieved only at lower temperature but it leads to indium segregation thus reducing the efficiency of LEDs. So we have to look into an alternative way to get more indium in InGaN without affecting the crystal quality.

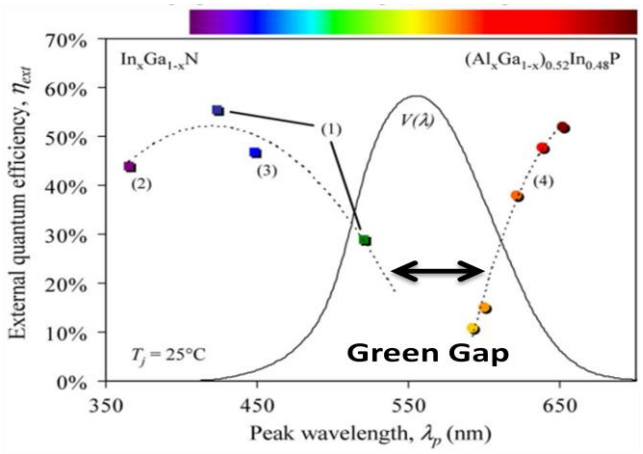

Figure 1.4 EQE vs peak wavelength graph

Anazawa et al had earlier shown the study of strain-compensated InGaN/AlN MQWs on c-plane GaN/ sapphire template by MOVPE [21]. AlN and InN have a lattice constant of 3.112 Aº and 3.545 Aº respectively. AlN having a small lattice constant shows tensile strain while InGaN alloy has compressive strain. By optimizing the In composition in InGaN and thickness of both AlN and InGaN will help in achieving strain balanced structure. The compressive strain of InGaN on tensile AlN will helps in achieving more indium composition in InGaN. Figure 1.5 shows the schematic of strain balancing structure using AlN and InGaN.

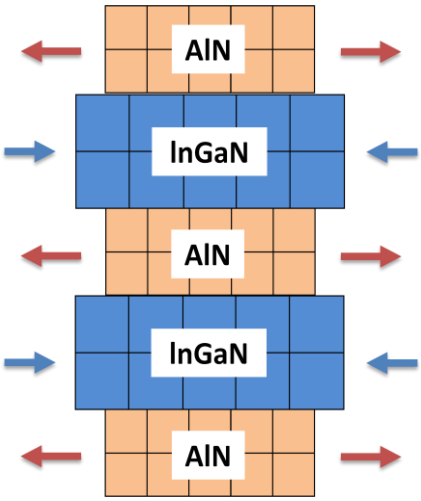

Figure 1.5 Schematic of strain balancing structure using InGaN and AlN

The growth conditions for both InGaN and AlN are opposite. For high indium in InGaN the growth temperature should be lower (~750℃) while for good quality AlN the growth temperature should be higher (>1100 ℃). If we grow InGaN at lower temperature and then ramp up the temperature for good crystal quality AlN then high temperature desorb indium resulting in less indium in InGaN. Secondly N_2 is used as a carrier for indium source in InGaN growth while H_2 is a carrier for Al source in AlN growth. Indium is highly unstable under H_2 condition causing removal of it from InGaN. Therefore it is difficult to grow both InGaN and AlN simultaneously under different conditions. To avoid this problem all of the experiments in this study we used N_2 as a carrier source for AlN.

1.5 References

[1] C. J. Humphreys, "Solid-state lighting," *MRS Bulletin*, vol. 33, pp. 459 (2008).

[2] N. Holonyak, S.F. Bevacqua, Appl. Phys. Lett. 1, 82 (1962).

[3] B. Johnstone, Brilliant!: Shuji Nakamura and the Revolution in Lighting Technology Prometheus Books, New York, (2007).

[4] M. Razeghi, *Int. J. high speed electron. Syst.,9,*, p. 161 (1998).

[5] O. H. Ambacher, *J., Journal of Applied Physics*, vol. 85, p. 3222 (1999).

[6] S. Nakamura and G. Fasol, The Blue Laser Diode ,Springer Verlag,(1997).

[7] F. Bernardini, V. Fiorentini and D. Vanderbilt, Phys. Rev. B 56, R10024 (1997).

[8] A. R. Smith, R. M. Feenstra, D. W. Greve, M.-S. Shin, M. Skowronski, J. Neugebauer and J. E. Northrup, Surf. Sci. 423, 70 (1999).

[9]M. Stutzmann, O. Ambacher, M. Eickhoff, U. Karrer, A. Lima Pimenta, R. Neuberger, J. Schalwig, R. Dimitrov, P. J. Schuck and R. D. Grober, phys. stat. sol. (b) 228, 505 (2001).

[10] S. Keller and S. P. DenBaars, J. Cryst. Growth 248, 479 (2003).

[11] M. Androulidaki, N. T. Pelekanos, K. Tsagaraki, E. Dimakis, E. Iliopoulos,A. Adikimenakis, E. Bellet-Amalric, D. Jalabert and A. Georgakilas, phys.stat. sol. (c) 3, 1866 (2006).

[12] F. Yun, M. A. Reshchikov, L. He, T. King, H. Morko¸c, S. W. Novak and L. Wei, J. Appl. Phys. 92, 4837 (2002).

[13] S. R. Lee, A. F. Wright, M. H. Crawford, G. A. Petersen, J. Han and R. N.Biefeld, Appl. Phys. Lett. 74, 3344 (1999).

[14] I. Vurgaftman, J. R. Meyer and L. R. Ram-Mohan, J. Appl. Phys. 89, 5815 (2001).

[15] J. Wu, W. Walukiewicz, K. M. Yu, J. W. Ager III, E. E. Haller, H. Lu and W. J. Schaff, Appl. Phys. Lett. 80, 4741 (2002).

[16] M. D. McCluskey, C. G. VandeWalle, C. P. Master, L. T. Romano and N. M. Johnson, Appl. Phys. Lett. 72, 2725 (1998).

[17] J. Wu, W. Walukiewicz, K. M. Yu, J. W. Ager III, S. X. Li, E. E. Haller, H. Lu and W. J. Schaff, Solid State Commun. 127, 411 (2003).

[18] Light's Labour's Lost: Policies for Energy-efficient Lighting , International Energy Agency, Paris, France, (2006).

[19] S. Pimputkar, J. S. Speck, S. P. DenBaars, and S. Nakamura, Nat. Photonics 3, 180 (2009).

[20] E. F. Schubert and J. K. Kim, *Science,* vol. 308,1274 (2005).

[21] K. Anazawa, S. Hassanet, K. Fujii, Y. Nakano, and M. Sugiyama, J. Cryst. Growth 370, 82 (2013).

[22] Y. Narukawa, M. Sano,T. Sakamoto,T. Yamada, and T. Mukai, Phys. Status Solidi A 205, 1081 (2008).

2 LED growth by MOVPE

This chapter will focus on process involved in the growth, characterization and fabrication of InGaN/GaN LEDs. The introduction part in section 2.1 will give a short introduction to different laboratory equipments used in the growth and fabrication of LEDs. Section 2.2, will focus on the experiment procedures for the growth and characterization of standard InGaN/GaN blue LEDs. The chapter ends with conclusion.

2.1 Introduction

2.1.1 Metal Organic Vapor Phase Epitaxy (MOVPE)

The main tools used in epitaxial growth of semiconductor materials are molecular beam epitaxy (MBE) and metalorganic vapor phase epitaxy (MOVPE). MOVPE is a chemical vapor deposition method of epitaxial growth of materials, especially compound semiconductors from the surface reaction of organic compounds or metalorganics and metal hydrides containing the required chemical elements. In MOVPE metalorganic precursors in gas phase are used to fabricate thin films. The precursors decompose thermally and the growth reaction takes place at the interface of the gas phase and the heated substrate. The reaction atmosphere is commonly nitrogen or hydrogen which is also used as carrier gases for the precursors. For example, gallium nitride could be grown in a reactor on a substrate by introducing trimethylgallium ($(CH_3)_3Ga$) and ammonia (NH_3) with the chemical reaction is (2-1).

$$Ga(CH_3)_3(l) + NH_3(g) + H_2(g) \rightarrow GaN(s) + 3CH_4(g) + H_2(g) \qquad (2\text{-}1)$$

Alternative names for this process include organometallic vapor phase epitaxy (OMVPE), metalorganic chemical vapor deposition (MOCVD) and organometallic chemical vapor deposition (OMCVD). All the crystal growth done in this work was done using AIXTRON (AIX 200/4 RF S) system. Figure 2.1 shows the schematic diagram of MOVPE apparatus. The metalorganic precursors are placed in steel cylinders called bubblers, which are kept in temperature controlled baths. Accurate temperature control of bubblers is needed, since the vapor pressures of precursors are extremely sensitive to temperature. When carrier gas is passed through a bubbler, it is saturated with gaseous metalorganic material. In this system trimethylgallium (TMGa) and triethylgallium (TEGa) are use as gallium source for bulk GaN and multi quantum well respectively.

Trimethylindium (TMIn), trimethylaluminum (TMAl) and bis-cyclopentadienylmagnesium (Cp 2 Mg) were used as gallium, indium, aluminum and magnesium sources, respectively. The gas flows are regulated with valves and mass flow controllers (MFCs) into the reactor. Gaseous ammonia (NH 3) and silane (SiH 4) were used as nitrogen and silicon sources respectively.

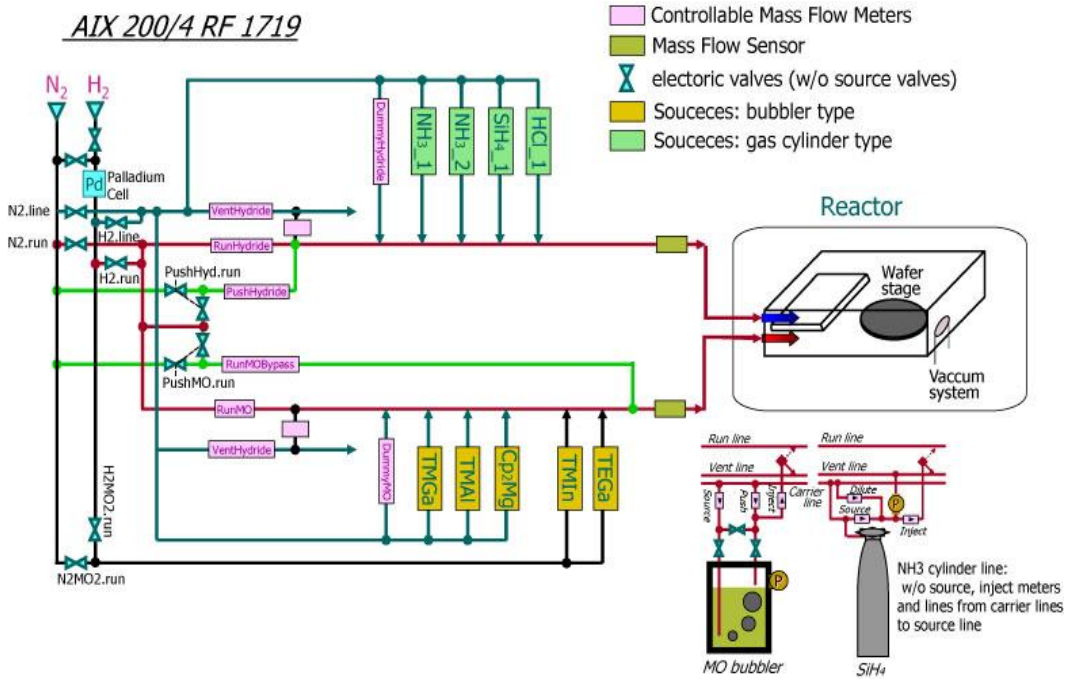

Figure 2.1 Schematic diagrams of the MOVPE apparatus

2.1.2 Reflectance Analysis

Laytec's EpiTT in situ reflectometry setup was used to analyze the growth rate, material properties and morphology of the material. EpiTT combines measurements of temperature and reflectance at three wavelengths in one tool. It uses three wavelengths of 405 nm, 633 nm and 950 nm to in-situ monitor the above properties of the crystal. 633 nm is ideal for monitoring GaN growth rate while 405 nm is used for monitoring InGaN growth. For True Temperature (TT), it uses emissivity corrected pyrometry, which delivers the precise surface temperatures of opaque materials at 950 nm (Si, GaAs, InP). For materials

that are transparent at 950 nm (GaN, Sapphire, SiC), EpiTT measures the temperature on the top side of the carrier.

During epitaxy, a convenient way to gain information from reflectance measurements is to take the so-called reflectance-transients. In this case, the intensity of light reflected at the substrate-layer-system is measured at one single wavelength as a function of time. If the growing layer is (at least partially) transparent at the wavelength of the incoming light, these transients show an intensity-modulation, related to interference effects. The period of the modulation can be used to measure the thickness and growth rate of the layer. As the incoming light is only partly reflected at the surface, another part penetrates into the layer. It will partly be reflected at the interface between layer and substrate. This reflected beam will travel back to the layer surface, where the same process will be repeated (the beam is partly reflected and partly leaves the sample) and so on. The overall intensity of the reflected light is then given by the superposition of all reflected beams. As there is a phase difference between the single beams, constructive or destructive interference will occur, leading to an intensity-modulation of the reflected light, the so-called Fabry-Pérot oscillations. The above mechanism is shown in figure 2.2.

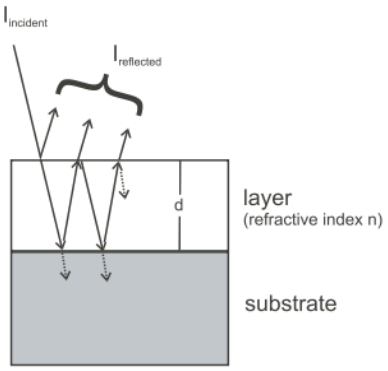

Figure 2.2 Reflection of light at transparent layer grown on top of absorbing surface.

The phase difference and thus the intensity of the reflected light depends on the thickness of the growing layer as well as on the optical constants of the materials and the wavelength of the light. For normal incidence constructive interference and a maximum reflectance occur, if the path difference between two beams is equal to an even number of the half wavelength

$$2nd = m\lambda \qquad (2\text{-}2)$$

Where n : refractive index, d: thickness of layer, M: even number, λ : incident wavelength. For destructive interference and minimum reflectance the path difference is equal to an odd number of the half wavelength

$$2nd = (m+1/2)\,\lambda \qquad (2\text{-}3)$$

Thus, by measuring Fabry-Pérot oscillations, the layer thickness can be derived from the intensity-transients of the reflected light. Since during epitaxy the layer thickness increases continuously with time t, the growth rate r = d/t can also be estimated

$$\text{maximum reflectance : } r.t = m\,\lambda/2n \qquad (2\text{-}4)$$

$$\text{maximum reflectance : } r.t = (m+1/2)\,\lambda/2n \qquad (2\text{-}5)$$

2.1.3 High-resolution X-ray Diffractometer (XRD)

X-ray diffraction (XRD) is a powerful and commonly available technique for identifying the presence of crystalline phase. The quantitative, high-accuracy measurements of interatomic spacings provided by XRD have motivated some detailed studies. The XRD patterns also provide information on strain, grain size, preferential orientation and epitaxy. In addition, XRD is non-destructive and can sometimes be used *in situ*.

X-rays with wavelength, λ, between 0.5 and 2Å are impinged upon a sample. The diffracted X-rays are measured at 2θ, the angel between X-ray source and detector. Diffracted waves from different atoms can interfere with each other and the resultant intensity distribution is strongly modulated by this interaction. If the atoms are arranged in a periodic fashion, as in crystals, the diffracted waves will consist of sharp interference maxima (peaks) with the same symmetry as in the distribution of atoms. Measuring the diffraction pattern therefore allows us to deduce the distribution of atoms in a material. The peaks in an x-ray diffraction pattern are directly related to the atomic distances. Let us consider an incident x-ray beam interacting with the atoms arranged in a periodic manner as shown in 2 dimensions in Figure 2.3. The atoms, represented as green spheres in the graph, can be viewed as forming different sets of planes in the crystal (colored lines in graph on left). For a given set of lattice planes with an inter-plane distance of d, the condition for a diffraction (peak) to occur can be simply written as:

$$2d\sin\theta = n\lambda \qquad (2\text{-}6)$$

which is known as the Bragg's law. In the equation, λ is the wavelength of the x-ray, θ the scattering angle, and n an integer representing the order of the diffraction peak. The Bragg's Law is one of most important laws used for interpreting x-ray diffraction data.

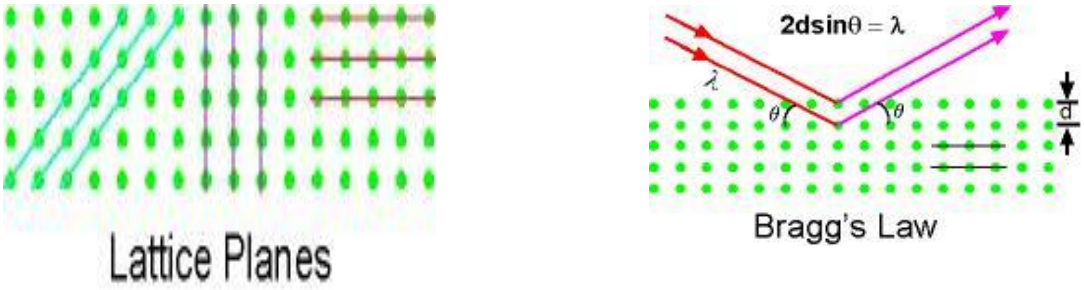

Figure 2.3 Lattice planes and Bragg's law [24].

2.1.4 Atomic Force Microscopy (AFM)

The atomic force microscope (AFM) is a very high-resolution type of scanning probe microscope, with demonstrated resolution of fractions of a nanometer. The AFM consists of a microscale cantilever with a sharp tip (probe) at its end that is utilized to scan the surface. The cantilever is typically silicon or silicon nitride with a tip radius of curvature in the order of nanometers. When the tip is brought into proximity of a sample surface, forces between the tip and the sample lead to a deflection of the cantilever. Typically, the deflection is measured using a laser spot reflected from the top of the cantilever into an array of photodiodes. The sample is mounted on a piezoelectric tube, which can move the sample in the z direction for maintaining a constant force, and the x and y directions for scanning the sample. A schematic and mode of AFM measurement are shown in figure 2.4 and 2.5 respectively.

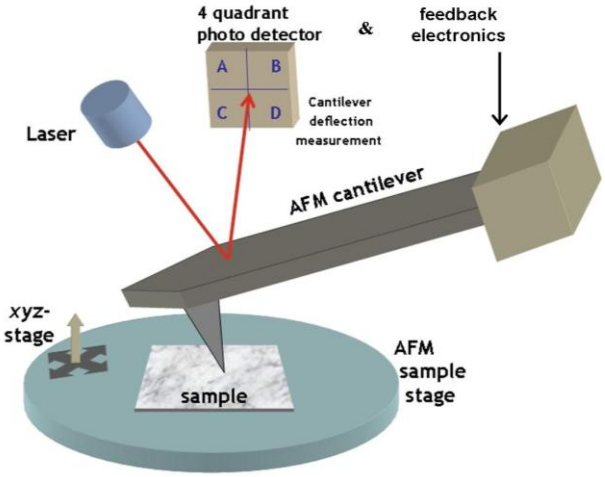

Figure 2.1 A schematic of AFM measurement [24].

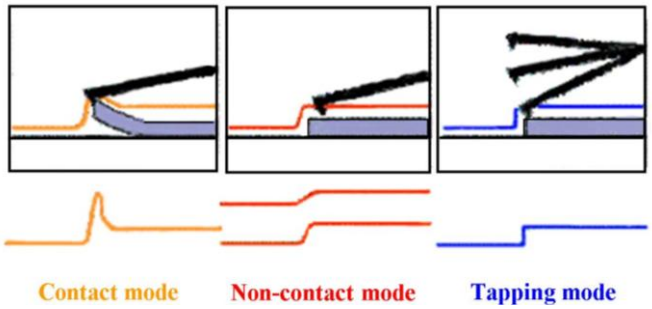

Figure 2.2 Modes of AFM measurement [24].

2.1.5 Photoluminescence (PL)

Photoluminescence is light emission from any form of matter after the absorption of photons (electromagnetic radiation). It is one of many forms of luminescence (light emission) and is initiated by photoexcitation (excitation by photons). The excitation typically undergoes various relaxation processes and then photons are re-radiated. The experimental setup for PL is presented with a schematic drawing as is shown in figure 2.6. The samples are mounted on closed circle refrigeration cryostat with temperature varying from 3.5 K to 300K, is excited by a He-Cd Laser with 325 nm wavelength. The luminescence signal is collected by lense, before which a long pass filter (cut-on 340 nm) is used to block the laser line signal. Finally the signal is detected by a photomultiplier tube and picked up by the computer via a data acquire module. To improve the signal/noise ratio, a standard optical chopper interfaced with a lock-in Amplifier is employed.

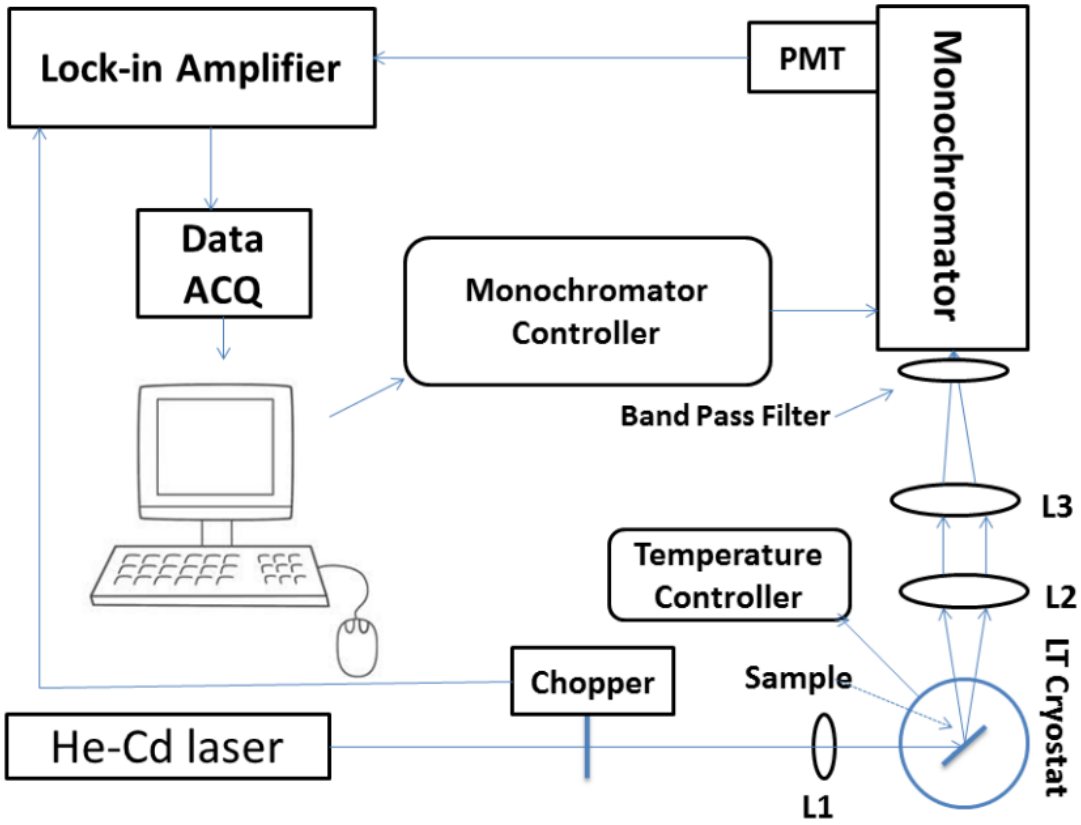

Figure 2.6 Experimental setup for photoluminescence spectroscopy [25].

In our experiments we have used two PL setups the first one with 325 nm laser was mentioned above other than that we used 405 nm μ-PL setup, to analyze some of the samples.

2.2 Growth and characterization of standard MQW blue LED

Since the first bright InGaN-based blue light emitting diodes (LEDs) were commercialized in 1993 [2], there has been considerable interest in improving their output power and expanding their emission wavelength. The output power has been significantly enhanced, from approximately 1 mW for the first commercialized LEDs to more than 300 mW today [3–9]. Moreover, the emission wavelength has also been extended, and now covers the range from deep ultra-violet to red light [10–21]. In 1996, white LEDs fabricated from blue LED chips combined with yellow phosphors ((Y 1 − a Gd a)3(Al 1 − b Ga b)5 O 12 , Ce 3+ (YAG)) were commercialized [22-23]. Most of the commercial white LEDs consists of blue LEDs coated with phosphor. These blue LEDs are made from InGaN/GaN multi quantum wells (MQWs). In this section we will focus on the growth and

characterization of conventional blue LED which will be used in our later part of study to make monolithic white LED.

The conventional MQW blue LEDs were grown on c-plane (0001) sapphire substrate. The metal organic precursors were TMGa, TMIn, TMA, TEGa. SiH_4 and Cp_2Mg were used as source for dopants. H_2 was the carrier gas for n-GaN and p-GaN while N_2 was used for the growth of MQWs. First the substrate was annealed at 1200 ºC for 10 min under H2 at 100 mbar pressure. Then the temperature was ramped down to 550 ºC to grow GaN nucleation layer at 200 mbar. After growing the nucleation layer the temperature was ramped up to 1130 ºC to grow 4 µm thick Si doped GaN cladding layer. Temperature was ramped down to grow InGaN/GaN MQWs at 780 ºC, 200 mbar. The barriers in the active regions were lightly doped with Si. MQWs were capped by 40 nm thick Mg-doped $Al_{0.15}Ga_{0.85}N$ electron blocking layer (EBL) at 1090 ºC,100 mbar, then the pressure was ramped to 200 mbar while keeping the temperature fixed to grow 125 nm thick Mg-doped p-GaN. The schematic cross section of the device structure is depicted in figure 2.7

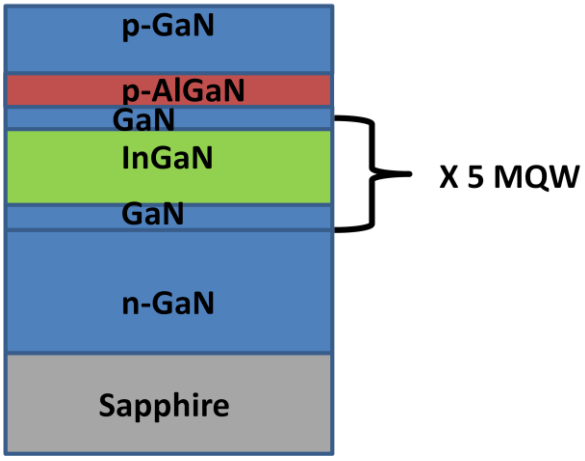

Figure 2.7 Schematic of InGaN/GaN MQW LED.

MQWs LED samples were characterized using HRXRD, PL and EL. Figure 2.8 shows HRXRD 2θ-ω scan for (0002) reflections for the LED samples. The dominant peak comes from the diffraction of n-GaN buffer layer under the MQWs and the satellite peaks comes from the diffraction of the InGaN/GaN MQWs. Spacing between the two nearby satellite peaks are same indicating uniform well and the barrier thickness in MQWs. The zeroth order peak almost coincides with the dominant peak indicating the strain balancing of well and the barrier layers. The sharp satellite peak indicates good crystal quality of MQWs. SL+1 is coming from $Al_{0.15}Ga_{0.85}N$ EBL layer. Total barrier and well thickness estimated from XRD was found to be 8nm and 1 nm respectively.

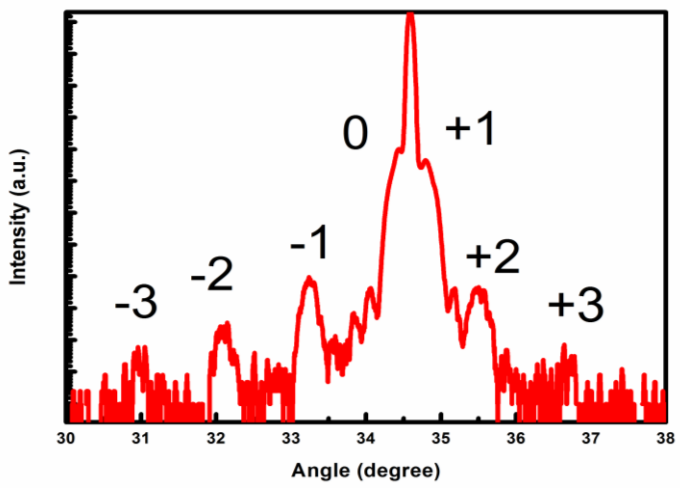

Figure 2.8 XRD (0002) 2θ-ω scan conventional MOVPE grown InGaN/GaN MQWs.

A room temperature (RT) µ-PL spectrum of InGaN/GaN MQWs LED is shown in Figure 2.9. PL was exited by 405 nm laser at an excitation power of 3 mW. The laser was focused onto the sample surface by an objective lens and the diameter of the exited area was 2 µm. PL spectrum had a peak wavelength of 433 nm and full width at half maximum (FWHM) of 14 nm.

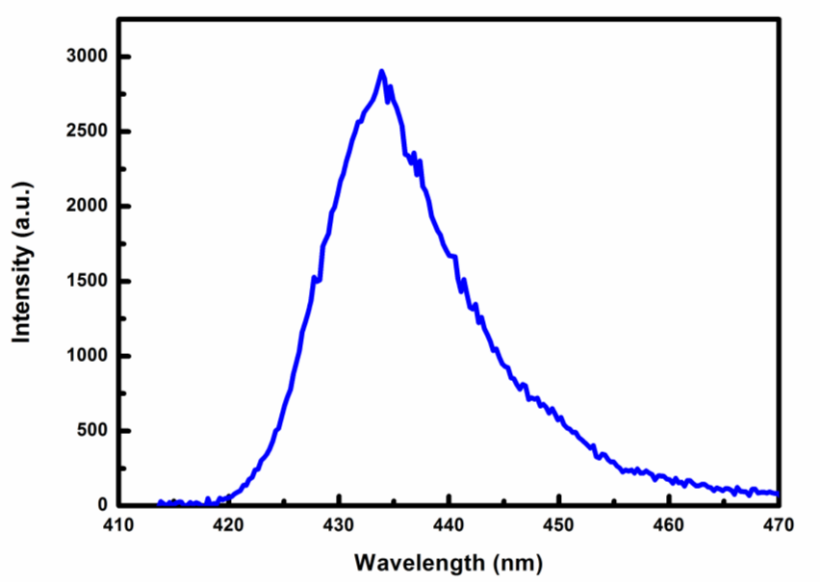

Figure 2.9 Room temperature µ-PL spectrum of InGaN/GaN MQWs LED.

LEDs were fabricated using Ni contacts of 300 µm diameter for p-GaN and indium contact for n-GaN. The turn on voltage of the LED was 3.2 V with the estimated device resistance of ~ 50 Ω. EL measurement was measured at room temperature under dc-biased

conditions. The EL spectrum of blue LED at 10 mA driving current is shown in figure 2.10. LEDs had a peak wavelength of 433 nm.

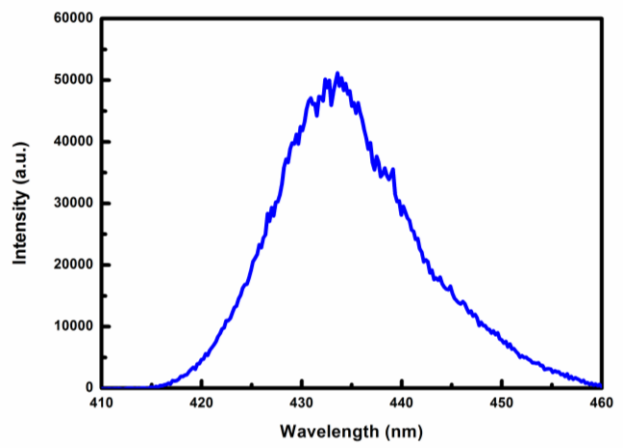

Figure 2.10 EL spectrum of InGaN/GaN MQWs LED

2.3 Conclusion

On comparing the EL and PL intensity the peak wavelength remained to be same at 433 nm. No blue shift in wavelength was observed on increasing the driving current indicating no effect of quantum confined stark effect. These blue LEDs when combined with yellow phosphor will emit white light. We will use this blue LED structure to make monolithic white LEDs, which will be discussed in chapter 6.

2.4 References

[1] A. C. Jones and P. O'Brien, *CVD of Compound Semiconductors: Precursor Synthesis, Development and Applications,* VCH, Weinheim,(1997).

[2] S.Nakamura, M. Senoh and T. Mukai, Japan. J. Appl.Phys., 32 L8 (1993).

[3] S.Nakamura, T Mukai and M. Senoh, J. Appl. Phys.,76 8189 (1994)

[4] S. Nakamura, M. Senoh, N. Iwasa and S. Nagahama, Japan.J. Appl. Phys. 34 L797 (1995)

[5] S.Nakamura, M. Senoh, N. Iwasa and S. Nagahama, Appl.Phys. Lett. 67 1868 (1995)

[6] T. Mukai, K.Takekawa and S. Nakamura, Japan. J. Appl.Phys. 37 L839 (1998)

[7] M. Yamada, T. Mitani, Y. Narukawa, S. Shioji, I. Niki, S. Sonobe, K. Deguchi, M. Sano and T. Mukai, Japan. J. Appl.Phys. 41 L1431(2002)

[8] Y. Narukawa, J. Narita, T. Sakamoto, K. Deguchi, T. Yamada and T. Mukai, Japan. J. Appl. Phys. 45 L1084 (2006)

[9] Y. Narukawa, M. Sano, M. Ichikawa, S. Minato, T. Sakamoto, T. Yamada and T. Mukai, Japan. J. Appl. Phys.46 L963 (2007)

[10] S .Nakamura, M. Senoh, N. Iwasa, S. Nagahama, T. Yamada and T. Mukai, Japan. J. Appl. Phys. 34 L1332 (1995)

[11] T.Mukai, H. Narimatsu and S.Nakamura, Japan. J. Appl.Phys. 37 L479 (1998)

[12] T. Mukai, M.Yamada and S.Nakamura, Japan. J. Appl.Phys. 37 L1358 (1998)

[13] T.Mukai, D.Morita and S. Nakamura, J. Cryst. Growth 189/190 778 (1998)

[14] T.Mukai and S.Nakamura, Japan. J. Appl. Phys. 38 5735 (1999)

[15] T.Tadatomo, H.Okagawa, Y .Ohuchi, T.Tsunekawa, Y. Imada, K.Kato and T.Taguchi, Japan. J. Appl. Phys. 40 L583 (2001)

[16] M. Yamada, Y. Narukawa and T. Mukai , Japan. J. Appl.Phys. 41 L246 (2002)

[17] D .Morita, M. Sano, M. Yamamoto, T. Murayama, S.Nagahama and T. Mukai, Japan. J. Appl. Phys. 41 L1434 (2002)

[18] M. Iwaya, S. Takanami, A. Miyazaki, Y. Watanabe, S. Kamiyama, H. Amano and I. Akasaki , Japan. J. Appl. Phys. 42 400 (2003)

[19] V. Adivarahan, W. H. Sun, A. Chitnis, M. Shatalov, S. Wu, H.P. Maruska and M. Asif Khan, Appl. Phys. Lett.85 2175 (2004)

[20] M. Shatalov, A. Chitnis, P. Yadav, Md. F. Hasan, J. Khan, V. Adivarahan, H. P. Maruska, W. H. Sun and M. Asif Khan, Appl. Phys. Lett. 86 201109 (2005)

[21] Y. Taniyasu, M. Kasu and T. Makioto, Nature 441 325 (2006)

[22] K. Bando, K.Sakano, Y.Noguchi and Y.Shimizu, J. LightVis. Environ. 22 2 (1998)

[23] Y. Narukawa, M. Ichikawa, D. Sanga, M. Sano and T. Mukai, J. Phys. D: Appl. Phys. 43, 354002 (2010).

[24] H. Sodabanlu, Metalorganic Vapor Phase Epitaxy and Fabrication of 1.5 μm GaN/AlN MQWs Intersubband All-Optical Switches, PhD Thesis, The University of Tokyo,17 (2010).

[25] W. Bao, Photoluminescence study of InGaN/GaN multiple quantum wells nanopillars, M.Phil Thesis, The University of Hong Kong, 23 (2012).

3 Effect of AlN on InGaN/GaN MQWs for broadband emission

This chapter will focus on the effect of AlN on the conventional blue LEDs discussed in chapter 2. Section 3.1, 3.2 will focus on broad band emission and thickness dependence of InGaN on the conventional blue LED then in section 3.3 the impact of 30 sec and 1 min AlN beneath first interface of InGaN/GaN will be investigated. Indium incorporation and broad band emission mechanism in the LEDs with AlN at interface of InGaN/GaN MQWs is explained in section3.4. The chapter ends with conclusion.

3.1 Broad band emission

Broad band emission in green gap region is very much important to realize monolithic white LEDs for solid state lighting. There is no report of external quantum efficiency (EQE) above 10% in yellow-green and yellow wavelength regions. The main problems for LEDs emitting in this region, namely, the large lattice mismatch, the miscibility gap in the InGaN crystal phase, and the quantum-confined Stark effect (QCSE) [1-4].There have been various efforts to make broad band emitter in the green gap region [5-10]. Mainly there are two approaches to obtain broad band emission. The first is to use of microstructures such as micro-rods, micro-strips and micro-pyramids using selective area growth (SAG) while the second approach is to grow InGaN at relatively lower temperature which results in the formation of dots but low temperature InGaN leads to lot of defects inside the crystal. Though we get the emission in the green gap region by the above two methods but the efficiency for these LEDs are still poor.

3.2 Effect of InGaN thickness on InGaN/GaN MQWs

Talalaev *et al* had earlier shown that indium composition in InGaN increases along the growth direction [11]. We used the above method for increasing the indium in InGaN by changing the InGaN growth time in the standard InGaN/GaN MQWs blue LEDs. The LEDs were grown on c-plane sapphire substrates by an AIXTRON 200/4 RF-S MOVPE system. A 25-nm thick low temperature GaN nucleation layer was grown at 550°C followed by a 3.4-μm-thick Si-doped n-type GaN. This served as the template for 3 batch of LED samples. All the batches had 5 MQWs grown at 780 °C and were capped by p-AlGaN and p-GaN layers. For the first batch we grew 5 InGaN/GaN MQW LEDs having an InGaN

growth time of 1 min, 2 min, 3 min and 4 min. All the four samples in this batch from now on will be referred to as batch A. Our conventional blue MQW LEDs discussed in chapter 2 had InGaN growth time of 1 min. Batch B had a AlN layer of 30 sec deposited on each GaN barriers, prior to the growth of InGaN wells. The growth temperature of AlN was same as that of InGaN in batch A. InGaN active layers in batch B were grown with the same growth conditions of batch A and the InGaN growth time was increased from 1 min to 4 min in interval of 1 min each. The third batch was similar to batch B except the AlN growth time was increased from 30 sec to 1 min. It also had four samples with InGaN growth time of 1min to 4 min in interval of 1 min each. The samples in this batch will be further referred to as batch C. The schematic cross sectional diagram for batch A is shown in Figure 3.1 (a) and for batch B and C is shown in Figure 3.1 (b).

All the three batches of LEDs were characterized by HRXRD, micro-PL, CL and EL. Figure 3.2. shows 2θ-ω scan for (0002) reflections for batch A. The dominant peak comes from the diffraction of n-GaN buffer layer under the MQWs. For 1 min InGaN the zeroth order peak is on the left side of dominant peak which is due to the compressive strain of InGaN. The SL-1 on the right side of dominant peak is coming from AlGaN electron blocking layer (EBL). Fringes can be observed on the both sides of the dominant peak reflecting to the good quality of crystal. When the InGaN growth time was increased to 2 min the zeroth order peak moved towards left indicating the compressive strain in InGaN. On further increasing the InGaN thickness zeroth order peak moved further left and only one satellite peak was observed for 3 and 4 min InGaN indicating strain relaxation in these wafers. Thus HRXRD result indicates that the longer InGaN growth time LEDs are degraded crystal quality due to strain relaxation.

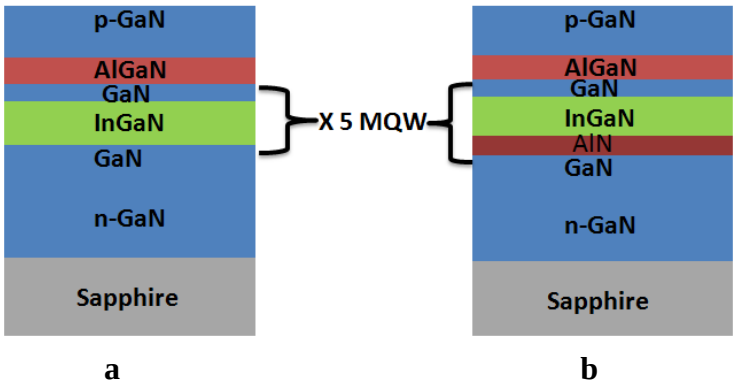

Figure 3.1 (a) Schematic of InGaN/GaN MQW LED (b) Schematic of InGaN/GaN with AlN layer at the interface of GaN and InGaN.

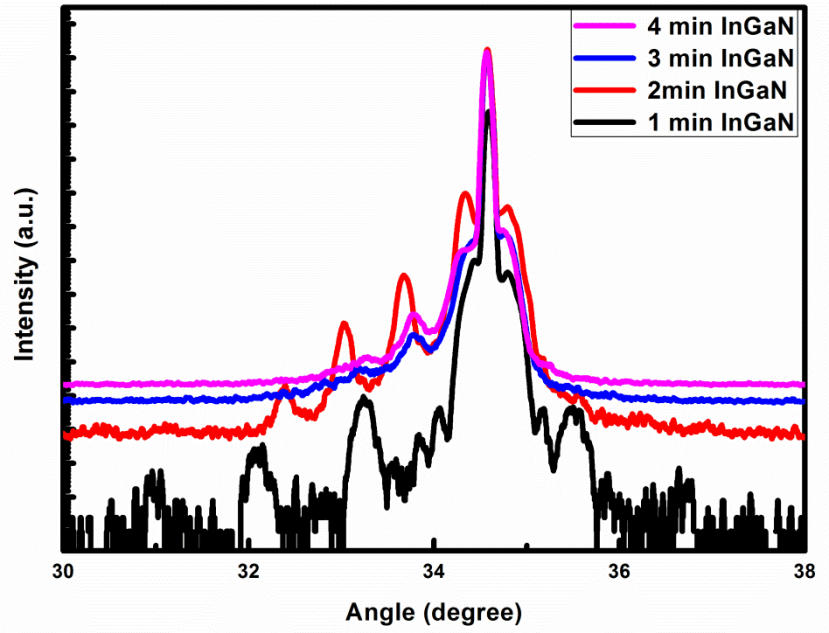

Figure 3.2 HRXRD 2θ-ω scan for the (0002) reflection from batch A.

These samples were further characterized using micro-PL measurement. PL was exited by a 405 nm laser at an excitation power of 3 mW. The laser was focused onto the sample surface by an objective lens and the diameter of the exited area was 2 μm. Figure 3.3. shows the PL measurement for sample A. The PL spectrum for 1 min InGaN had a peak wavelength of 432 nm and on increasing the InGaN growth time to 2 min the wavelength red-shifted to 454 nm but it also reduced the PL intensity. Further increasing of InGaN thickness deteriorated the crystal quality and no emission peaks were observed for these LED structures. This is due to strain relaxation of InGaN on GaN.

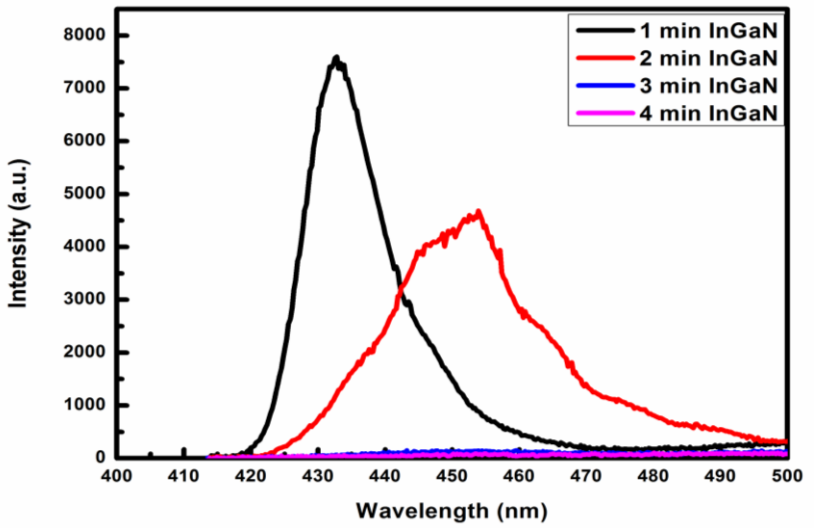

Figure 3.3 Room temperature µ-PL spectrum for batch A.

CL observation of the active layers for all the four samples in the batch was carried out at room temperature in order to investigate the differences in the LED characteristics. Figure 3.4 (a-d) shows the images of the samples for batch A. For the first sample with InGaN growth time of 1 min CL image showed uniform indium deposition throughout the wafer at 430 nm and when the indium growth time was increased from 1 min to 2 min the wavelength got red-shifted to 450 nm. Indium seems to be segregated at some places due to increase in growth time of InGaN which is depicted in figure3.4 (b). On further increasing the InGaN growth time to 3 min and 4 min the CL spectrum had a peak wavelength of 437 and 432 nm respectively. No red shift in wavelength was observed in the wafers but the wavelength remained similar to 1 min InGaN growth time wafer. The CL images for both the samples shows island like structures in sub-micrometer scales at isolated places due to spatial fluctuation of indium composition in InGaN layers. For the last sample in batch A with 4 min InGaN (figure 3.4 d) growth time indium seems to be segregated at one place on the wafer. Thus from the CL images we conclude that on increasing the InGaN thickness in the quantum wells leads to indium segregation and effects the crystal quality of LEDs.

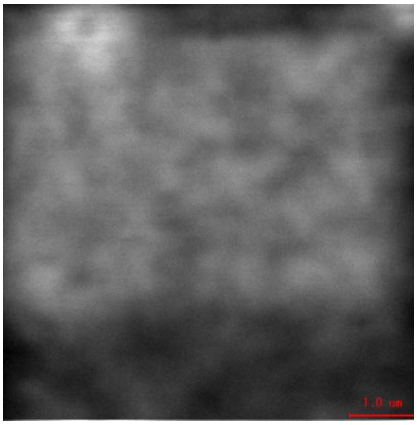

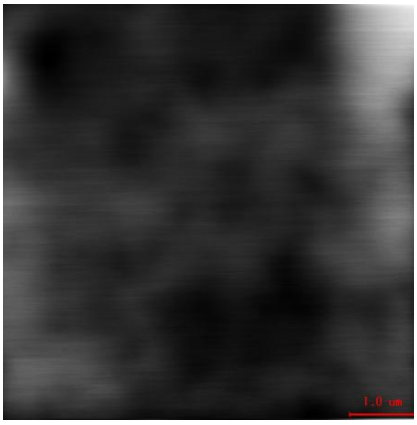

c

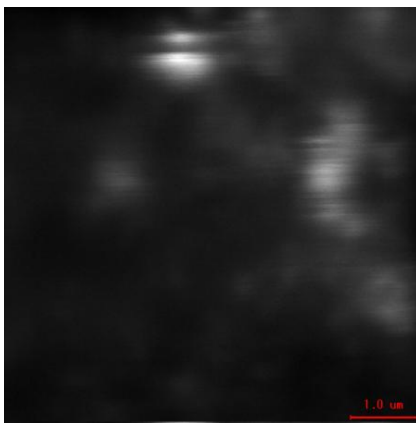

d

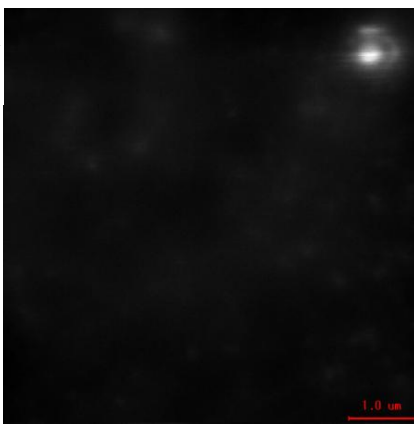

Figure 3.4 CL images taken for samples in batch A at room temperature.

All the four LEDs in batch A were fabricated using Ni (20 nm)/Au (80 nm) ohmic contacts using thermal evaporation for p-GaN and indium contact for n-GaN. The diameter of Ni/Au contact was 300 μm for all the samples. Figure 3.5 shows the current-voltage (I-V) characteristics for the samples in batch A. The turn on voltage for 1 min InGaN LED was lower as compared to other three LEDs. Threshold voltage increased with increase in InGaN due to indium segregation. The turn on voltage for 1 and 2 min InGaN were 2.9V and 3.1 V respectively, 2 min InGaN had higher resistance as compared to 1 min InGaN. Threshold voltage for 3 and 4 min InGaN was same at 4.5 V. EL for all the four samples were measured at room temperature under dc-biased conditions. Wavelength got red shifted from 435 nm to 459 nm with increasing the InGaN growth time from 1 min to 2 min, while for the other two samples the intensities from LEDs were too weak to be measured but they appeared to be in blue color. Figure 3.6 shows the graph total well and barrier thickness and EL wavelength as a function of InGaN growth time. Inset shows the picture of blue LEDs for 3 and 4 min growth time. The black line in the graph represents well and the barrier thickness, while blue line represents the EL wavelength. The well and the barrier thickness were determined from 2θ-ω scan using HRXRD. Thickness of the well and the barrier increased with increase in InGaN growth time. The thickness was found to be 8, 14, 16.5 and 17.5 nm for 1,2,3 and 4 min InGaN growth respectively.

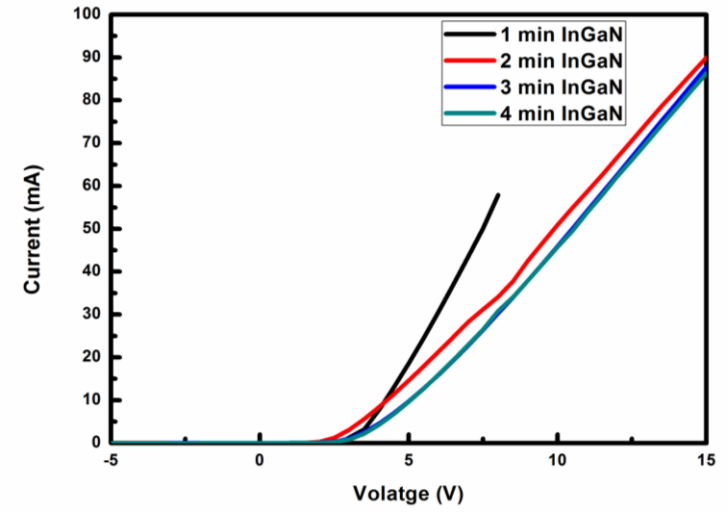

Figure 3.5 I-V characteristics for samples in batch A measured at room temperature.

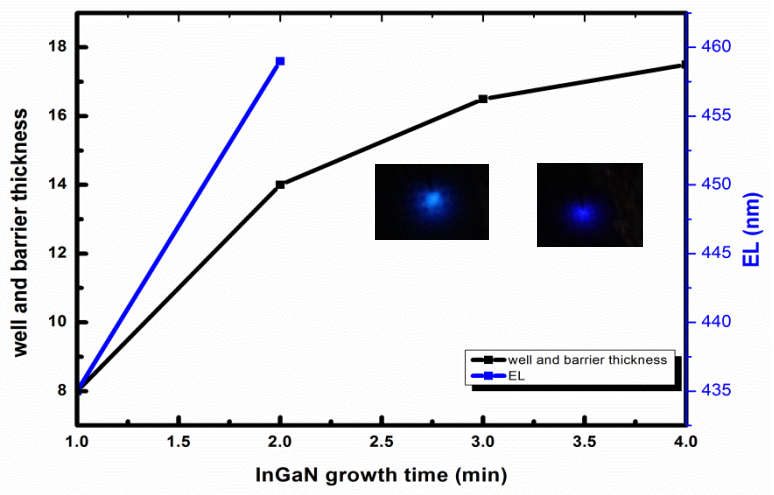

Figure 3.6 Total well and barrier thickness and EL wavelength as a function of InGaN growth time for batch A LEDs. Inset shows the color of LEDs for 3 and 4 min growth time.

By looking at all the characterization result it was observed that thick InGaN does not result in red shift in wavelength but thick InGaN leads to strain relaxation and degradation of crystal quality. So increasing the InGaN thickness is not an effective way to make LED emitting in green-gap region.

3.3 Effect of AlN on InGaN/GaN MQWs

In order to get an emission in the green gap region we looked back at the lattice constant vs band gap diagram. Wurtzite GaN, AlN and InN have a lattice constant of 3.191, 3.112 and 3.545 A° respectively. Since AlN having a small lattice constant compared to InN thus the tensile strain of AlN and compressive strain of InGaN will help in achieving high indium content in InGaN.

For set B we inserted a thin AlN for 30 sec between first InGaN/GaN interfaces of each quantum wells which was described in section 3.1.1. All the four samples in set B were characterized using HRXRD, micro-PL, CL and EL.

Figure 3.7. shows 2θ-ω scan for (0002) reflections for batch B. The dominant peak came from the diffraction of n-GaN buffer layer under the MQWs which is similar to that of batch A. From the graph we can observe that for 1 min InGaN on 30 sec AlN the zeroth order peak is coinciding with the dominant peak and as we increased the InGaN thickness the satellite peak shifted towards the left side of the dominant peak which indicates compressive strain in the layers due to thick InGaN. The thickness of InGaN increased with

increase in InGaN growth time which can be interpreted from reduction in distances between the satellite peaks. Compared to batch A the satellite peak are broadened confirming the formation of 3D structure. The total well and the barrier thickness was estimated to be 8, 9, 10, 12 nm for 1, 2, 3 and 4 min InGaN growth respectively.

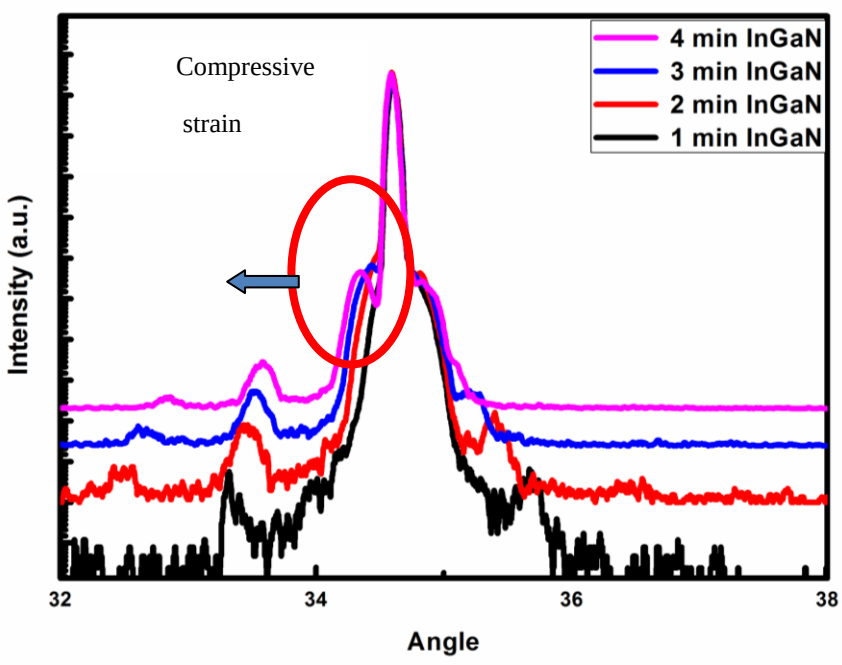

Figure 3.7 HRXRD 2θ-ω scan for the (0002) reflection from batch B.

In order to analyze AlN crystal quality we grew 30 sec AlN on GaN template. The growth conditions of GaN and AlN were exactly the same as mentioned in section 3.1.1. Since we grew AlN at the same temperature as that of barrier and well, so it was necessary to analyze the surface of AlN. Figure 3.8 displays (1 µm x 1 µm) image of 30 sec AlN grown at 780 °C. AlN on GaN template was rough with lot of dots on the surface. In order to get a smooth AlN surface it is necessary to grow AlN at higher temperature but high temperature growth of AlN layer will lead to desorption of indium layer beneath. Root mean square (RMS) roughness of AlN was found to be .3 nm.

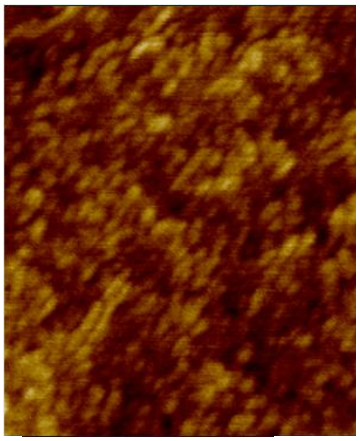

Figure 3.8 AFM image of 30 sec AlN on GaN template.

CL measurement was done for all the four samples. Figure 3.9 (a-d) shows room temperature CL mapping for all the four wafers in batch B. Figure 3.9 (a) shows a large number of dots emitting at 429 nm for 1 min InGaN with 30 sec AlN. Since AlN surface was rough and thin InGaN deposition on these rough AlN formed nano dots. On further increasing the InGaN growth time to 2 min the dot became more prominent and larger with the emission wavelength of 460 nm. The compressive strain of InGaN had helped in having more indium in InGaN with larger size which is depicted in figure 3.9 (b). For 3 min InGaN on rough AlN a broad spectrum in the yellow luminescence was observed with the peak wavelength of 562 nm. Figure 3.9 (c) shows the image for 3 min InGaN growth. 3 min InGaN does not have contrast in image like that observed for 1 and 2 min InGaN. When the growth time was increased to 4 min the CL emission was in yellow-green region with the peak wavelength of 551 nm. The blue shift in wavelength is due to the characterization performed at different places in the wafer. For 3 and 4 min InGaN there was no contrast in the scanned image indicating high and uniform InGaN deposition.

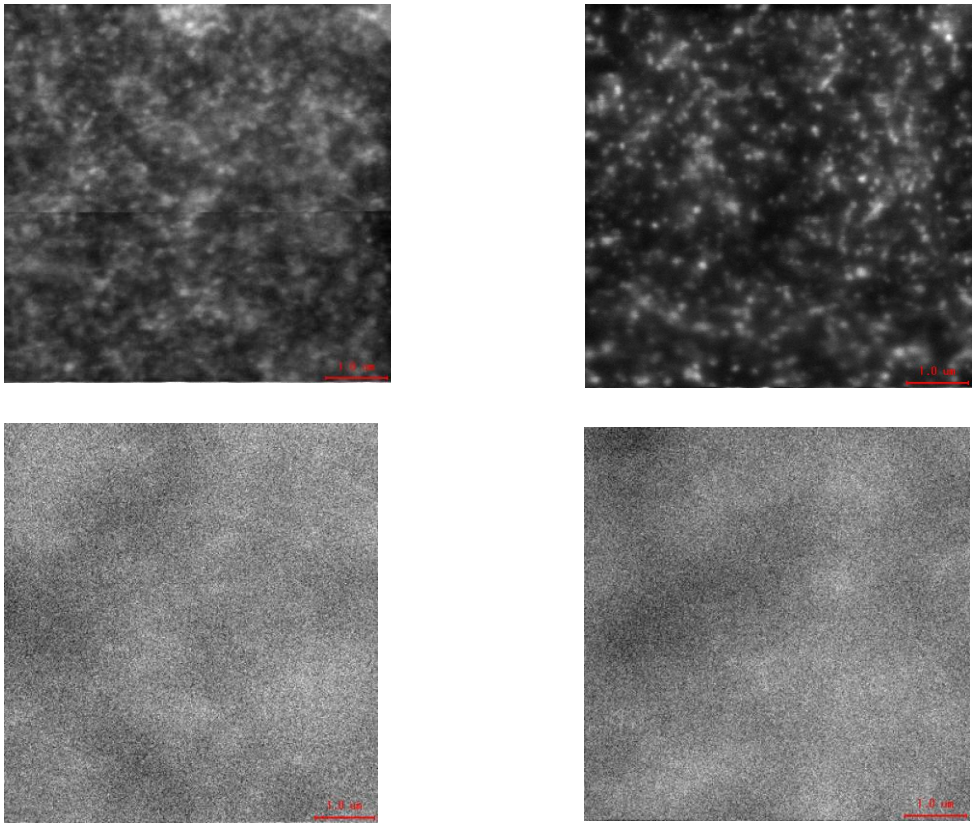

Figure 3.9 CL images taken for samples in batch B at room temperature.

PL measurement was performed with the same micro-PL setup mentioned in section 3.1.1. Figure 3.10 shows the room temperature μ-PL spectrum for batch B. For 1 min InGaN the peak intensity was at 426 nm and on increasing the InGaN growth time the wavelength got red-shifted to 436 nm. There were two peaks observed for 2 min InGaN. On further increasing the InGaN growth time to 3 min the peak wavelength shifted to 471 nm and the spectrum became broader. When the InGaN growth time was increased to 4 min a very broad spectrum was observed. The intensity of 1 min InGaN was less than all the three samples because InGaN layers could not completely cover the rough AlN layer.

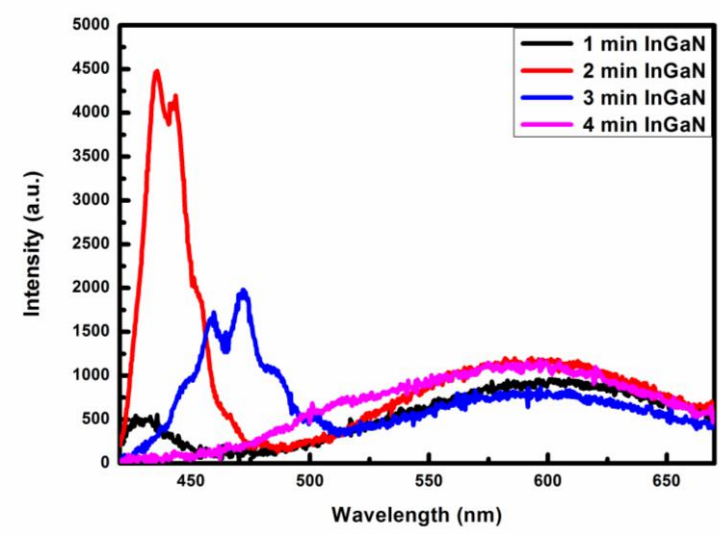

Figure 3.10 Room temperature µ-PL spectrum for batch B.

All the LEDs in batch B were fabricated using Ni (20 nm)/Au (80 nm) ohmic contacts using thermal evaporation for p-GaN and indium contact for n-GaN. The diameter of Ni/Au contact was 300 µm for all the samples. Figure 3.11 shows the current-voltage (I-V) characteristics for the samples in batch B. Resistance for 1 min InGaN was higher compared to 2 min InGaN on 30 sec AlN. This may be due to inability of InGaN to cover all AlN nanoislands. Resistance of LEDs further increased when InGaN thickness was increased for 3 and 4 min. This may be due to crystal defect originating from high compressive strain of InGaN.

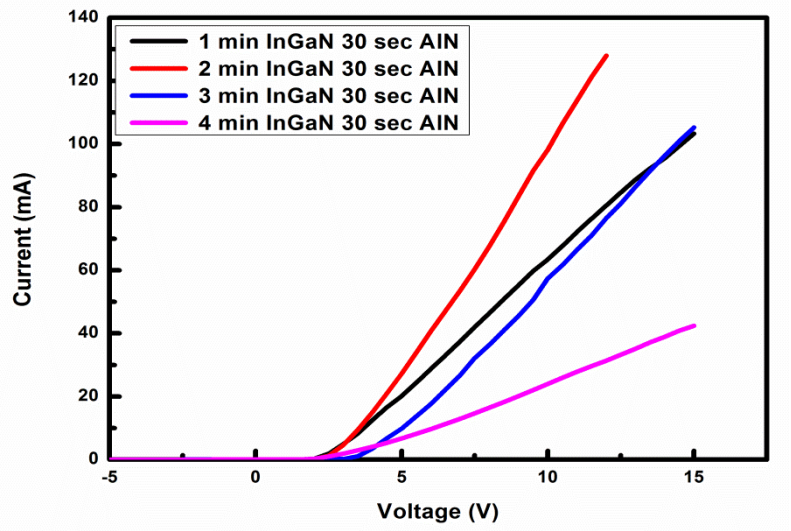

Fig. 3.11 I-V characteristics for batch B.

The total well and barrier thickness was calculated using XRD. Figure 3.12 shows the graph representing total well and barrier thickness with respect to increase in InGaN for 30 sec AlN and without AlN. The well and the barrier thickness increases with increase in InGaN growth time. The well and the barrier thickness in batch B is less than batch A due to run-to-run variations during growth.

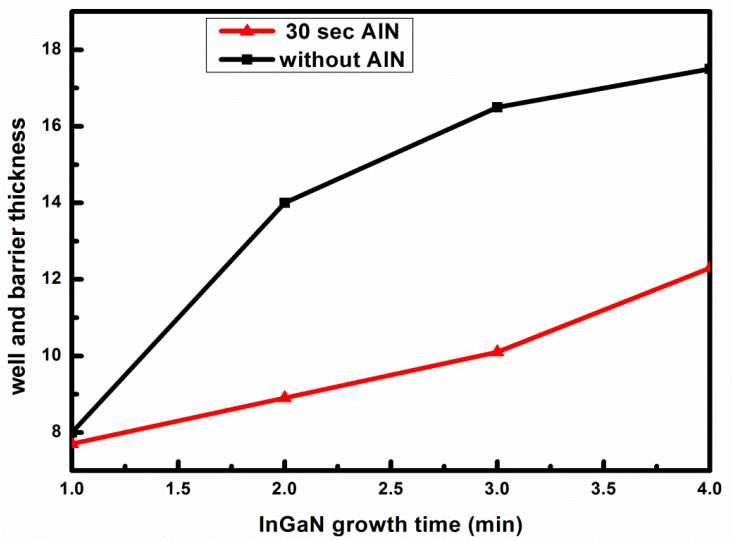

Figure 3.12 Well and barrier thickness vs InGaN growth time for batch Aand B.

EL was measured at 50 mA under room temperature. Figure 3.13 shows normalized EL intensity of all the four LEDs and insets shows the pictures of all the four LEDs corresponding to their wavelength. For a 1 min InGaN the LEDs had a peak wavelength emission of 427 nm and on increasing the InGaN thickness to 2 min the wavelength got red shifted to 458 nm. On further increasing the InGaN growth time to 3 min the wavelength again got red shifted to 483 nm. This time the wavelength became broad. When the growth time was increased to 4 min the wavelength further red shifted by 62 nm and there was a peak wavelength emission at 545 nm. The emission at this wavelength was broader than the emission with 3 min InGaN.

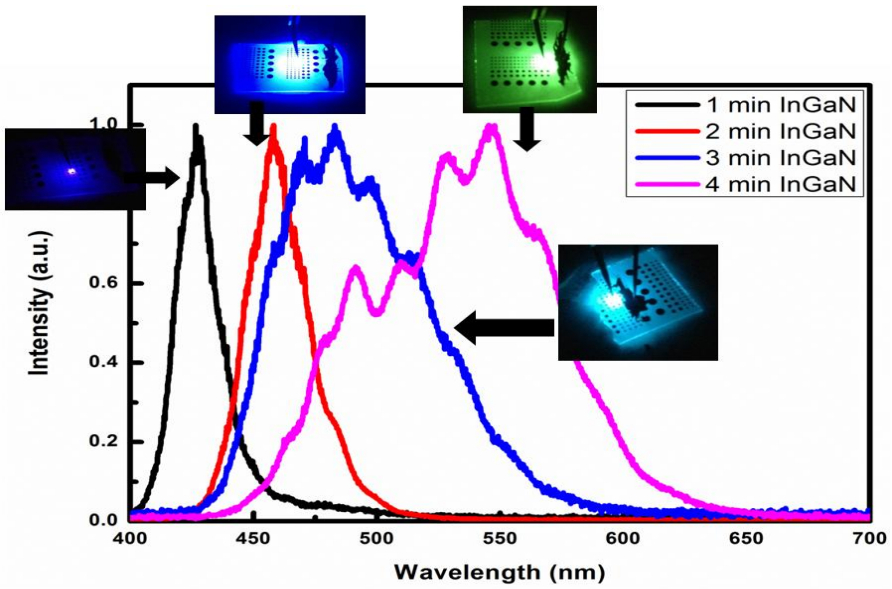

Fig 3.13 shows normalized EL intensity of all the four LEDs and insets shows the pictures of all the four LEDs corresponding to their wavelength.

On comparing the EL results for LEDs in batch A and B we found that insertion of thin AlN layer red-shifted the emission wavelength. Figure 3.14 shows EL comparison graph for LEDs with and without AlN layer. For 1 and 2 min InGaN in batch A the peak wavelength emission was 435 and 459 nm respectively while for batch B the peak emission wavelength was 427 and 458 nm respectively. The peak wavelengths showed the similar behavior for both the conditions. When the InGaN growth time for batch A was increased to 3 and 4 min then there was no further red shift in wavelength while for batch B there was a drastic red shift in wavelength. Red shift in batch B was due to high compressive strain of InGaN on tensile AlN helped in more In incorporation in InGaN.

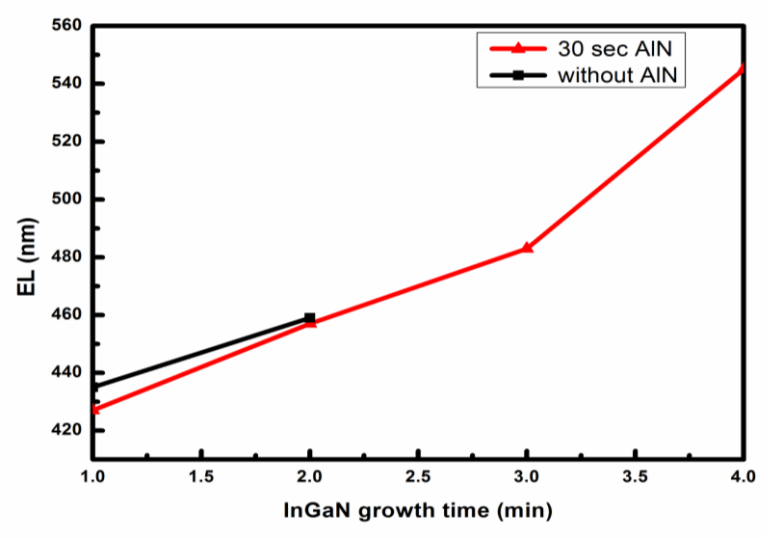

Figure 3.14 shows EL comparison graph for LEDs with and without AlN layer.

In order to further analyze the effect of thickness of both AlN and InGaN we further increased the AlN growth time from 30 sec to 1 min for all the MQWs. The four samples in this batch will be further referred to as C. Figure 3.15 shows room temperature μ–PL for batch C. For 1 min InGaN with 1 min AlN the peak wavelength emission was 438 nm and on further increasing the InGaN growth time the wavelength got red shifted to 529 nm. The wavelengths for both the cases were very broad in comparision to samples in batch A and B. For 3 min InGaN the peak wavelength shifted to 565 nm with a very broad emission and as the growth time of InGaN was increased to 4 min the peak wavelength again got red-shifted to 612 nm.

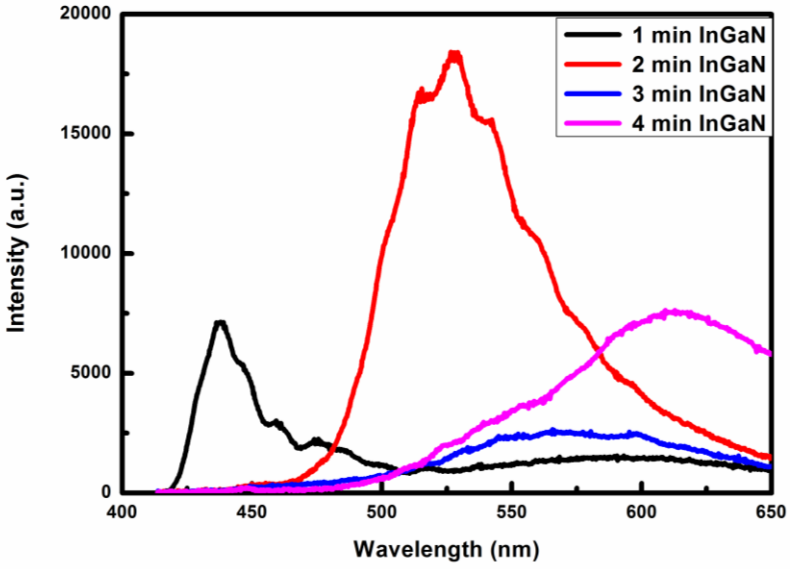

Fig 3.15 room temperature µ-PL for batch C

The crystal quality of AlN was analyzed by growing 1 min AlN on the GaN template. The surface analysis of AlN was done using AFM. Figure 3.16 displays (1 µm x 1 µm) image of 1 min AlN grown at 780 °C. A big dot size image can be clearly observed from the AFM image. These dots were formed due to low temperature growth of AlN. The RMS roughness of the sample was found to be .39 nm which is larger compared to 30 sec AlN.

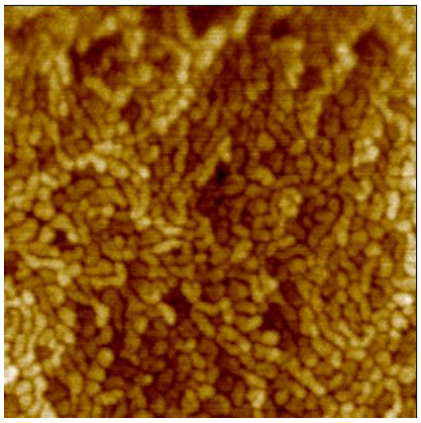

0 1

Figure 3.16 AFM image of 1 min AlN on GaN template.

The samples in batch C were further analyzed using 2θ-ω scan for (0002) reflections. Figure 3.17 shows HRXRD 2θ-ω scan for the (0002) reflection from batch C. From the graph we observe that for 1 min InGaN the zeroth order peak coincides with the dominant peak and as the InGaN thickness is increased to 2 min the zeroth peak emerges to the left of dominant peak. When the InGaN thickness is increased to 3 min the zeroth peak properly emerges out and for 4 min InGaN the peak further moves towards left of dominating peak. This shift in the zeroth peak is due to the compressive strain due to thicker InGaN. Increase of InGaN thickness with increasing InGaN growth period can be confirmed from the decrease in distances between satellite peaks. This tendency is similar to batch B samples. While if we compare it with batch A sample there was no observance of zeroth peak shift for 3 and 4 min InGaN growth period thus with the samples with thin AlN helps in thicker InGaN.

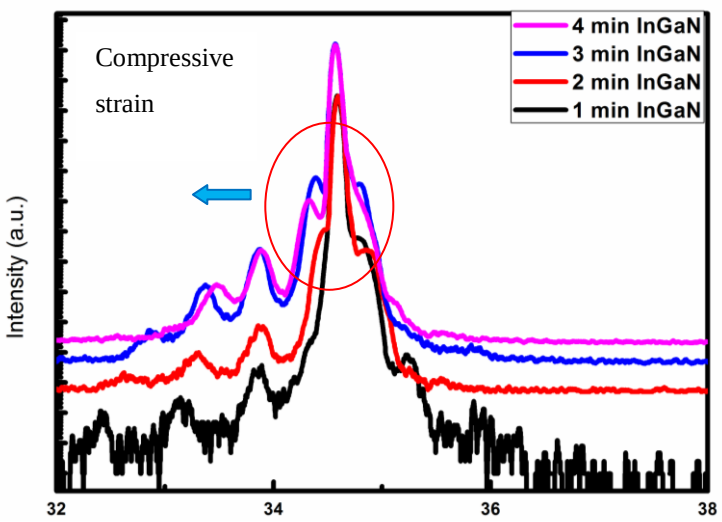

Figure 3.17 HRXRD 2θ-ω scan for the (0002) reflection from batch C.

CL for all the four samples in batch C was measured at room temperature. Figure 3.18 (a-d) shows CL images of four samples with 1 min AlN. 1 min InGaN in sample C showed lot of scattered dots having the peak wavelength of 444 nm. The emission from scattered places is coming due to rough AlN. 1 min InGaN is not enough to cover the complete AlN so the emission comes from scattered places. On comparing this sample with 1 min InGaN in batch B there is a red shift of 15 nm. Thicker AlN helped in having more tensile stress on InGaN resulting in more indium in InGaN. Samples with 2, 3 and 4 min InGaN in batch C had a peak wavelength of 557 nm, 560 nm and 554 nm respectively. The CL images had broad emission regions at some places of all the three samples which is due indium fluctuations on the wafers.

All the LEDs in batch C were fabricated in the similar way as that of batch B.. Figure 3.19 shows the current-voltage (I-V) characteristics for the samples. Resistance for 1 min InGaN was higher compared to 2 min InGaN due to uncovering of rough AlN by InGaN at some places. This tendency is similar to batch B sample with 1 min InGaN. 2 min InGaN growth time on 1 min AlN has lowest turn on voltage and resistance as compared to rest of the samples in batch C and the resistance and turn on voltage further increase with increase in InGaN thickness. The increase in resistance may be due crystal defects due to thicker InGaN.

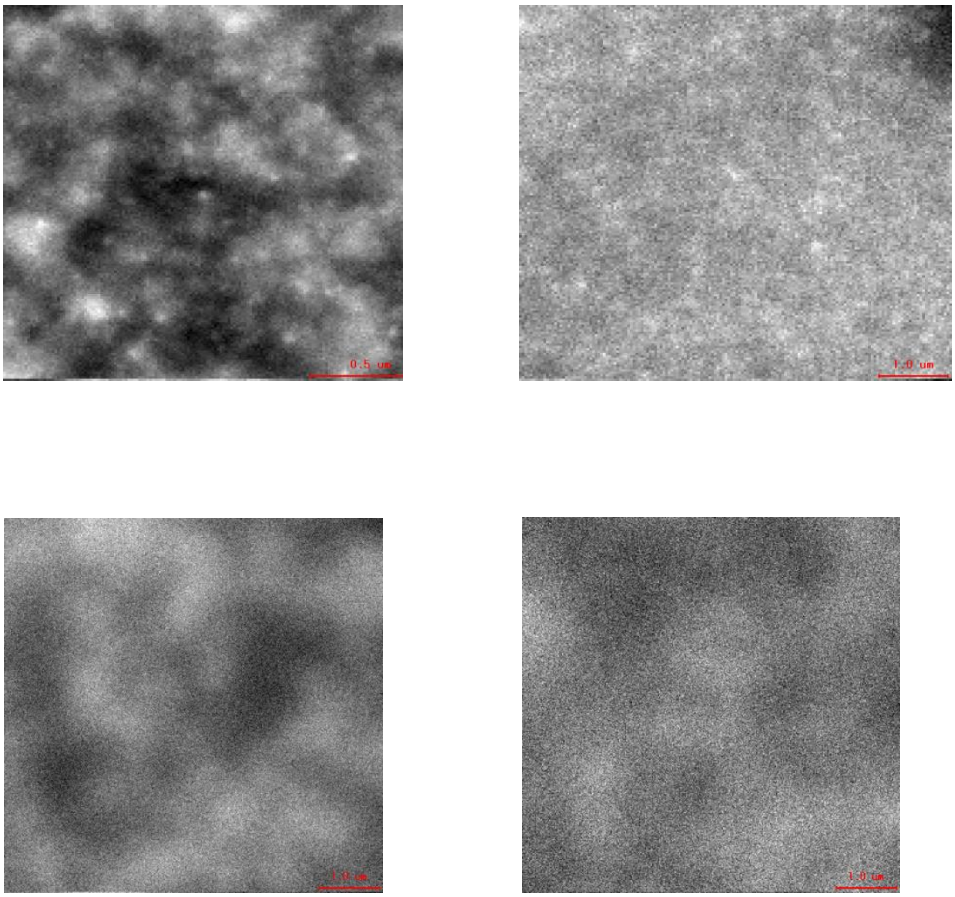

Figure 3.18 CL images taken for samples in batch C at room temperature.

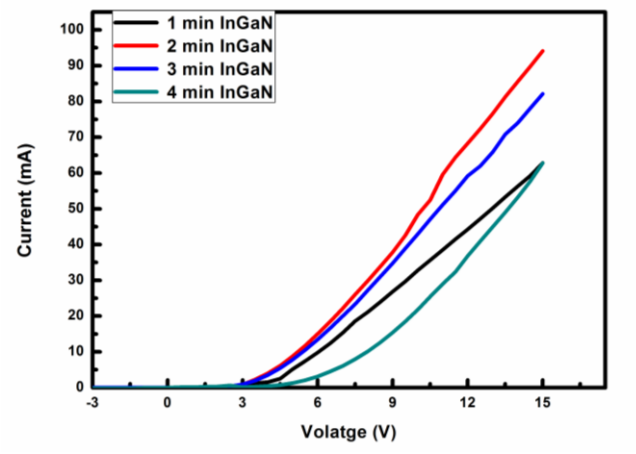

Figure 3.19 I-V characteristics for batch C

EL was measured at 50 mA under room temperature for batch C. Figure 3.20 shows normalized EL intensity of all the four LEDs and insets shows the pictures of all the four LEDs corresponding to their wavelength. For a 1 min InGaN the LEDs had a peak wavelength emission of 492 nm and on increasing the InGaN thickness to 2 min the wavelength got red shifted to 504 nm. On further increasing the InGaN growth time the wavelength got further red shifted to 575 nm. The emission for 3 min was broader as compared to previous two samples. For 4 min InGaN growth time the wavelength got further red shifted to 588 nm. There was also an emergence of another weak at 487 nm. The EL results were similar to that obtained in μ–PL measurements with the exemption of 1 min and 4 min InGaN which may be due to indium composition fluctuation in the samples. From the EL emission we may conclude that thick InGaN on rough AlN results in more indium incorporation in InGaN resulting in red shift in wavelength.

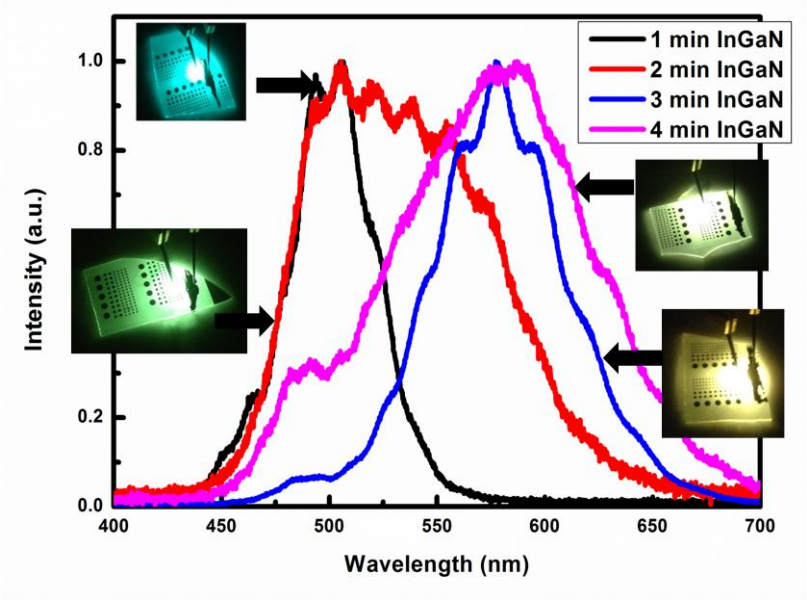

Fig 3.20 shows normalized EL intensity of all the four LEDs and insets shows the pictures of all the four LEDs corresponding to their wavelength.

The total well and barrier thickness for batch C were calculated using XRD. Figure 3.21 shows the graph representing total well and barrier thickness with respect to increase in InGaN for batch A, B and C. The well and the barrier thickness increases with increase in InGaN growth time and the total well and barrier thickness was larger in batch C compared to batch A and B. Total well and barrier thickness for 1,2,3 and 4 min InGaN were 13, 15, 18 and 22 nm respectively.

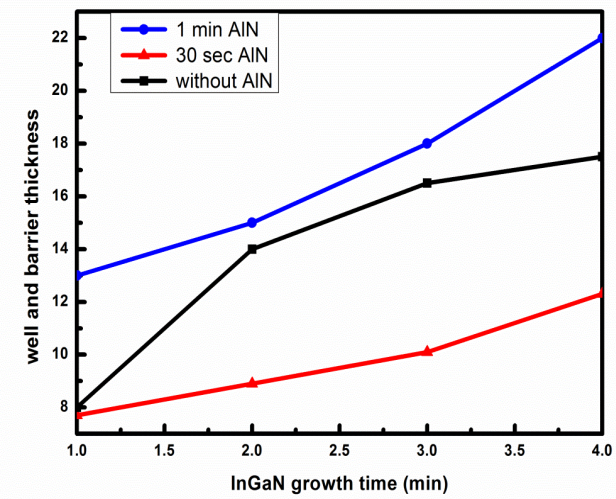

Figure 3.21 Well and barrier thickness vs InGaN growth time for batch A,B andC.

On comparing the results of batch A,B and C we found that insertion of rough AlN layer helped in red-shift of wavelength. Figure 3.22 shows EL comparison graph for LEDs for batch A,B and C. From the figure we observe that increasing the AlN growth time in batch C helped in red-shifting of peak EL compared to batch A and B . For 1 min InGaN the wavelength shift in batch C was 66 nm compared to batch A. Similarly for 2, 3 and 4 min InGaN growth time the wavelength shift in batch C were 47, 95 and 43 nm respectively compared with batch A.

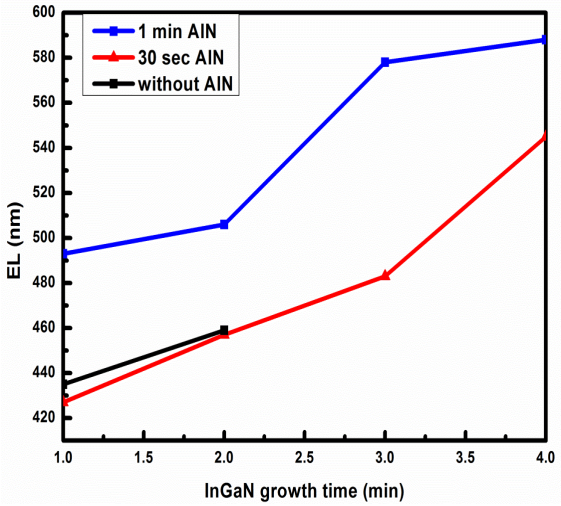

Figure 3.22 EL vs InGaN growth time for batch A,B and C.

Figure 3.23 shows the high angle annular dark field scanning transmission electron microscopy (HAADF-STEM) image for the sample with 3 min InGaN in batch C. The

bright region in the figure represents InGaN while the gray region represents GaN. The black region between InGaN and GaN represents AlN. The GaN barrier thickness was 11 nm and the InGaN thickness was ~ 7 nm which is in accordance with the total well and barrier thickness calculated by HRXRD. AlN thickness was ~0.6 nm. There was no contrast observed in InGaN representing uniform indium composition throughout the wafer.

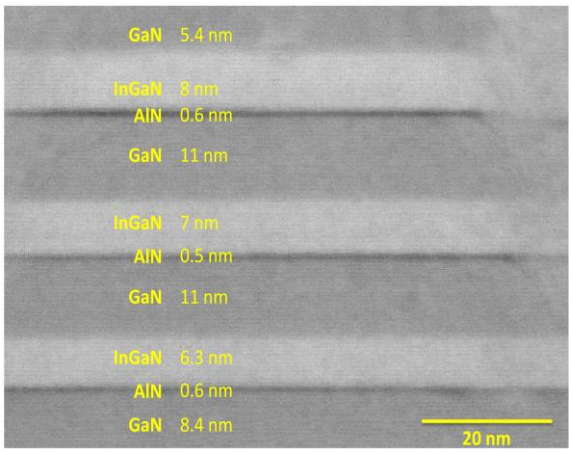

Figure 3.23 HAADF STEM image of 3 min InGaN growth time in batch C

EDX was used to measure the indium composition on the above sample . 6 points were selected on the sample. Figure 3.24 a shows the EDX points on the sample. Indium composition on the defect area at point 1 was 8 percent while at point 2 it was 22 percent. All the other points had a uniform indium composition of 28 percent.

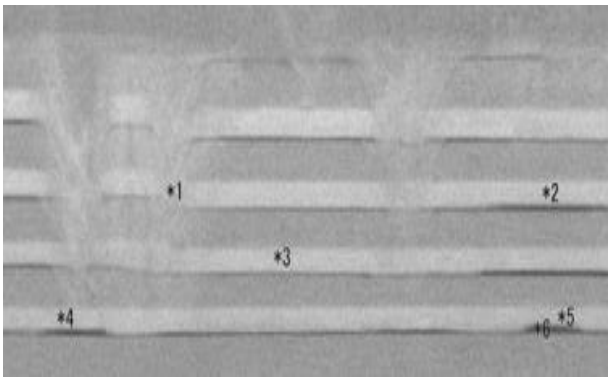

Figure 3.24 EDX points on sample with 3 min InGaN in batch C

3.4 Mechanism of indium incorporation

First we look into the mechanism that deteriorated the samples in batch A. Talalaev et al had shown that the indium composition increases along the growth direction with increase in InGaN thickness [11]. When the InGaN thickness is less than critical thickness then InGaN is coherently strained. Increasing the thickness of InGaN beyond critical thickness, results in strain relaxation [12-14]. Due to strain relaxation there is indium segregation on the wafers which deteriorates the crystal quality. Figure 3.25 represents the cross sectional and top view schematic of segregated InGaN over GaN template.

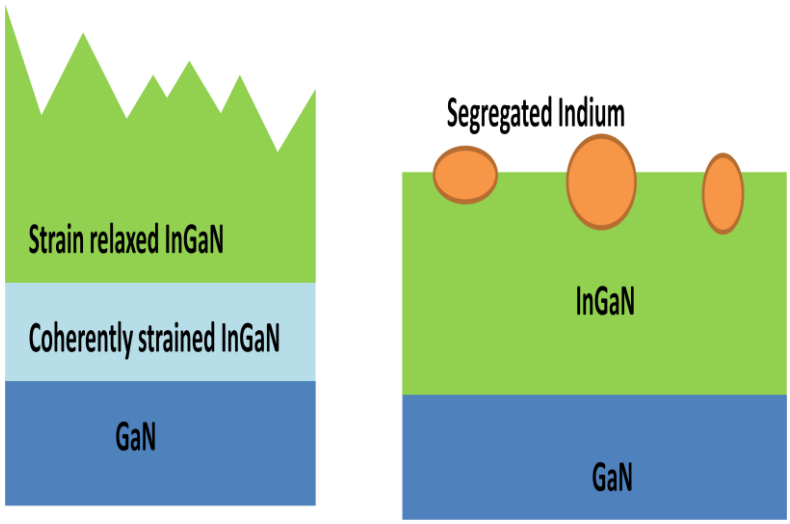

Figure 3.25 (a) cross sectional schematic of thick InGaN over GaN (b) top view of segregated InGaN

When rough AlN layer is inserted beneath first interface of each InGaN/GaN MQWs then

1. Red shift in wavelength with increasing InGaN and AlN thickness.
2. Broadening of emission wavelength.

Insertion of AlN layers exerts tensile stress on the above InGaN layer. The compressive stress of InGaN on rough and tensile AlN helps in diffusion of indium in InGaN. Kisielowski *et al* had earlier reported sudden increase in indium at InGaN/AlGaN interface when InGaN was capped with AlGaN. As tensile strain is introduced by AlGaN, it eases the indium incorporation limitation due to existing compressive strain of InGaN [15]. His results were further simulated by Talalaev *et al* which showed the reason for increase in InGaN [11]. When the InGaN thickness is increased beyond the critical thickness with AlN at the bottom, the tensile strain of AlN prevents compressive strain of InGaN to relax. Due

to tensile nature of AlN indium in InGaN seems to move in the opposite to growth direction thus preventing segregation of indium beyond the critical thickness. Thus on increasing the AlN thickness more tensile stress is exerted on the upper compressive InGaN leading to more indium diffusion in InGaN and hence red shift in wavelength.

LEDs in batch B and C exhibited broad emission spectrum with increase in InGaN growth time. HAADF-STEM image for sample showed no contrast in the InGaN region indicating uniform indium in quantum wells. The disadvantage of TEM image is that high energy electron beam used in TEM damage InGaN QWs, resulting in potentially unreliable structural data [16-18].Atom probe tomography (APT) is more appropriate then TEM since three-dimensional nature of the APT data set is more appropriate to the development of a three-dimensional model than the two-dimensional projections usually recorded in TEM. For quantum wells grown at a single temperature, with x = 0.18 and 0.25, the APT data revealed the $In_x Ga_{1-x}N$ within the quantum well to be a random alloy [19]. The samples in batch B and C had more indium composition compared to standard blue LED in which the indium composition is ~ 18%. The high indium composition in InGaN leads to indium composition fluctuation inside the quantum wells. Due to this composition fluctuation LEDs emit a broad spectrum. Fig 3.26 shows the mechanism of indium fluctuation in InGaN due to presence of AlN.

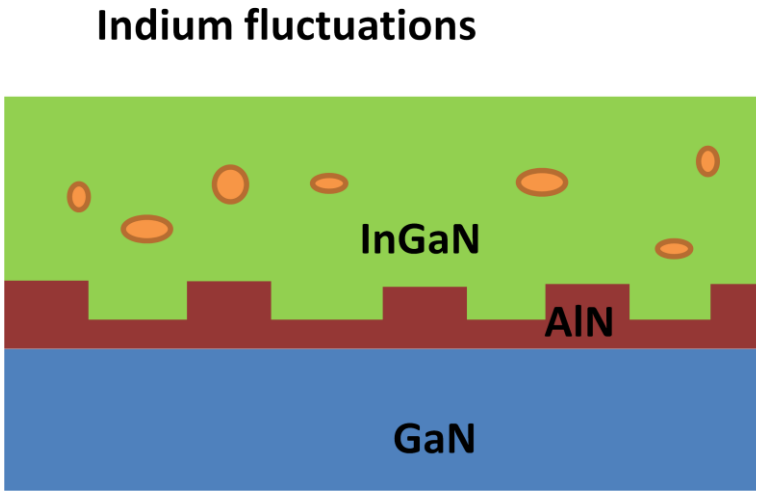

Figure 3.26 Schematic of indium fluctuation in InGaN due to AlN.

3.5 Conclusions

From the above sections we have investigated the effect of AlN on standard InGaN/GaN LEDs . Results indicated that AlN have a crucial role in the red-shift of wavelength. High indium fraction in InGaN was due to the underlying tensile AlN layer which resulted in more indium in InGaN due to its compressive nature. Broad wavelength emission in these LEDs was due to indium composition fluctuations inside the QWs. Though the morphology of AlN grown at lower temperature is not good but it still helped in longer wavelength emission.

3.6 References

[1] M. Shimizu, K. Hiramatsu, and N. Sawaki, J. Cryst. Growth 145, 209 (1994).

[2] A. Koukitu, N. Takahashi, T. Taki, and H. Seki, J. Cryst. Growth 170, 306 (1997) .

[3] F. Bernardini, V. Fiorentini, and D. Vanderbilt, Phys. Rev. B 56, R10024(1997).

[4] S. Chichibu, T. Azuhata, T. Sota, and S. Nakamura, Appl. Phys. Lett.6,9 4188 (1996).

[5] C. B. Soh, W. Liu, S. J. Chua, S. S. Ang, R. J. N. Tan, and S. Y. Chow, J. Appl. Phys. 108, 093501 (2010)

[6] S. P. Chang, Y. C. Chen, J. K. Huang, Y. J. Cheng, J. R. Chang, K. P. Sou, Y. T. Kang, H. C. Yang, T. C. Hsu, H. C. Kuo, and C. Y. Chang, Appl. Phys. Lett. 100**,** 061106 (2012).

[7] Y. J. Hong, C. H. Lee, A. Yoon, M. Kim, H. K. Seong, H. J. Chung, C. Sone, Y. J. Park, and G. C. Yi, Adv. Mater. 23, 3284 (2011).

[8] T. Kim, J. Kim, M. S. Yang, S. Lee, Y. Park, U. I. Chung, and Y. Cho, Appl. Phys. Lett. 97**,** 241111 (2010).

[9] C. C. Chen, C. H. Chiu, S. P. Chang, M. Shih, M. Y. Kuo, J. K. Huang, H. C. Kuo, S. P. Chen, L. L. Lee, and M. S. Jeng, Appl. Phys. Lett. 102, 011134 (2013).

[10] S. P. Chang, J. R. Chang, K. P. Sou, M. C. Liu, Y. J. Cheng, H. C. Kuo, and C. Y. Chang, Opt. Express 21, 23030 (2013).

[11] R. A. Talalaev, S. Yu. Karpov, I. Yu. Evstratov, and Yu. N. Makarov,phys. stat. sol. (c) 0, No. 1 (2002).

[12] Liliental-Weber, Z; Benamara,M; Washburn,J;Piner, E; Roberts, and Bedair, S.M., J. Electron. Mat. 30,439 (2001).

[13] S. Pereira, M. R. Correia, E. Pereira, K. P. O'Donnell, E. Alves, A. D. Sequeira, N. Franco, I. M. Watson and C. J. Deatcher, Appl. Phys. Lett. *80* , 3913 (2002).

[14] M. Shimizu, Y. Kawaguchi, K. Hiramatsu and N. Sawaki, JJAP 36, 3381(1997)

[15] C. Kisielowski, Z. Liliental-Weber, and S . Nakamura , Jpn. J. Appl. Phys. 36, 6932 (1997).

[16] M. J. Galtrey, R. A. Oliver, M. J. Kappers, C. J. Humphreys, P. H.Clifton, D. Larson, D. W. Saxey, and A. Cerezo, J. Appl. Phys. 104,013524 (2008).

[17] S. E. Bennett,D. W. Saxey,M. J. Kappers, J. S. Barnard, C. J. Humphreys,G. DW Smith,

and R. A. Oliver 1,Appl. Phys. Lett. 99, 021906 (2011).

[18] R A Oliver , S E Bennett , T Zhu , D J Beesley , M J Kappers ,D W Saxey , A Cerezo and C J Humphreys,J. Phys. D: Appl. Phys. 43, 354003 (2010).

[19] T. M. Smeeton, M. J. Kappers, J. S. Barnard, M. E. Vickers, and C. J. Humphreys, Appl. Phys. Lett. 83, 5419 (2003).

4 Growth and fabrication of nanodisk LEDs

This chapter will focus on the growth and fabrication of nanodisks. Introduction to different nanostructures and growth mechanism of InGaN/AlN is described in section 4.1 and 4.2 respectively. The effect of strain neutral layer on nanodisk will be investigated in section 4.3 followed by mechanism for broad emission in nanodisk will be explained in section 4.4. Comparison of nanodisk structure with other works will be compared in section 4.5 finally the chapter would end with conclusion in section 4.6.

4.1 Introduction

In comparison to conventional thin film LEDs used today, GaN based nanorods (or nanowires) offer many potential advantages. GaN nanorods with high aspect-ratio and large surface-to-volume ratio can dramatically reduce the dislocation density in the upper part of the nanorods [1]. Besides, nanorods with a small footprint help to relieve the strain induced by thermal expansion mismatch and avoid cracks generation, which is a big problem for GaN growth on large substrates or substrates with large thermal expansion coefficient difference to GaN, e.g., Si. The light extraction efficiency is expected to increase owing to the non-planar geometry of nanorods [2]. There are two main methods for making nanostructures. The first method is self-organized nanorods and the second method is selective area growth (SAG). Nanostructures generated by self assembly process have random distribution in terms of size which causes inhomogeneous broadening of EL spectra [3]. This broad spectrum in the green gap region will be helpful in realizing monolithic white LEDs. Nanostructures structures grown by SAG can have uniform nanostructure throughout the wafer however this technique is not feasible for commercial application because its time consuming, unreliable and expensive [4]. Furthermore, LEDs have to undergo subsequent p-GaN growth and annealing for Mg activation which is carried out at a temperature much higher than that for the growth of indium rich InGaN QDs. This will lead to unavoidable spectra broadening and blueshift in peak wavelength [5].

Wang et al has reported on the effect of increasing the annealing temperature for p-GaN activation in InGaN QDs based LEDs [6]. With the annealing temperature at 830°C , degradation of the QDs takes place through atomic diffusion of indium into the underlying

wetting layer, leading to the formation of a wide InGaN QWs with higher indium contents. These effects enhance the blueshift in the emission wavelength at a higher drive current.

In order to solve the issue of InGaN diffusion in GaN we have look for an alternative material having higher bond energy than InN so that it can stop the diffusion of InN into barrier. Al-N bond energy is higher than Ga-N and In-N bond energy (Al-N=11.52 eV/atom, In-N=7.72 eV/atom and Ga-N=8.92 eV/atom) [7]. Use of AlN will help in preventing the diffusion of InGaN into barrier hence increase the indium content in InGaN well and enhancing the emission in green gap region [8,9]. In this chapter the growth and fabrication of self assembled InGaN/AlN nanodisk will be described in detail.

4.2 Growth and fabrication of nanodisks LEDs

Long wavelength InGaN LEDs require higher indium contents, which causes degradation of material quality due to lattice mismatch between InGaN and (Al)GaN layers. The formation of high indium composition in InGaN takes place at a lower growth temperature (~700°C), due to the unfavorable vapor pressure of indium over the compound, which hampers defect free epitaxial growth [10]. In order to solve this problem we have used AlN as a barrier instead of a conventional GaN barrier in our LED structure. The tensile strain of AlN and compressive strain of InGaN leads to higher indium incorporation [11].

In the previous section we have seen that an insertion of thin AlN beneath first interface of each InGaN/GaN MQW resulted in high indium incorporation in InGaN which is very much essential to solve the green gap problem. High indium composition in InGaN and broad emission combined will be helpful in replacing phosphor for white LEDs. In order to get a broad emission it is necessary to have a 3D structure rather than 2D structure. This motivation helped in replacing the GaN barrier with AlN barrier. Here we report, to the best of our knowledge, the first demonstration of LED using InGaN/AlN nanodisk structure emitting from orange to yellow in color. The nanodisk structure was grown at a relatively high temperature of 780°C, which is approximately the same growth temperature as that of the conventional blue LED [12].

Self assembled InGaN/AlN nanodisks were grown using an AIXTRON (AIX 200/4 RF S,) horizontal flow, low pressure MOVPE reactor on single side polish c-plane (0001) sapphire substrate. The metalorganic precursors were trimethyl-gallium (TMGa), trimethyl-indium (TMIn), trimethyl-aluminium (TMA) and triethyl-gallium (TEGa). Silicon tetra-

hydride (SiH_4) and bis-cyclopentadienylmagnesium (Cp_2Mg) were used as sources for dopant. H_2 was used as a carrier gas for the growth of n-GaN and N_2 was used for InGaN and AlN layers.

After annealing the substrate, a 30 nm thin low temperature GaN nucleation layer was grown at 550°C on sapphire substrate, then the temperature was ramped up to 1130°C to grow a 4 μm thick Si doped GaN cladding layer. Temperature was then ramped down to 780°C to grow nanodisks active layers at 100 mbar pressure. The active layers consisted of AlN and InGaN. There was no temperature swing between InGaN and AlN during growth. Nanodisks were formed due to crack formation in the first AlN layers. The succeeding InGaN/AlN layers introduce the branching of nanodisks from the initial cracks of AlN layer. Five layers of InGaN/AlN layers were formed on the initial cracked AlN layer. Finally, the structure was capped with a 120 nm thick Mg doped GaN layer grown at 1020 °C and 200 mbar. The schematic cross section of the device structure is depicted in Figure 4.1

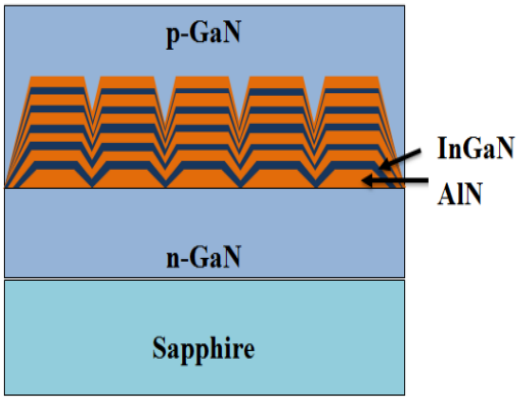

Figure 4.1 Schematic of InGaN /AlN nanodisk LED

Figure 4.2 shows high resolution X-ray diffraction (HRXRD) 2θ-ω scan for the (0002) reflections of self-assembled nanodisk LED sample, having 5 periods of InGaN/AlN layers. The dominant peak comes from the diffraction of n-GaN buffer layer under the nanodisk and the satellite peak comes from the InGaN/AlN multi-layer structure of nanodisk. The zero-th order peak coincides with the dominant peak, which indicates strain balancing between GaN and nanodisk layers.

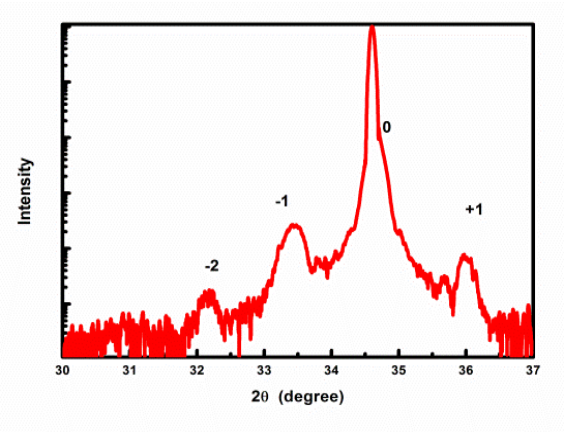

Figure 4.2 HRXRD 2θ-ω scan for the (0002) reflection from the InGaN/AlN nanodisk LED.

In order to investigate the formation of nanodisks, three different samples were grown. The first sample had a thin AlN layer on the GaN template. The second sample had an AlN layer followed by InGaN layer on GaN template with top InGaN layer uncapped. The third sample had five stacks of AlN and InGaN and was capped with an AlN layer. All the above samples were grown at the same conditions as that of the nanodisk LED. AFM was used to study the surface morphology of the nanodisk structure. Figure 3a, b, c. displays the (1 µm × 1 µm) images of single AlN layer on GaN, InGaN over single AlN layer and five layers of AlN/InGaN layers respectively. Figure 4.3 (a) shows small disk-like structure on the GaN template. The origin of initial disk-like growth in AlN is due to the low growth temperature of AlN i.e. 780 °C and nitrogen as a carrier for Al source. The average diameter of the disks were ~20 nm. A layer of InGaN grown over the initial AlN disks resulted in a lateral ncrease of disk size and the average disk diameter was increased to ~27nm as shown in Figure 4. 3 b. Further growth of InGaN and AlN resulted in the increase in disk size in both lateral and vertical directions. Five stacks of AlN/InGaN had an average diameter of ~47nm for nanodisks as shown in Figure 4.3 c. Nanodisks can be clearly observed in the AFM images.

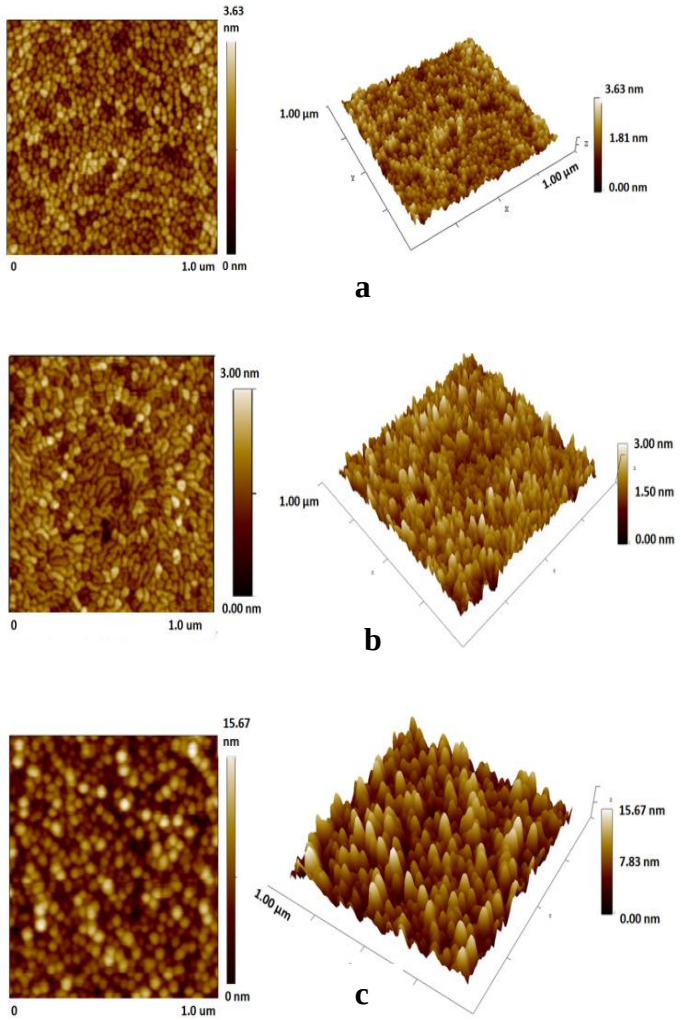

Figure 4.3 AFM images of (a) first AlN layer on GaN template. (b) InGaN deposition on first AlN layer (c) five InGaN/AlN layered structure

In-situ growth monitoring of InGaN/AlN nanodisks was performed using reflectance measurement from a 405 nm laser. Laytec EpiTT in-situ sensor was used for this purpose. Figure 4.4 (b) shows the reflectance for the whole LED growth while Figure 4.4 (a) shows the enlarged image of reflectance during nanodisk growth. The initial peak of the curve (Figure 4.4 (b)) represents the nucleation layer, followed by a straight line representing a smooth n-GaN buffer layer. After the buffer growth, AlN layer was deposited, which resulted in the decrease of reflectance, which can be clearly observed in Figure 4. 4 (a). The decrease in reflectance suggests the formation of cracked AlN surface rather a smooth surface. In other words, the slope of the reflectance graph can be interpreted as the formation of 3 dimensional (3D) structures. Subsequent growth of five periods of InGaN/AlN layers on the initial AlN reduced the reflectance further, confirming the

formation of 3D structures. After the nanodisk formation, Fabry-Perot oscillations were observed, corresponding to the p-GaN layer.

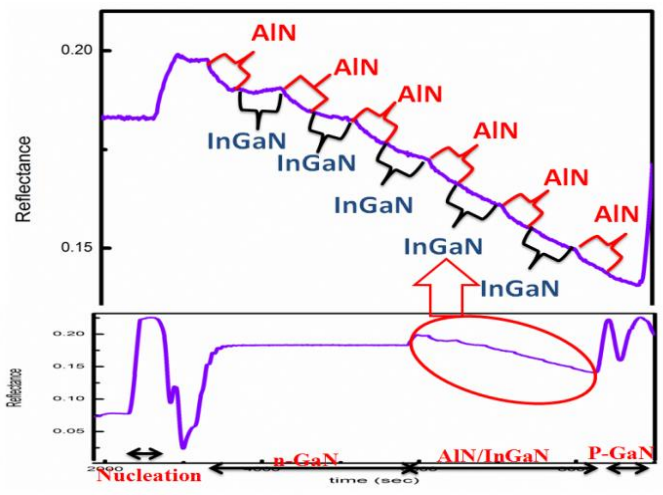

Figure 4.4 405 nm reflectance of InGaN/AlN nanodisk (a) represents enlarged view of reflectance for nanodisk LED (b) represents reflectance for whole nanodisk LED growth.

A room temperature (RT) micro-photoluminescence (μ-PL) spectrum of InGaN/AlN nanodisks is shown in Figure 4. 5. PL was excited by a 405 nm laser at an excitation power of 3 mW. The laser was focused onto the sample surface by an objective lens and the diameter of the excited area was about 2 μm. The spectrum shows broad emission and Fabry-perot reflectance is observed due to thick sapphire/n-GaN/air cavity interfaces [12]. The nanodisks have a peak wavelength around 538 nm. We believe that the broad emission in PL is due to the nanodisk structure.

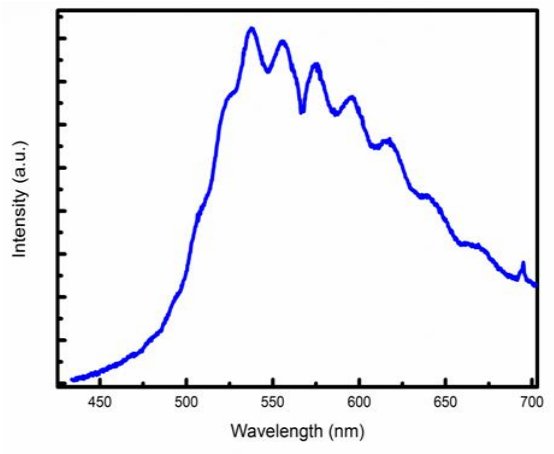

Figure 4.5 Room temperature μ-PL of InGaN/AlN nanodisk

The emission properties of this structure was further investigated by temperature dependent PL measurements and was compared with standard blue LEDs described in chapter 2. The samples were optically excited by a He-Cd laser at a wavelength of 325 nm. The excitation power for both the samples were 1.4 mW. Figure 4. 6 shows the temperature- dependent PL spectra for nanodisk LED as recorded from 10 to 300K. For nanodisk LED at room temperature (300K), the emission was mainly dominated by yellow luminescence having a peak wavelength of 556 nm with no luminescence in the blue region. On reducing the temperature to 10 K the wavelength there was no blue shift in wavelength and the peak wavelength remained at 556 nm. Figure 4.7 shows Arrhenius plot of the PL intensities of nanodisk LEDs with standard blue LEDs. The IQE is assumed to be close to unity at 10 K as non-radiative recombination is mostly suppressed at low temperature. The PL intensities are constant at low temperatures and then gradually decreases with increase in temperature. The carrier dynamics are well stabilized at lower temperature while increasing temperature leads to nonradiative recombination centers. The PL intensity for MQW LEDs reduced to 1.2 % at room temperature while for nanodisk LED the intensity reduced to 29 %. The IQE of nanodisk LED was 23 times higher compared to QWs LED.

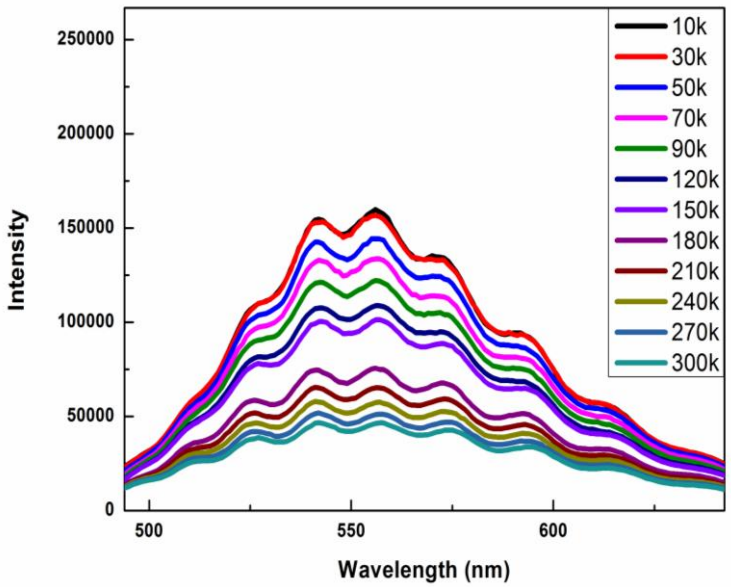

Figure 4.6 Temperature- dependent PL spectra for nanodisk LED from 10 to 300K

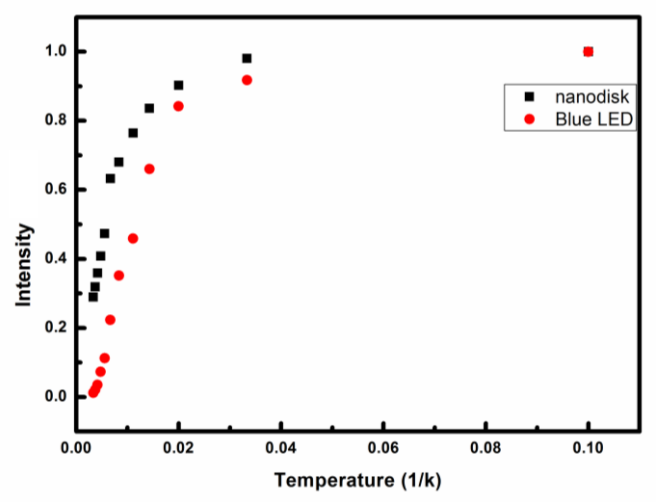

Figure 4.7 Arrhenius plot of the PL intensities of nanodisk LEDs with standard blue LEDs.

Figure 4.8 shows the cross-sectional HAADF-STEM image of InGaN/AlN nanodisk LED structure. Nanodisks of different sizes can be observed from the image. The brighter region in the naodisk represents InGaN, while dark region represents AlN. There is no contrast in the InGaN region which indicates that indium composition is uniform in InGaN. The threading dislocation in the LED structure is mainly due to threading dislocations present in the underlying n-GaN layer, there is almost no threading dislocation due to the formation of nanodisk, which confirms the good quality of nanodisk LED structure.

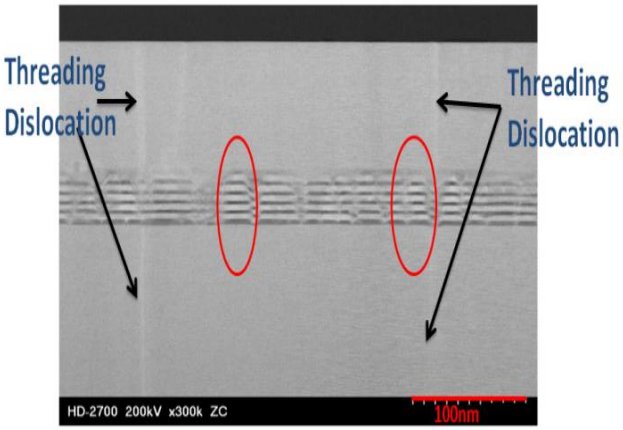

Figure 4. 8 HAADF image of InGaN/AlN nanodisk

LEDs were fabricated using Ni contacts of 300 μm daimeter for the p-GaN and In contact for n-GaN . The turn on voltage of the LED was around ~3.9V and the device

resistance is estimated to be ~75 Ω. The reason for low turn on voltage and low device resistance in LED inspite of having AlN is due to the current injection from sides of nanodisks in InGaN from p-GaN region. EL for InGaN/AlN nanodisk was measured at room temperature under dc-biased conditions. At low injection current of 10 mA the LED emitted orange light at a peak wavelength of 605 nm, when increasing the current to 20 mA the color changed to orange-yellow with a peak emission wavelength of 598 nm. At 30 mA current the peak wavelength blue shifted to yellow with a wavelength at 586 nm. Beyond 30 mA, the peak wavelength was stable at 586 nm. Figure 4.9 (a) shows the variation of EL peak wavelength as a function of driving current (inset shows the pictures of orange, orange-yellow and yellow LED lit at 10, 20 and 40 mA current respectively). Figure 4.9 (b) shows EL spectrum of InGaN/AlN nanodisk at various injection current levels and compared it with intensity of InGaN/GaN LED. Intensity of InGaN/GaN LED was 6 times larger than nanodisk LED. The spectrum from nanodisk has a broad linewidth of 100 nm as compared to InGaN/GaN LED. Broad wavelength in the nanodisk LED was due to indium composition fluctuation at the centre and edges of nanodisk. Edges of nanodisks had more indium composition due to relaxation while centre of nanodisk had less indium composition in InGaN. The possible reason for large EL blue shift from 605 nm to 586 nm with increase in the injection current is due to weakening of QCSE due to high injection current [13].

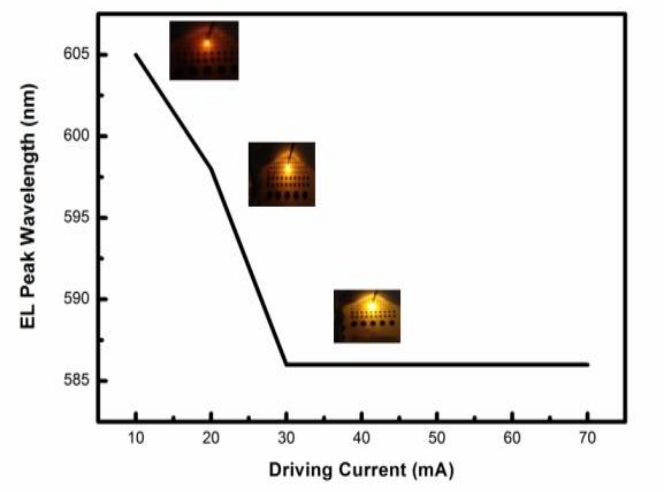

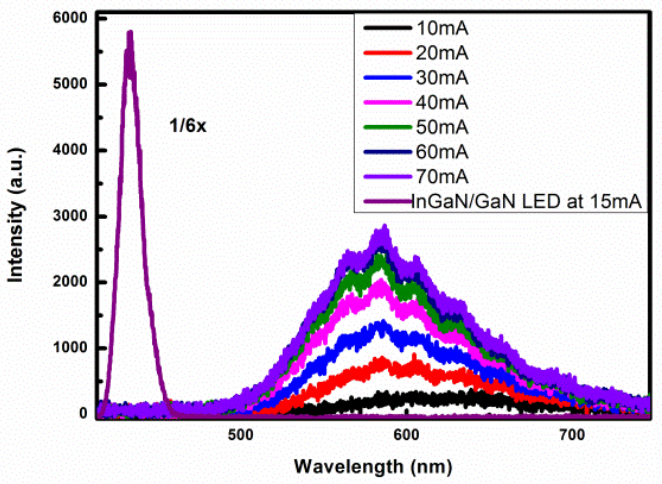

Figure 4. 9 (a) Variation of EL peak wavelength as a function of driving current. Inset shows the pictures of orange, orange-yellow and yellow LED lit at 10, 20 and 30 mA current respectively. (b) EL spectrum of InGaN/AlN nanodisk at various injection current levels and compared it with intensity of InGaN/GaN LED.

We have successfully grown self assembled InGaN/AlN nanodisks on sapphire substrate and fabricated LEDs having a variable wavelength from 605 nm to 586 nm. The large blue shift in our InGaN/AlN nanodisk was due to weakening of the QCSE due to high injection current. High indium composition in InGaN is achieved by strain relaxation of InGaN on AlN in a nanodisk.

4.3 Growth and fabrication of nanodisks LEDs with strain neutral layer

To further improve the quality of nanodisk we introduced a thin GaN strain neutral layer at the interface of AlN and GaN. Nanodisks with strain neutral layers were grown on single side polished c-plane (0001) sapphire substrate. After annealing the substrate, a 30 nm low temperature GaN nucleation layer was deposited at 550°C, then the temperature was ramped up to 1130°C to grow a 4-µm-thick Si doped GaN cladding layer. A thin AlN barrier layer was deposited on n-GaN template at 780°C, 100 mbar. Nitrogen was used as a carrier gas for trimethylaluminium (TMA) and triethylgallium (TEGa) precursors for Al and Ga in the active region. High temperature is essential for good crystalline quality of AlN. Since the initial AlN layer in nanodisk was grown at the same temperature as that of GaN barrier in our standard blue LED, it resulted in the formation of three dimensional (3D) nanoislands rather than two dimensional (2D) structure. This initial AlN nanoislnds forms the base for the nanodisks. Surface morphology of the samples was examined using atomic force microscopy atomic force microscope (AFM). Figure 4.10 (a). depicts the cross-

sectional schematic image and 1 μm x 1 μm AFM image of AlN grown on GaN template. Nanoislands are clearly visible in the AFM image. A 4-nm thick layer of InGaN was grown over the initial AlN nanoislands this resulted in the growth of InGaN in the vertical direction. InGaN growth conditions for this nanodisk with strain neutral layer was same as that of our standard MQW blue LED but the growth time for InGaN in nanodisk was increased by 3 min. Increasing the growth time of InGaN lead to more compressive strain on underlying tensile AlN layer which in turn resulted into high indium composition. A monolayer of GaN was deposited between the AlN and InGaN interface to improve the quality of the crystal. GaN having a lattice constant between InGaN and AlN acts a strain neutral layer thus helping in improving the quality of the nanodisks. Figure 4.10 (b) shows the cross-sectional schematic image and corresponding AFM of InGaN over AlN nanodisk. The succeeding InGaN/AlN layers introduce the branching of nanodisks from the initial cracks of AlN layer. Further growth of InGaN and AlN increases the size of the disk in the vertical direction and also narrowing of nanodisk takes place at top. Five layers of InGaN/AlN layers with a monolayer of GaN at their interface were formed on the initial cracked AlN layer for sample B. The cross-sectional schematic and AFM image of five layers of InGaN/AlN nanodisk capped with AlN is shown in figure 4.10 (c). As we can see from the AFM image that the size of the nanodisk becomes large with the stacking of AlN and InGaN layers. Finally, the nanodisks were capped with a 120-nm- thick Mg doped GaN layer grown at 1020°C and 200 mbar. Capping of nanodisks by p-GaN reduces the surface roughness to .44 nm and it also flattens the top surface of the disk. Figure 4.10 (d) shows the cross sectional schematic and AFM image of the final nanodisk LED structure. No cracks were observed on the surface of the 2 inch wafer with nanodisk LED structure. The indium composition for this nanodisk LED with strain neutral layer was found to be 26% by energy dispersive X-ray (EDX). A cross-sectional high angle annular dark-field scanning transmission electron microscopy (HAADF-STEM) result confirms the formation of InGaN/AlN nanodisks as show in Figure 4.11 Brighter region represents InGaN, while the dark grey region represents AlN. There was no contrast in the InGaN region indicating uniform indium composition inside the nanodisks. As discussed in chapter 3 it is difficult to obtain nanoscale fluctuation in InGaN from TEM. There can be possibility of indium fluctuation in InGaN. The image also indicates that no threading dislocations were generated due to the formation of nanodisks. The initial AlN layer in nanodisk was 5 nm thick while the remaining AlN barrier layers were 3 nm thick while the thickness InGaN was 4 nm. The total threading

dislocation density in nanodisk was found to be 1.6 x 10^{8} cm^{-2} using STEM. The diameter of nanodisks varied from 10 nm to 30 nm.

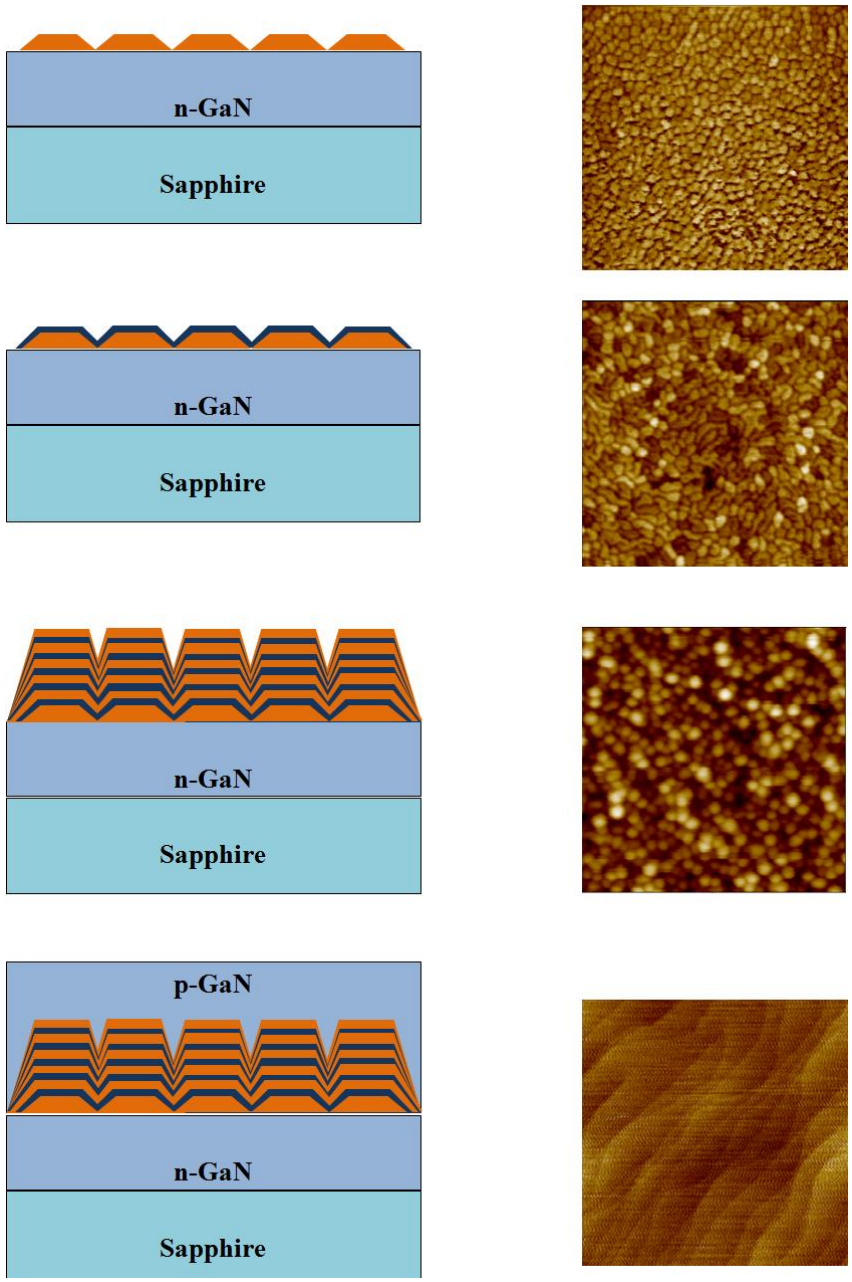

Figure 4. 10 (a) the cross-sectional schematic image and 1 μm x 1 μm AFM image of AlN grown on GaN template. (b) cross-sectional schematic image and corresponding AFM of InGaN over AlN nanodisk. (c) cross-sectional schematic and AFM image of five layers of InGaN/AlN nanodisk capped with AlN (d) cross sectional schematic and AFM image of the final nanodisk LED structure.

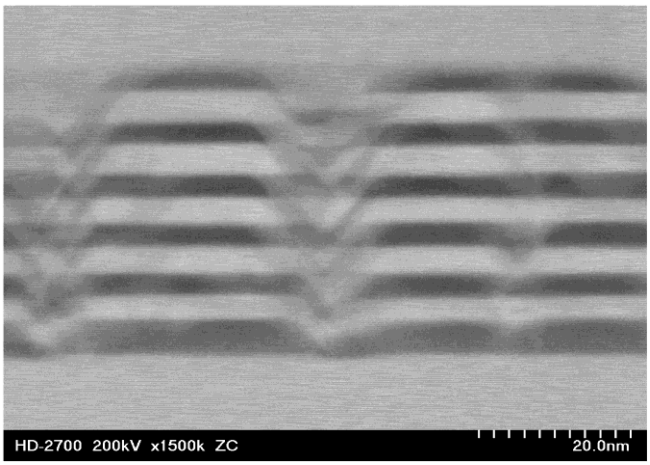

Figure 4.11 cross-sectional high angle annular dark-field scanning transmission electron microscopy (HAADF-STEM) image of nanodisks.

The emission properties nanodiks were investigated by temperature dependent photoluminescence (PL) measurements. The sample was optically excited by a He-Cd laser at a wavelength of 325 nm. The excitation power for both the samples were 1.4 mW. Figure 4.12 shows the temperature- dependent PL spectra for nanodisk LED recorded from 10 to 300K. At room temperature (300K), the emission was mainly dominated by yellow luminescence having a peak wavelength of 551 nm with no luminescence in the blue region. On reducing the temperature to 10 K the wavelength blue-shifted to 547nm. This small blue shift of 4 nm at low temperature might be coming from trapped states at the InGaN/AlN interface. Figure 4.13. shows Arrhenius plot of the integrated PL intensities for nanodisk LEDs with strain neutral layer and standard blue LED. The IQE is assumed to be close to unity at 10 K as non-radiative recombination is mostly suppressed at low temperature. The integrated PL intensities are constant at low temperatures and then gradually decreases with increase in temperature. The carrier dynamics are well stabilized at lower temperature while increasing temperature leads to nonradiative recombination centers. The PL intensity for MQW LEDs reduced to 1.2 % at room temperature while for nanodisk LED the intensity reduced to 46%. The IQE of nanodisk LED was 38 times higher as compared to QWs LED. If we compare the IQE of nanodisk LED with strain neutral layer and without a strain neutral layer we can see 1.6 times improvement in IQE with introduction of strain neutral layer.

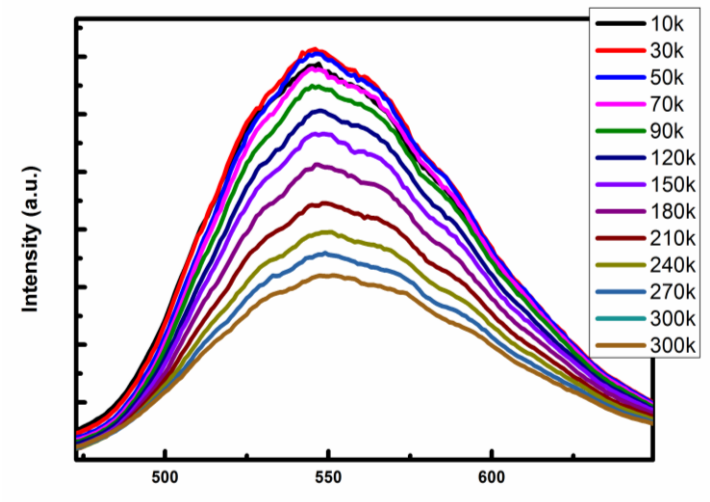

Figure 4.12 Temperature- dependent PL spectra for nanodisk LED

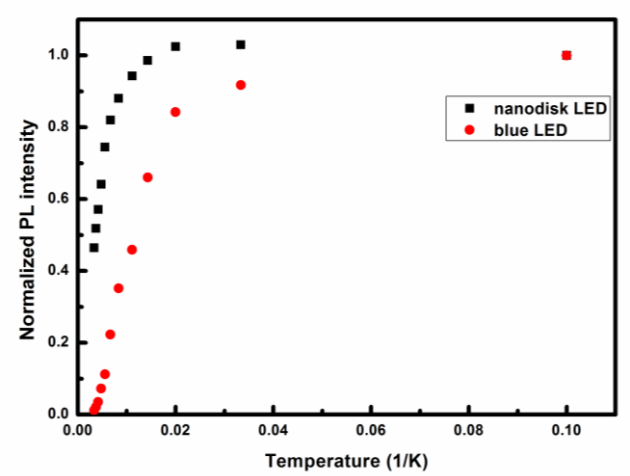

Figure 4.13 Arrhenius plot of the integrated PL intensities for nanodisk

LEDs were fabricated using Ni/Au contact of 20 nm/60 nm for p- GaN and indium contact for n-GaN. Figure 4.14. Shows the current-voltage (I-V) characteristic for both the LEDs. The series resistance of nanodisk LED was higher compared to that of normal QW LEDs due to the presence of AlN. Though AlN exhibits high resistance but the effect of resistance was reduced in nanodisk due to current injection from sides inside the nanodisks rather than vertical injection. The EL spectrum for both the samples was measured at room temperature under dc-biased conditions. Blue LED had a peak wavelength of 407 nm and it remained constant with increasing the injection current. For nanodisk LED at low injection current of 10 mA the LED emitted red light with a peak wavelength of 613 nm, on increasing the current to 20 mA the color changed from red to yellow with the peak

wavelength of 573 nm. At 30 mA current the peak wavelength blue shifted to 556 nm and at 40 mA the emission spectrum had a peak wavelength of 541 nm. Figure 4.15 shows the EL vs driving current for nanodisk LEDs. On further increasing the injection current did not shift the peak wavelength and it remained stable at 541 nm. Figure 4.16 shows the EL spectrum comparison for both the samples. EL was measured under the same conditions. The full width at half maximum (FWHM) was 18 nm for blue LED at 10mA and 63 nm for nanodisk at 60 mA. The blue shift in the nanodisk LEDs was due to the band-filling effect of localized energy states.

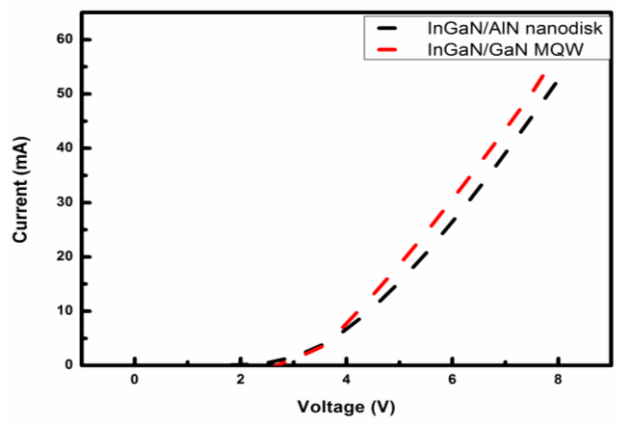

Figure 4.14 current-voltage (I-V) characteristic comparison for blue and nanodisk LEDs .

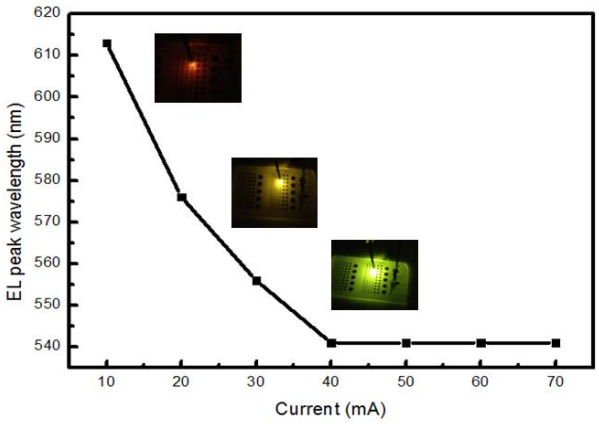

Fig 4.15 Variation of EL peak wavelength as a function of driving current. Inset shows the pictures of orange, yellow and green LED lit at 10, 20 and 40 mA current respectively.

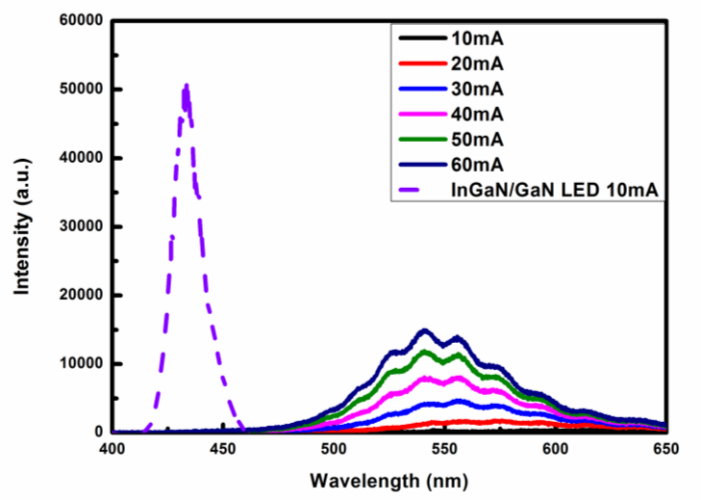

Figure 4.16 EL spectrum of InGaN/AlN nanodisk at various injection current levels and compared it with intensity of InGaN/GaN LED

Self-assembled InGaN/AlN nanodisk green LED structure with GaN strain neutral layer was successfully grown on sapphire substrate. Fabricated LEDs had a higher IQE as compared InGaN/GaN LED grown under the same conditions. The peak wavelength of nanodisk LED was 541 nm while blue emission of 407 nm was observed for the InGaN/GaN MQW LEDs. The tensile strain of AlN enables high indium incorporation in InGaN. Nanodisk LEDS exhibited higher turn on voltage due to the presence of AlN layer. The emission wavelength of nanodisk LEDs are dependent on injection current. The large blue shift in wavelength with increase in injection current is due to band filling effect of localized energy of state.

4.4 Mechanism in nanodisk

In section 4.2 and 4.3 we have looked into the growth and fabrication of InGaN/AlN nanodisk. The following four properties were observed in nanodisks LEDs.

1. High indium composition.
2. Low turn on voltage.
3. Broad band spectrum.
4. Blue shift in wavelength

First we look into the mechanism of getting high indium composition in InGaN. Lobanova et al. studied the critical thickness vs InN molar fraction in InGaN and found that as the indium mole fraction increases to 30 percent the critical thickness reduces to less than a nanometer for an InGaN grown on GaN [15]. On replacing the GaN with AlN the tensile

behavior of AlN helps in getting more indium composition in InGaN due to compressive nature of InGaN. More the compressive stress then more is the indium in InGaN on tensile AlN. The combination of both tensile and compressive stress helps in achieving more indium in InGaN. Usually InGaN layers are capped by GaN layer in MQWs for standard blue LEDs. There is always a diffusion of InN into GaN during the growth of LED structure resulting in composition fluctuation and less indium in standard blue LEDs. In section 4.1 we discussed about the bond energy of Al-N is much higher than Ga-N and In-N bond. Hence capping the InGaN with AlN prevents the diffusion of indium into barriers. Secondly the upper AlN cap is tensile in nature hence it will also attract the indium atom towards itself [14]. Therefore InGaN layer sandwiched between AlN have more indium composition due to strain mechanism and anti-diffusion phenomenon. Figure 4.17 depicts the schematic of strain in nanodisks.

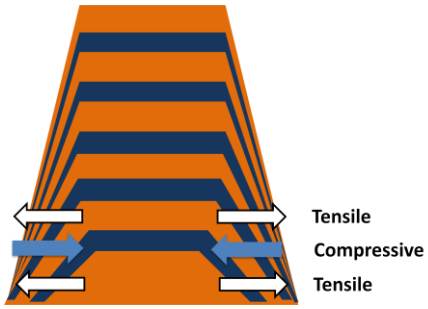

Figure 4.17 Schematic of strain in nanodisks.

AlN has a band gap of 6.28 eV, so it should have a high resistance but on comparing the I-V characteristics for both the nanodisks with the standard InGaN/GaN blue LED it was found that the resistance of nanodisk LEDs was little higher than standard LEDs. The hypothesis for low turn on voltage and low device resistance in LED in spite of having AlN is due to the current injection mechanism in nanodisks. The current injections in nanodisks were from sides rather from top in the disks. Figure 4.18 shows the current injection mechanism in nanodisk LEDs. The emission in these LEDs was not due the leakage current because in that condition there should no increase in intensity with increase in injection current. The V shape structure in nanodisk is helpful in injecting carrier inside the nanodisks. Since the mobility of holes in GaN is 60 times less than that of electron so the migration of holes from top to bottom of quantum well is very difficult in standard blue LEDs but due to the V shape of these nanodisks the hole can penetrate deep into the bottom of nanodisks from the sides.

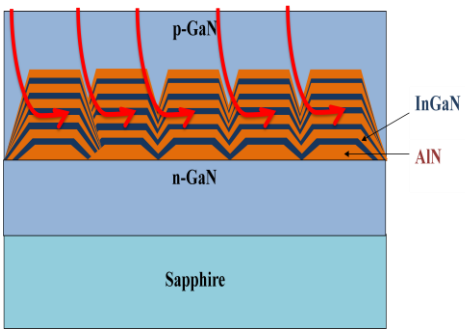

Figure 4.18 Current injection mechanism in nanodisk LEDs.

Both the nanodisk LED exhibited a broad band emission. As discussed earlier in nanodisk LEDs InGaN is sandwiched between two tensile strained AlN. The hypothesis of getting a broad band emission may be due to two reasons. First the tensile strain of AlN from both the direction on InGaN will cause indium fluctuation at the interface of AlN and InGaN. Secondly AlN has 3 dimensional structures and InGaN on AlN is strain released there can be indium rich portions at the corner of the nanodisks. Figure 4.19 shows indium rich portions in nanodisks.

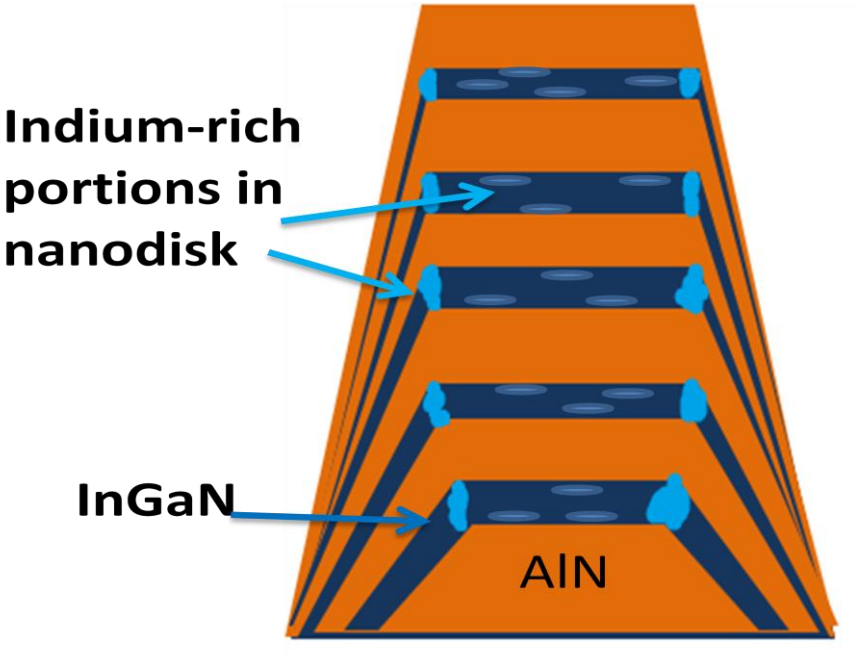

Figure 4.19 Indium rich portions in nanodisks.

Lastly a large blue shift in wavelength was observed on increasing the driving current in nanodisks LEDs. This was due to quantum confined stark effect (QCSE). The internal electric field shifts the electron and holes in opposite sides of the nanodisks. This reduced overlap decreases the radiative recombination efficiencies and shift emission wavelength to longer wavelengths [16-18]. At low injection current, the carriers within the nanodisk provide relatively small coulomb potential to counterbalance the polarization induced electrical field, leading to stronger band bending. When the current injection in nanodisk is increased the large number of carriers are excited in nanodisk, the large coulomb potential can produce a stronger repulsive field to cancel the polarization induced field in the nanodisks. Then the band in naodisks becomes less tilted and thus blue shift in wavelength. Figure 4.20 illustrates the schematic band structure of nanodisk.

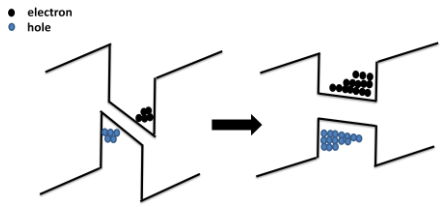

Figure 4.20 Schematic band structure of nanodisk.

4.5 Comparison of nanodisk LEDs with other broadband emission LEDs

There are mainly two methods for getting broad band emission in the green gap region. The first method is to grow InGaN at low temperature resulting in dot like structure while the second method is to use selective area growth (SAG) [5,12,19]. Here we will compare our nanodisk structure with the quantum dot structure by Soh *et al* and SAG nanopyramid structure from Chang *et al* [5, 12]. Table 4.1 shows the comparison of self assembled nanodisk with quantum dot and SAG nanopyramid structure.

Table 4.1 Comparison of self assembled nanodisk with quantum dot and SAG nanopyramid structure

	Nanodisk	**Quanum dot [5]**	**SAG nanopyramid [12]**
Equipment	MOVPE	MOVPE	MOVPE
Technique	Self assemble	Self assemble	Selective area growth
Material	InGaN/AlN	InGaN/GaN capped with thin AlN	InGaN/GaN
Growth temperature	780°C	725°C	GaN-800°C, InGaN-710°C
Peak wavelength (EL)	586 nm	562 nm	495 nm
Regrowth	No	No	Yes
FWHM	100 nm	~80 nm	57 nm

From the table we observe that all the structures were grown by MOVPE. Our nanodisk structure and quantum dot structure use self assembly technique while nanopyramid structure uses SAG which requires regrowth. Regrowth makes the process expensive and complicated. Nanodisk structure was grown at the same temperature as that of blue LEDs, which is higher compared to other two methods. Low temperature InGaN growth often results in degradation of crystal structure. Comparing the peak wavelength our nanodisk LED had a longer wavelength of 586 nm even though we grew the samples at relatively higher temperatures than the other two methods. We also had a broader FWHM compared to other two techniques. FWHM of quantum dot structure was not mentioned so we approximated it from the EL spectrum.

4.6 Conclusions

On comparing the results of nanodisk with and without strain neutral layer we can see that the insertion of strain neutral layer has improved the IQE. Insertion of strain neutral layer also resulted in blue shift of wavelength it may be due to different partial pressure for InGaN growth conditions. On comparing the IQE of nanodisk LEDs with standard blue LEDs it was found that IQE of nanodisk LEDs were 23 times higher. AlN helped in accommodating more indium in InGaN by its tensile strain and stopping diffusion to overlying layers. Our nanodisk structure emitted broad and longer wavelength compared to other broad emitting sources.

4.7 References

[1] D. Zubia and S. D. Hersee, J. Appl. Phys. 85, 6492 (1999).

[2] S. Li and A.Waag, J. Appl. Phys. 111, 071101 (2012).

[3] C. Adelmann, J. Simon, G. Feuillet, N. T. Pelekanos, B. Daudin, and G. Fishman, Appl. Phys. Lett. 76, 1570 (2000).

[4] P. Chen, A. Chen, S. J. Chua, and J. N. Tan, Adv. Mater. 19, 1707 (2007).

[5] C. B. Soh, W. Liu, S. J. Chua, S. S. Ang, R. J. N. Tan, and S. Y. Chow, J. Appl. Phys. 108, 093501 (2010).

[6] Q. Wang, T. Wang, J. Bai, A. G. Cullis, P. J. Parbrook, and F. Ranali, Appl. Phys. Lett. 93, 081915 (2008).

[7] Pearton S J and Shul R J 1998 Gallium Nitride (GaN) I vol 50 (London: Academic).

[8] Queren D, Schillgalies M, Avramescu A, Brüderl G, Laubsch A, Lutgen S and Strauß U J. Cryst. Growth 311, 2933(2009).

[9] Shioda T, Yoshida H, Tachibana K, Sugiyama N and Nunoue S , Phys. Status Solidi a 209, 473(2012).

[10] F. Scholz, Semiconductor Science and Technology, 27, 024002 (2012).

[11] H. Chen, C. Lu, D. Yeh, C. Huang, J. Huang and C Yang, IEEE Photonics Technology Letters, 18,2269 (2006).

[12] S. P. Chang, Y. C. Chen, J. K. Huang, Y. J. Cheng, J. R.Chang, K. P. Sou, Y. T. Kang, H. C. Yang, T. C. Hsu, H. C. Kuo, and C. Y. Chang, Appl. Phys. Lett. 100 , 061106 (2012).

[13] C. H. Chen, S. J. Chang, Y. K. Su, G. C. Chi, J. K. Sheu, and J. F. Chen, IEEE J. Sel. Top. Quantum Electron. 8, 284 (2002)

[14] R. A. Talalaev, S. Yu. Karpov, I. Yu. Evstratov, and Yu. N. Makarov,phys. stat. sol. (c) 0, No. 1 (2002).

[15] A. V. Lobanova,A. L. Kolesnikova,A. E. Romanov,S. Yu. Karpov, M. E. Rudinsky,and E. V. Yakovlev ,Appl. Phys. Lett. 103, 152106 (2013)

[16] T. Takeuchi, H. Amano, and I. Akasaki, Jpn. J. Appl. Phys., Part 1 39, 413 (2000).

[17] T. Takeuchi, S. Sota, M. Katsuragawa, M. Komori, H. Takeuchi, H. Amano, and I. Akasaki, Jpn. J. Appl. Phys., Part 2 36, L382 (1997).

[18] D. A. B. Miller, D. S. Chemla, T. C. Damen, A. C. Gossard, W. Wiegmann, T. H. Wood, and C. A. Burrus, Phys. Rev. Lett. 53, 2173 (1984).

[17] S. Albert, A. Bengoechea-Encabo, P. Lefebvre, F. Barbagini, M. A. Sanchez-Garcia, E. Calleja, U. Jahn and A. Trampert, Appl. Phys. Lett. 100 , 231906 (2012)

5 Impact of AlN and InGaN growth conditions on nanodisks

In the previous section we have seen the growth and fabrication of nanodisk LEDs. The entire nanodisk LEDs grown in the last section we had only changed the In partial pressure while all other parameters were kept constant. In this section we would look into the impact of change in different parameters like partial pressure, temperature etc on the nanodisk. In order to do this study we made single stack of nanodisk rather than 5 stacks. Impact of parameters like InGaN partial pressure and growth time, AlN growth temperature, AlN cap temperature, AlN doping on nanodisk will be discussed in detail.

5.1 Introduction

All the single nanodisk structure used in this study was grown on (0001) c-plane sapphire substrate. A thick n-GaN template was grown on the sapphire substrate, followed by nanodisk. All the naodisks were capped by p-AlGaN EBL and p-GaN. Figure 5.1 shows the schematic image of single nanodisk structure.

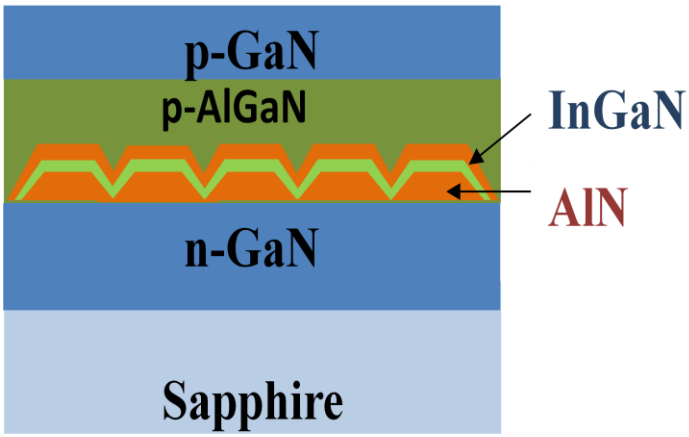

Figure 5.1 Schematic image of single InGaN/AlN nanodisk.

5.2 Effect of InGaN growth time on single nanodisk

In order to study the effect of InGaN growth time on nanodisk LEDs we changed the InGaN growth time from 1 min to 5 min while keeping the TMA, TMI partial pressure constant. InGaN and AlN were grown at the same temperature of 780 °C, 200 mbar. Four samples with InGaN growth time of 1, 2, 3 and 5 min were grown while keeping the AlN

growth time fixed for 2 min. The structural analysis of the sample was done with the help of PL with 325 nm He-Cd laser. Figure 5.2 shows room temperature PL of single InGaN/AlN nanodisk. From the figure we can see that there is not much change in the peak position in PL intensity at 550 nm but we can see emergence of peak at around 450 nm when the InGaN growth time from 1 min to 5 min. The peak for the 5 min InGaN is much broader compared to all other peaks. The GaN peak intensity increases with increase in InGaN thickness referring to good crystal quality.

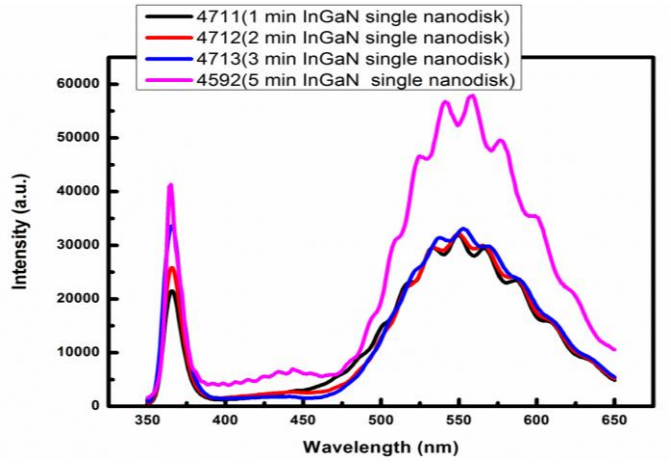

Figure 5.2 Room temperature PL of single InGaN/AlN nanodisk with different InGaN growth time.

LEDs were fabricated for all the four samples with Ni/Au contact for p-GaN and indium contact for n-GaN. Figure 5.3 shows room temperature EL characteristics for all the four LEDs. EL was measured at 20 mA for all the LEDs at almost the same measurement conditions. From the graph we can see that for 1 min InGaN the EL had a broad emission with a peak wavelength of 464 nm. On increasing the InGaN growth time to 2 min the wavelength got red shifted to 495 nm. Similarly for 3 min and 5 min InGaN growth period the peak emission intensity was at 515 and 540 nm respectively. Thus from the EL graph we can see that on increasing the InGaN thickness results in red shift in wavelength. The more compressive strain of InGaN on tensile AlN had resulted in high indium incorporation in InGaN. Secondly it can also be seen that the intensity of the wavelength also increases with increase in InGaN thickness which can be referred to as good crystal quality. Usually increasing the InGaN thickness always results in degraded crystal quality due to indium segregation in InGaN. The low intensity for 1 min InGaN may be due to thin InGaN compared to AlN which may result in large series resistance.

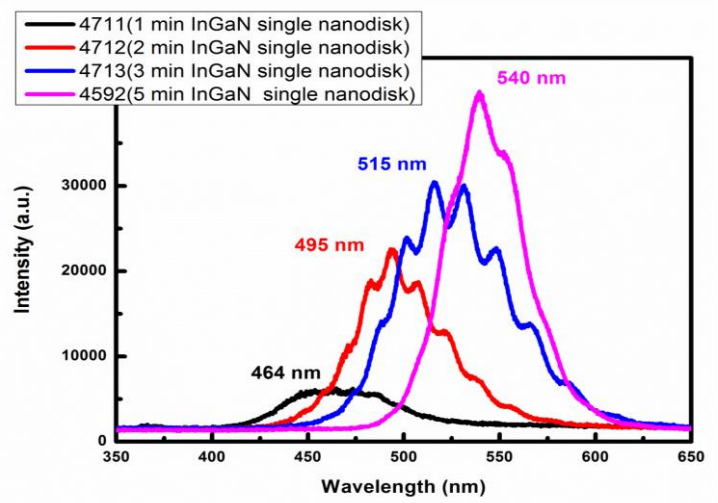

Figure 5.3 Room temperature EL of single InGaN/AlN nanodisk with different InGaN growth time measured at 20 mA.

5.2.1 Discussion

As discussed in the previous chapter AlN has a crucial role in accommodating more indium in InGaN alloy. As the InGaN growth time is increased, it results in more compressive stress. When the high compressive stress material is placed on the 3 D tensile material like AlN then InGaN tries to release strain by accommodating more indium in it. This phenomenon was earlier observed by C. Kisielowski *et al* and later on theoretically confirmed by R. A. Talalaev *et al* [1-2].The three dimensional structure of nanodisk structure is also helpful in release of strain in LEDs.

5.3 Effect of indium partial pressure on single nanodisk

After looking into the impact of InGaN thickness on nanodisk we then changed the indium partial pressure to see its effect on nanodisk. In our all the previous growth we were growing InGaN with the partial pressure of 30 $x10^{-3}$ mbar. So in this experiment we changed the indium partial pressure from 10 $x10^{-3}$ mbar to 30 $x10^{-3}$ mbar and tried to see the effect on the luminescence. Figure 5.4 shows the room temperature PL for single nanodisk with In partial pressure of 10, 20 and 30 $x10^{-3}$ mbar. The PL intensity was higher for 10 x 10^{-3} mbar and it was minimum for 20 $x10^{-3}$ mbar at 550 nm wavelength. No shift in wavelength was observed in PL with the change in indium partial pressure.

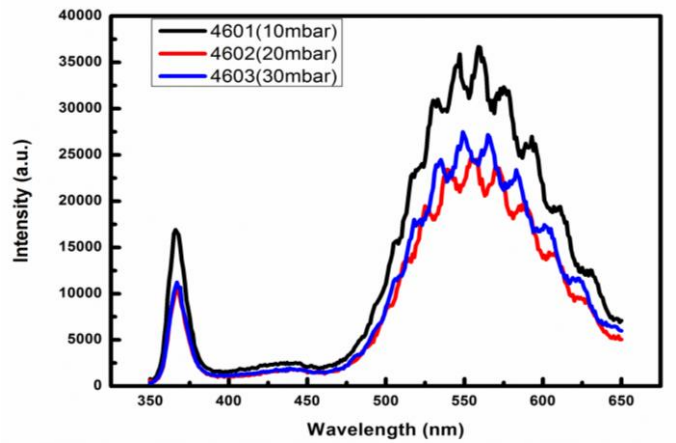

Figure 5.4 Room temperature PL of single InGaN/AlN nanodisk with different In partial pressure.

LEDs were fabricated from all the three samples and EL measurement was done at room temperature under the same setup. Figure 5.5 shows the EL spectrum of LED at different In partial pressure conditions. At a low In partial pressure of 10 x 10^{-3} mbar the peak wavelength was 497 nm and on increasing the partial pressure to 20 x 10^{-3} mbar the wavelength got red shifted to 519 nm and on further increasing the partial pressure the wavelength again red shifted to 523 nm. There red-shift in the latter case was only 4 nm as compared to 22 nm between chance in partial pressure from 10 x 10^{-3} mbar to 20 x 10^{-3}. From this result we can deduce that on increasing the In partial pressure results in red-shift in wavelength which in turn help in higher indium incorporation in InGaN.

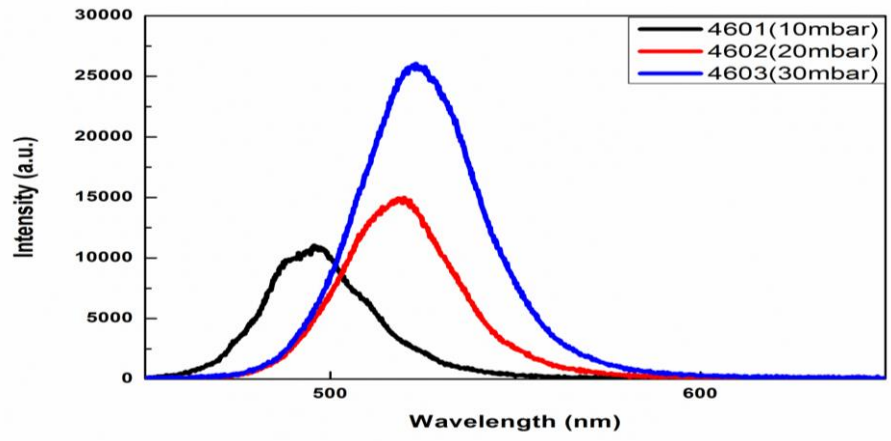

Figure 5.5 Room temperature EL of single InGaN/AlN nanodisk with different In partial pressure measured at 20 mA.

5.3.1 Discussion

Lee *et al* had earlier demonstrated that on increasing the TMIn flow rate and keeping TMGa flow to a fixed value results in saturation of In mole fraction in InGaN [3]. The same phenomenon was observed for the nanodisk LEDs except nanodisk had more indium composition. For the low TMIn flow we observed low indium fraction in InGaN and on increasing the TMIn flow rate further the indium fraction in InGaN got saturated. On comparing the results of MQW blue LEDs and nanodisk LED it can be observed that more indium fraction is obtained in InGaN nanodisk due to AlN tensile strain.

5.4 Effect of AlN cap growth temperature on single nanodisk

For all the nanodisks grown so far had an AlN growth temperature of 780 °C which was same as that of InGaN. In this section we studied the effect of AlN cap (AlN layer over InGaN) temperature on nanodisks. The device structure was similar to that of the single nanodisk shown in Fig.5.1. The initial AlN and InGaN layers were grown at 780 °C and we varied the top AlN cap growth temperature from 700 °C to 800 °C with interval of 50 °C. EL was measured for all the three samples at room temperature under the same measurement conditions. Figure 5.6 shows the EL spectrum for all the three samples with different AlN growth temperature measured at 20 mA current. The peak emission wavelength for AlN cap growth temperature of 700,750 and 800 °C were 558,540 and 532 respectively. This indicates that on increasing the AlN cap growth temperature there is a blue-shift in wavelength.

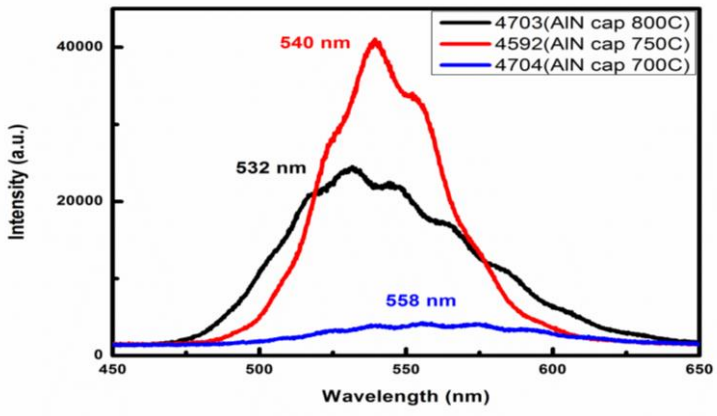

Figure 5.6 Room temperature EL of single InGaN/AlN nanodisk with different AlN cap temperature measured at 20 mA.

5.4.1 Discussion

Higher AlN cap temperature results in desorption of In from InGaN during the temperature ramping up process from InGaN to AlN, thus leading to blue shift in emission wavelength. Intensity of AlN cap grown at 750 °C was higher compared to other samples because there was no swing in temperature between InGaN and AlN thus having better 3D surface. AlN grown at 700 °C are much rougher in comparison to that grown at 750 °C, this might have resulted in increase in resistance. On the other hand for 800 °C AlN cap, the resistance might be higher due to flatter or 2D AlN which could have increased the device resistance and thus reducing the intensity.

5.5 Effect of AlN cap thickness on single nanodisk

In this section we analyzed the AlN cap thickness on the nanodisk. The structure was similar to that mentioned in section 5.4 with the bottom AlN and InGaN grown at 750 °C. The AlN cap thickness was varied by changing the growth time of AlN. AlN cap growth time was varied from 1 min to 3 min with interval of 1 min. LEDs were fabricated for all the three samples and EL was measured under room temperature at 20 mA current under the same setup conditions. For a thin AlN of 1 min the peak emission wavelength was 562 nm and on increasing the AlN cap thickness to 2 and 3 min resulted in change in wavelength to 542 and 566nm respectively. LEDs with 1 and 2 min AlN cap had higher intensities as compared to 3 min AlN. Thicker AlN cap increased the device resistance thus affecting the intensity of LED. Thinner AlN offers lower resistance to the device. Figure 5.7 shows room temperature EL of single InGaN/AlN nanodisk with different AlN cap thickness measured at 20 mA.

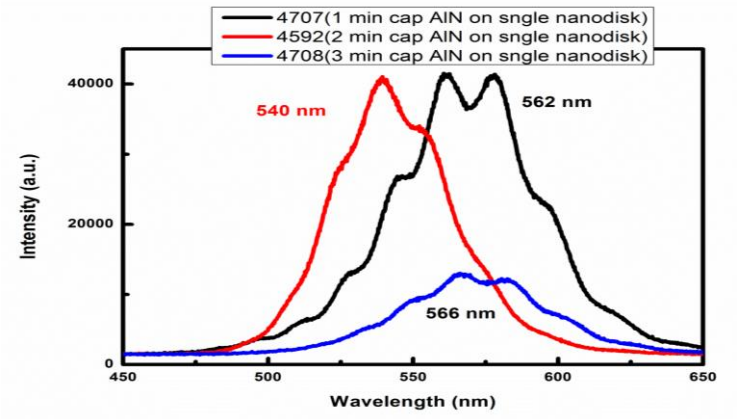

Figure 5.7 Room temperature EL of single InGaN/AlN nanodisk with different AlN cap thickness measured at 20 mA.

5.5.1 Discussion

From the results it can be observed that thicker AlN is helpful in getting more indium composition in InGaN by its tensile nature and preventing the diffusion of InGaN in the barrier [2,4]. However, the thicker AlN also increases the resistance of the device due to their larger bandgap. Thus there is a tradeoff between wavelength and resistance. Since 2 min AlN cap was grown at different time so there was a change in wavelength it is due to the run to run variation in growth inside the reactor.

5.6 Effect of AlN temperature on nanodisks

The growth temperature of AlN plays the crucial role in the formation of nanodisks. Many studies have been done in the past to study the crystal quality of AlN at different temperatures, but for all these studies the carrier source for Al was H_2 [5]. In our study we use N_2 as a carrier for Al, so it was important to study the surface quality of AlN at different temperature with N_2 carrier. In this section we will look into the impact of AlN growth temperature on nanodisk LEDs.

In order to investigate the effect of temperature on AlN surface quality, we grew only the AlN underlayer on a GaN template at different temperatures from 750 °C to 950 °C. The growth time of AlN described in chapter 4 was 2 min, so we grew 2 min AlN on the GaN template. Temperature was varied in the interval of 50 °C. The surfaces of these AlN layers were characterized by atomic force microscope Figure 5.8 shows (1 μm × 1 μm) AFM image of AlN grown from 750 °C to 950 °C. AlN grown at 750 °C had a dot like structure with the root mean square roughness (RMS) of 0.84 nm. When the temperature was increased to 800 °C the RMS roughness reduced to .39 nm but the structure still had dot like structure. Further increasing the AlN growth temperature to 850and 900 °C RMS roughness changed to .38 and .37 nm respectively. AlN grown at 950 °C had comparatively smooth planer surface with RMS roughness of 0.33 nm.

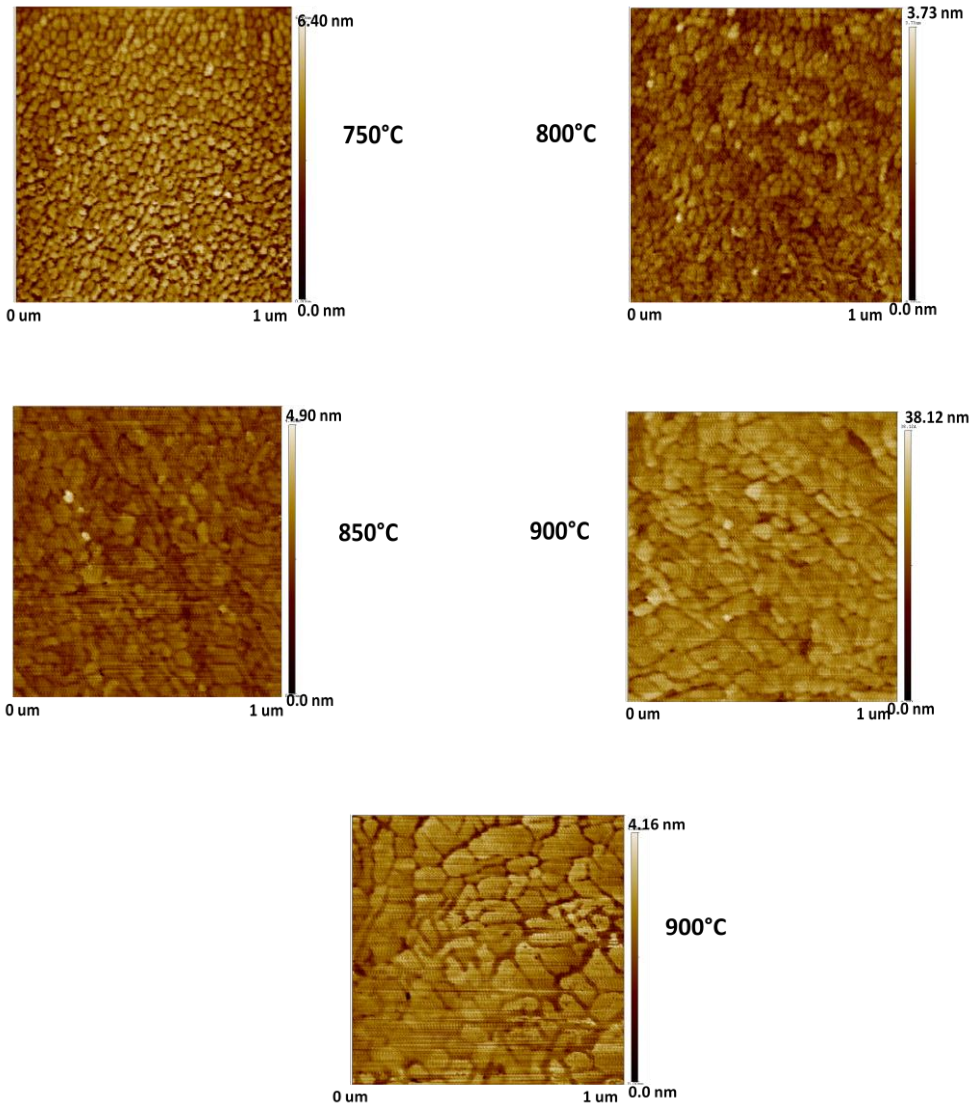

Figure 5.8 (1 μm × 1 μm) AFM image of AlN grown from 750 °C to 950 °C

Self-assembled InGaN/AlN structures were grown on single-sided-polished c-plane (0001) sapphire substrate. A template layer, 4-μm thick Si-doped GaN, was grown on the substrate via a nucleation layer. Five stacks of InGaN/AlN active layers were grown on these GaN templates. Five samples were grown with AlN growth temperature varied from 750 °C to 950 °C with the interval of 50 °C, while the growth temperature of InGaN was kept constant at 750°C. Finally all the structures were capped with 120 nm thick Mg doped GaN layer grown at 1020 °C, 200 mbar. The device structure is shown in Figure 5.9 LEDs were fabricated using Ni/Au and indium contacts for p-GaN and n-GaN respectively.

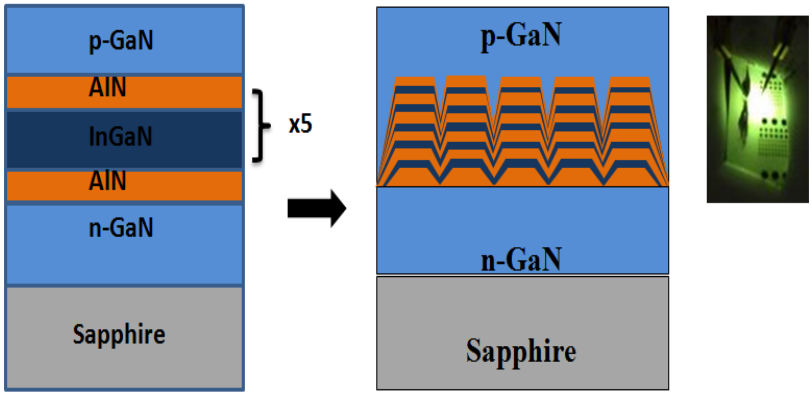

Figure 5. 9 Schematic image of InGaN/AlN LED Structure and the corresponding image of nanodisk structure grown at 750°C. Inset shows the picture of green LED from nanodisk LED

The emission properties of all the LED structures with different AlN growth temperature were investigated using PL measurements. Samples were excited by a 325 nm He-Cd laser with an excitation power of 1.4 mW. Figure 5.10 shows PL spectrum for nanodisk LED grown with different AlN temperature. From the graph it can be observed that at low growth temperature of 750 °C of AlN there was a broad emission in the yellow green region while there was no emission in the shorter wavelength region. As the temperature was increased to 800 °C a shorter wavelength starts to appear along with long wavelength broad band emission. At 850 °C shorter wavelength with peak wavelength at 432 nm was clearly visible along with emission in the yellow region. On further increasing the temperature to 900 and 950 °C the wavelength again blue shifted to 417 and 410 nm.

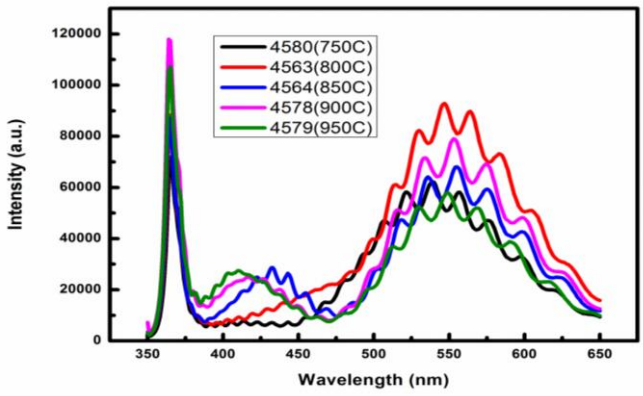

Figure 5. 10 PL spectrum of InGaN/ AlN LED structure at different AlN growth temperature

Electroluminescence was measured for all the five samples at room temperature under dc biased conditions as shown in Figure 5.11. AlN grown at 750°C had a peak wavelength of 569 nm and on increasing the temperature to 800 °C the wavelength blue shifted to 520 nm. The peak wavelength of devices with AlN grown at 850 , 900 and 950°C were 440, 433 and 423 nm respectively. The tendency is consistent with the enhancement of indium incorporation due to AlN surface roughness. There is a little variation between PL and EL peak wavelength due to compositional fluctuation in the wafers.

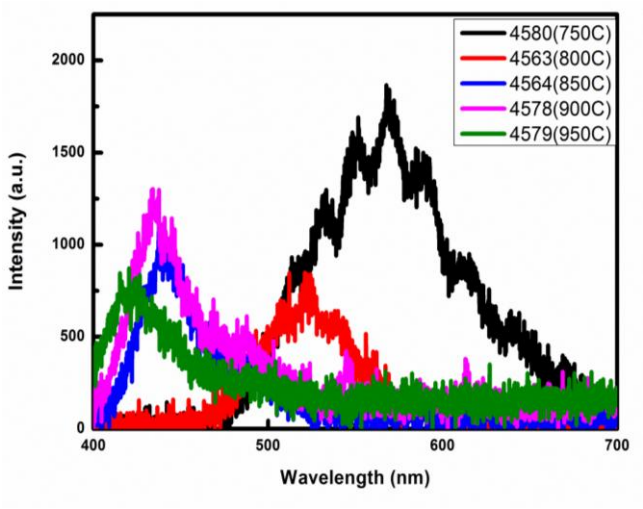

Figure 5. 11 EL spectrum of InGaN/ AlN LED structure at different AlN growth temperature

Figure 5.12 shows the I-V characteristics for all the five LEDs. Resistance for nanodisk LEDs grown at lower temperature had lower resistance compared to that grown at temperature greater than 850°C. Though AlN exhibits high resistance properties, the resistance in the LEDs with low-temperature AlN was less compared to LEDs with high temperature AlN. Low temperature AlN had three dimensional (3D) structures and current can be injected to the nanodisks via the gap among AlN islands, while the samples having high temperature AlN had two dimensional (2D) structures and current injection to the InGaN layer suffers from high resistance due to the AlN barrier.

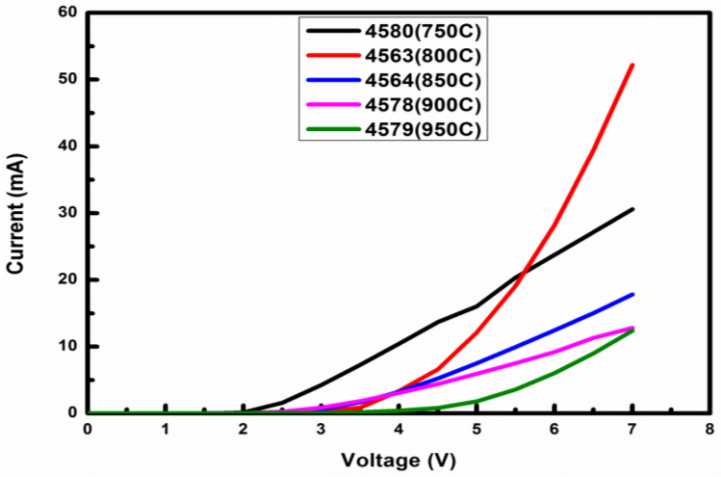

Figure 5. 12 EL spectrum of InGaN/ AlN LED structure at different AlN growth temperature

5.6.1 Discussion

AlN grown at lower temperature of 750 °C exhibited a 3D structure which enabled the formation of InGaN nanodisk with high indium content and the electroluminescence at longer wavelengths. These LEDs with low-temperature AlN had low resistance due to current injection to InGaN nanodisks via the gap in AlN. The capability of nanodisk LEDs for broadband visible electroluminescence clearly depends on the structure of AlN beneath InGaN. High temperature AlN had more flatter surface so it exhibited high resistance due to current injection in these nanodisks were in vertical direction. InGaN was grown at lower temperature of 750°C while the highest temperature AlN was grown at 950°C. There was growth interruption of 2 min between the temperature ramps. NH_3 was continuously flown during the ramping periods. Since indium is highly unstable at higher temperature it results in less indium in InGaN and thus shorter wavelength. In order to prove this mechanism, a single nanodisk structure was grown with bottom AlN grown at 950°C and then InGaN and top AlN cap was grown at 750°C. LED was fabricated for this structure and EL was compared with the single nanodisk structure with both bottom and top AlN temperature of 950°C. On capping the InGaN with AlN at same temperature resulted in longer wavelength which prevented the evaporation of indium during ramping of temperature. Figure 5.13 shows the EL spectrum of single nanodisk with bottom AlN at 950°C and top AlN cap at 750°C and 950°C.

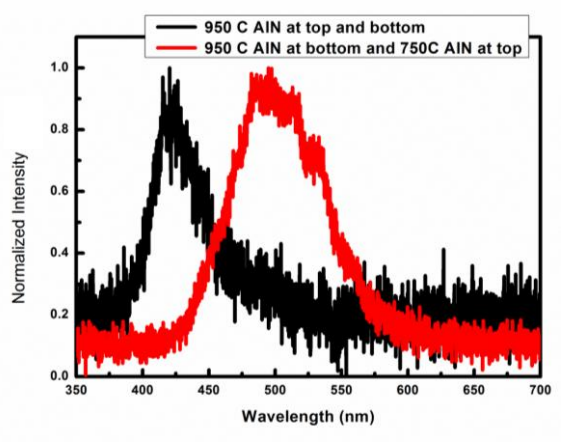

Figure 5. 13 EL spectrum of single nanodisk with bottom AlN at 950°C and top AlN cap at 750°C and 950°C.

5.7 Effect of AlN doping in nanodisk

In this section we analyzed the effect of doping in AlN for nanodisk LEDs. The LED structure is the same as discussed in section 5.1. We grew three samples with different doping for AlN. The first sample was a single nanodisk with both AlN barrier undoped. In second sample both the barriers were doped with Mg to obtain p-doping in AlN. Third sample had its upper AlN barrier p-doped while lower barrier was undoped.

PL was performed on the samples with 325 nm He-Cd laser under room temperature. Figure 5.14 shows the PL spectrum for the samples with different AlN doping. The PL intensity of undoped AlN was much higher compared to doped AlN. Insertion of Mg in AlN may produce defects in crystal which may result in reduction in intensity. When both the barriers were p-doped it reduced the PL intensity due to Mg doping.

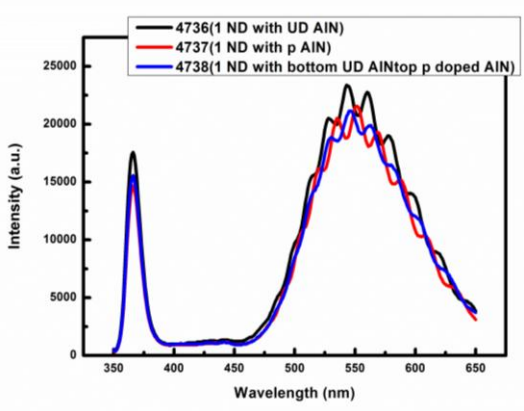

Figure 5. 14 PL spectrum with different AlN doping.

LEDs were fabricated for all the three structures with Ni/Au (20 nm/ 60 nm) for p-contact and indium contact for n-contact. Figure 5.15 shows EL characteristics for these LEDs at room temperature. When the barrier was undoped then it resulted in low intensity in emission while on doping the barrier increased the intensity and also helped in redshift and broadening of wavelength.

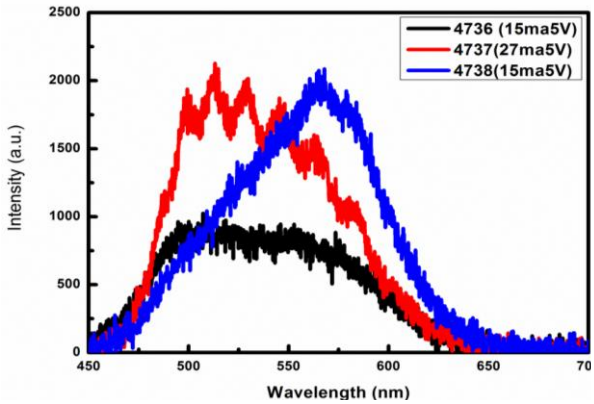

Figure 5. 15 EL spectrum with different AlN doping.

5.7.1 Discussion

For the first case with undoped AlN the intensity was less and resistance was high because the large barrier height prevented the flow of electron and holes inside the nanodisks. When both the barriers were p-doped the upper doped AlN helped in injecting more holes inside the well while the lower barrier helped in preventing carrier overflow (due to high mobility of electron) to some extent by recombination and hence more radiative recombination inside the well. Dual doping also helps in reducing resistance of the device. In third case where the upper barrier was p-doped while the lower was undoped. The electron from the bottom can reach the well faster due their mobility and most of the recombination might be taking place at the top layer of InGaN well. As we have discussed earlier there is more indium composition at the InGaN/AlN interface thus resulting in longer wavelength.

5.8 References

[1] C. Kisielowski, Z. Liliental-Weber, and S . Nakamura , Jpn. J. Appl. Phys. 36, 6932 (1997).

[2] R. A. Talalaev, S. Yu. Karpov, I. Yu. Evstratov, and Yu. N. Makarov,phys. stat. sol. (c) 0, No. 1 (2002).

[3] S. Lee “Luminescence, structure and growth of wide band gap semiconductors”, Sandia National Laboratories.

[4] Q. Wang, T. Wang, J. Bai, A. G. Cullis, P. J. Parbrook, and F. Ranali, Appl. Phys. Lett. 93, 081915 (2008).

[5] J.-S. Yang et al., H. Sodabanlu, M. Sugiyama, Y. Nakano , Y Shimogaki, Journal of Crystal Growth 314, 252–257 (2011).

6 Monolithic white Light Emitting Diodes

This chapter will start with the introduction about monolithic white LEDs in section 6.1 followed by growth and fabrication of monolithic white LEDs using nanoislands in section 6.2. Section 6.3 will show monolithic white LEDs using the combination of blue LEDs and nanodisk. The impact of MQW on nanodisk LEDs will be explained in section 6.4. Section 6.5 will demonstrate white LEDs growth and fabrication using blue MQW, nanodisk and blue SQW. Final section will compare our LED structure with LEDs grown by other research groups.

6.1 Introduction

Most of the commercial white LEDs are made up of blue LED chip coated with yellow phosphor [3-6]. The yellow phosphor absorbs a portion of blue photons and re-emits yellow light. The conversion of these blue photons to the yellow spectral range leads to losses of about 20-30% because of stoke shift which in turn effects the overall luminous efficacy of the white LED [1]. Use of phosphor also adds to the cost for manufacturing LEDs [7].

There are various approaches for the fabrication of monolithic or phosphor less LEDs. The basic approach for fabricating monolithic white LED is to use a dichromatic or trichromatic source which combine two or three quantum wells each emitting blue, green/yellow light [8-17]. The same principal has also been applied in microfacet and nanowires LEDs [18-20]. The efficiency of theses monolithic LEDs is still poor compared to phosphor coated LEDs due to the degraded quality of InGaN in the quantum wells. High indium content in InGaN is required for green/yellow emission which is achieved by growing InGaN at low temperature which increases the chances of indium segregation and misfit dislocation [21]. The other approach of getting a white LED is using InGaN/GaN yellow-green light converter but the efficiency of the device is reduced because of inefficient optical pumping [22]. We have shown earlier that high indium composition in InGaN can be achieved at high temperature by using InGaN/AlN nanodisk structures [23]. The tensile strain of AlN and compressive strain of InGaN leads to higher indium incorporation. We adopted the principles of strain management and enhancement of In incorporation for this work. Therefore, we were able to achieve high indium composition in

InGaN for monolithic white LED structure using AlN nanoislands at a relatively high growth temperature of 780°C which is approximately the same temperature as that of conventional InGaN/GaN blue LEDs.

6.2 Monolithic white LEDs using nanoislands

The LEDs were grown on c-plane sapphire substrates. A 25-nm thick low temperature GaN nucleation layer was grown at 550°C followed by a 3.4-µm-thick Si-doped n-type GaN. This formed a template for two samples. In order to compare the results with blue LEDs we grew two set of samples. Sample A was a reference sample, consisting of five stacks of $In_{.13}Ga_{.87}N$/GaN quantum wells grown on n-GaN template at 780°C. Sample B was a monolithic white LED structure in which AlN layers were deposited on each GaN barriers, prior to the growth of InGaN wells. The growth temperature of AlN was same as that of GaN and InGaN in sample A. Low growth temperature of AlN resulted in the formation of three dimensional (3D) nanoislands rather than two dimensional (2D) layers [23]. InGaN active layers in sample B were grown with the same growth conditions of sample A, except for the growth time of InGaN which was increased by three minutes in sample B. Increasing the growth time of InGaN lead to more compressive strain on tensile AlN layer resulting in high indium composition. Five stacks of InGaN/GaN layers with AlN nanoislands at their interface were grown. Finally 40-nm thick Mg-doped $Al_{0.15}Ga_{0.85}N$ layer followed by 125-nm thick Mg-doped p-GaN were grown on both samples. The schematic cross sectional diagram of sample B is shown in Figure 6.1. Both the LEDs were fabricated using Ni (20 nm)/Au (80 nm) ohmic contacts using thermal evaporation for p-GaN and indium contact for n-GaN. The diameter of Ni/Au contact was 10 µm for both the samples.

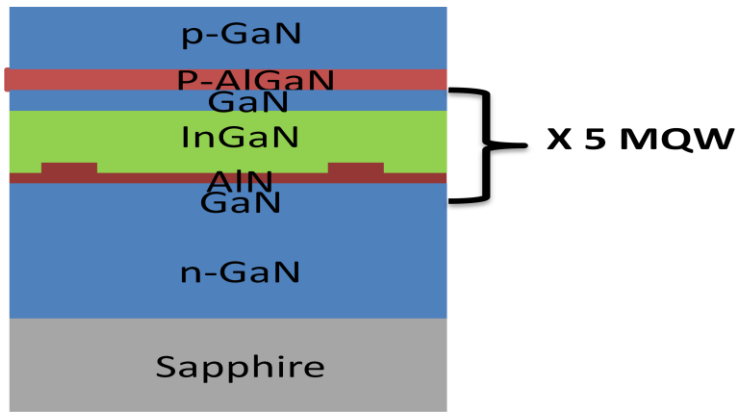

Figure 6. 1. A schematic cross sectional structure of monolithic white LED structures with AlN nanoislands inserted between InGaN and GaN.

In order to characterize the active layer of monolithic white LED, high-angle annular dark-field (HAADF) analysis was employed. Figure 6. 2 shows the cross sectional HAADF image for the active region of sample B. Brighter region represents InGaN, while the dark grey region represents GaN. There was no contrast in the InGaN region indicating that indium composition was uniform. The thickness of InGaN was measured to be 7 nm from the HAADF image. AlN nanoislands are clearly distinguishable (black region) at the InGaN/GaN interfaces in the QWs. The thickness of these nanoislands were approximately 1.8 nm, while the thickness of the GaN barriers was 11 nm. There was no degradation in crystal quality in spite of growing AlN at relatively low temperature.

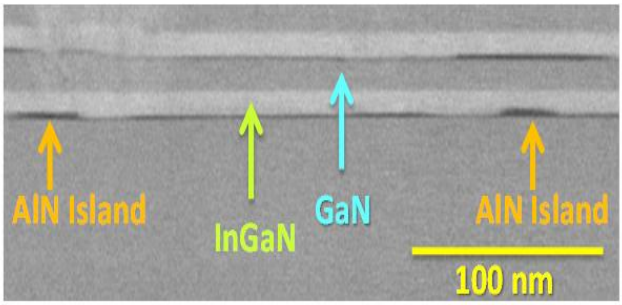

Figure 6. 2 Cross-sectional HAADF image of the active layers of the monolithic white LED. It clearly shows AlN nanoislands in the InGaN well layers.

The emission properties of both the samples were investigated using temperature-dependent photo luminescence (PL) measurements. The samples were optically excited by a 325 nm wavelength He-Cd laser. Fig 6. 3(a). and figure 6. 3(b). shows the temperature-dependent PL spectra for sample A and B respectively as recorded from 10 to 300K. For sample A, single peak luminescence fixed at 426 nm wavelength was observed for all temperatures between 10 K and 300 K. On the other hand, for sample B at room temperature (300K), the emission was mainly dominated by yellow luminescence having a peak wavelength of 555 nm with no luminescence in the blue region. Reducing the temperature to 240 K, the blue luminescence having a peak wavelength of 456 nm emerged along with the broad yellow wavelength. At 10 K two peaks of blue and yellow could be distinctively observed with a peak wavelength of 446 nm and 538 nm respectively. Blue luminescence had a blue-shift of 10 nm in peak wavelength when the temperature was reduced from 300 to 10 K. In case of yellow luminescence the wavelength remained constant at 555 nm with the temperature range from 300 to 120 K, but further reducing the

temperature to 10 K blue shifted the peak wavelength to 538 nm. This large blue shift of 17 nm at low temperature might be coming from trapped states at the InGaN/AlN interface.

The electroluminescence (EL) measurement was carried out for sample B at various injection current levels. Figure 6. 4 shows the EL spectra for sample B at injection current of 10, 30, 50 and 70 mA as compared with sample A at a fixed driving injection current of 15 mA. Regardless of current, there was only single peak emission from sample A stemming from the InGaN/GaN QWs. For sample B at low injection current of 10 mA, both blue (481 nm) and yellow (580 nm) peaks were observed. The intensity of the yellow peak was higher compared to that of blue peak. The hypothesis behind the dual peak emission is that the blue emission is coming from band edge emission in the InGaN/GaN QWs while the yellow emission may be due to the presence of high indium traps in the vicinity of AlN nanoislands. At low injection current most of the recombination is taking place in the traps causing the emission to be dominated by the yellow wavelength peak. Increasing the injection current to 30 mA, the blue and yellow peaks were blue shifted to 479 nm and 576 nm, respectively. The blue shift is owing to the band filling of the localized low-energy state and weakening of the QCSE. As the injection current was increased to 50 mA the intensity of both wavelengths increased while the peak wavelength remained unchanged from the case of 30 mA injection current. At 70 mA the emission was mainly dominated by blue light while the intensity of yellow light decreased and becomes flattened. This behavior is most likely due to filling of trap states. Combination of blue and yellow emission gives white LED. The inset in figure 6. 4 shows the picture of white LED at 70 mA injection current. For sample A, there was only single mode emission at 423 nm.

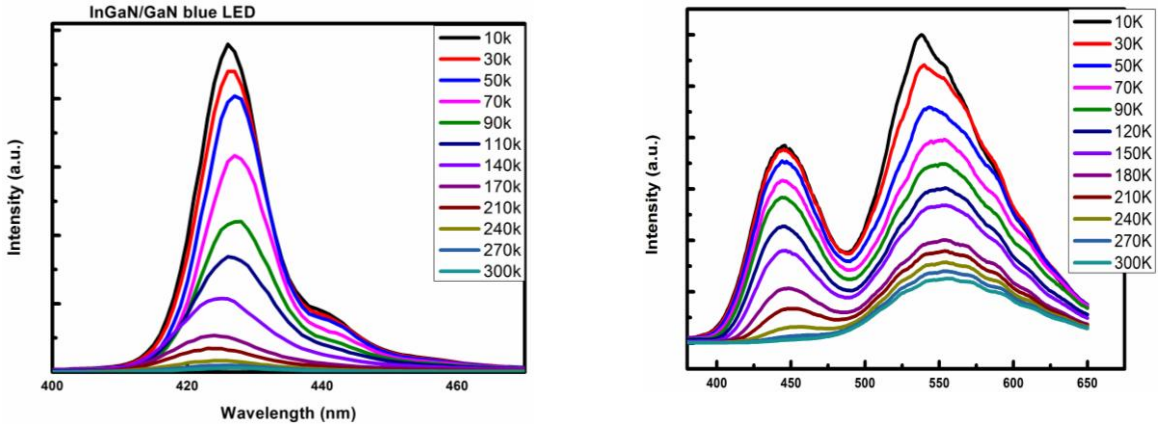

Figure 6. 3 (a) Temperature-dependent PL spectra for InGaN/GaN QWs (b) temperature-dependent PL spectra for monolithic white LEDs with AlN nanoislands.

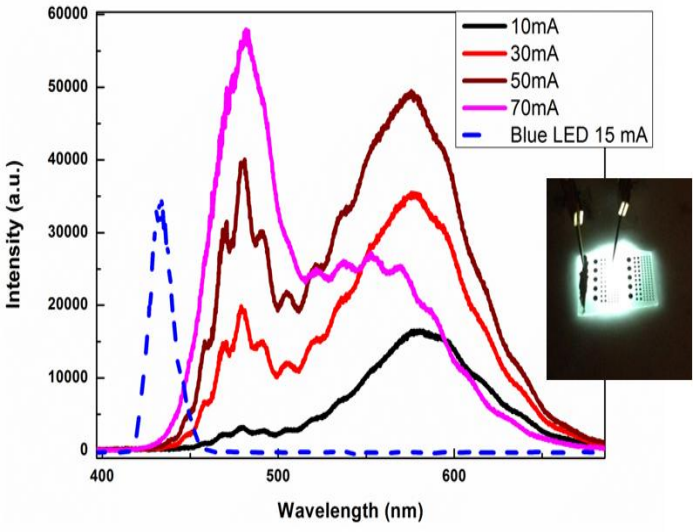

Figure 6. 4. EL spectra comparison for monolithic white LED at injection current of 10, 30, 50 and 70 mA compared with InGaN/GaN QW blue LED having a fixed driving injection current of 15 mA. Inset shows the picture of white LED at 70 mA injection current.

We measured the CIE-1931 chromatic coordinates for monolithic white LED at different injection current, together with those of the black body temperature curve in the chromicity diagram shown in Figure 6. 5. The chromatic coordinates were closed to that of the black body temperature curve. Color temperature changed from 2500 K to 4500 K with the increase in injection current from 10 to 70 mA. The color temperature of 4500 K corresponded to cool white light emission. Figure 6.6 shows the I-V characteristic curve comparison for sample A and B. The turn on voltage of monolithic white LED was approximately 3.9 V which was close to that of the reference blue LED. The device resistance was estimated to be ~70 Ω. Series resistance of white LED was a bit larger as compared to InGaN QW LEDs because of the presence of AlN nano islands.

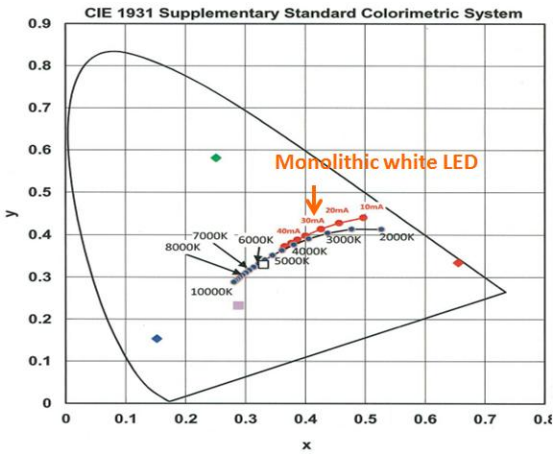

Figure 6. 5 CIE-1931 chromatic coordinates for monolithic white LED at different injection current. (the black line represents the black body emission curve)

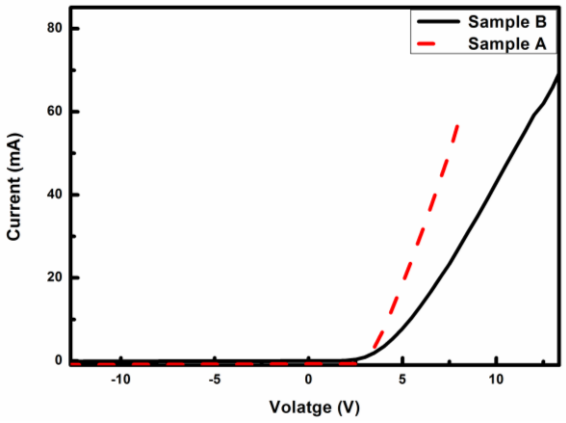

Figure 6. 6 I-V characteristic curve comparison for sample A and B.

In summary, we reported that the fabrication of monolithic white LED could be achieved by introducing AlN nanoislands prior to InGaN wells in each QW. The white light was attributed to a mixture of blue and yellow light as shown in the EL spectra. HAADF images confirmed the presence of nanoislands in the monolithic white LED, while the sample without nanoislands had only single peak emission in the blue region. The broad wavelength emission of the monolithic white LED came from the AlN/InGaN interface where the emission traps present at this interface. The blue emission was from recombination in planer InGaN/GaN QWs. The turn on voltage of the white LED was approximately 3.9 V. The device resistance was a bit higher than that of the blue LED due

to the presence of AlN in the QWs. Since the growth conditions for monolithic white LED is as same as that of conventional blue LED therefore this technique can be very useful in reducing the cost of LEDs in SSL.

6.3 Monolithic white LEDs using MQWs and nanodisks

In the previous section we had fabricated monolithic white LEDs using nanoislands but the problem with these LEDs were that it requires very high injection current to drive these LEDs. We had also demonstrated broad emission LEDs emitting in green gap region in chapter 4, but these LEDs missed blue emission which is essential requirement for making white LEDs. In order to make monolithic white LED we used the concept of combining blue and nanodisk LEDs.

The LEDs were grown on c-plane sapphire substrates. A 25-nm thick low temperature GaN nucleation layer was grown at 550°C followed by a 3.4-μm-thick Si-doped n-type GaN. Then five stacks of $In_{.13}Ga_{.87}N$/GaN quantum wells were grown on n-GaN at 780°C. AlN was grown on top of MQWs at the same temperature as that of MQWs. Low growth temperature of AlN resulted in the formation of three dimensional (3D) nanodisk rather than two dimensional (2D) layers. InGaN active layers were grown on top of 3D AlN layers. The growth time of InGaN was increased by 4 min compared to that of blue MQW. Active InGaN layer on top of AlN was capped by AlN. Finally 40-nm thick Mg-doped $Al_{0.15}Ga_{0.85}N$ layer followed by 125-nm thick Mg-doped p-GaN were grown on the sample. The schematic cross sectional diagram of sample B is shown in Figure 6.7 LEDs were fabricated using Ni (20 nm)/Au (80 nm) ohmic contacts using thermal evaporation for p-GaN and indium contact for n-GaN. The diameter of Ni/Au contact was 300 μm.

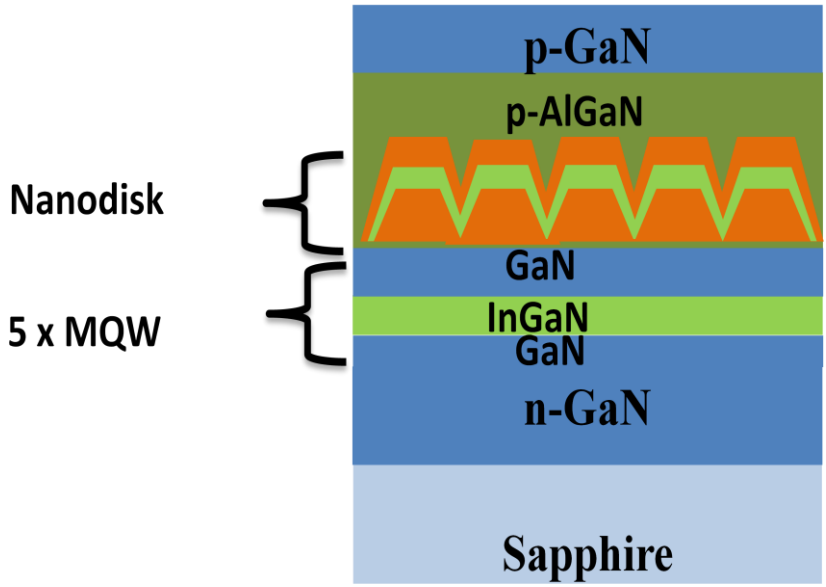

Figure 6. 7. A schematic cross sectional structure of monolithic white LED structures with blue MQW and nanodisks.

The structural analysis of the sample was done with the help of PL with 325 nm He-Cd laser at room temperature. Figure 6.8 shows PL spectrum for monolithic white LED with combination of MQW and single nanodisk. Two peaks are clearly visible in the spectrum. The shorter wavelength peak at 401 nm is coming from the MQWs while the longer order wavelength with broader emission is coming from the top of the nanodisks. The combination of these two wavelengths results in white light.

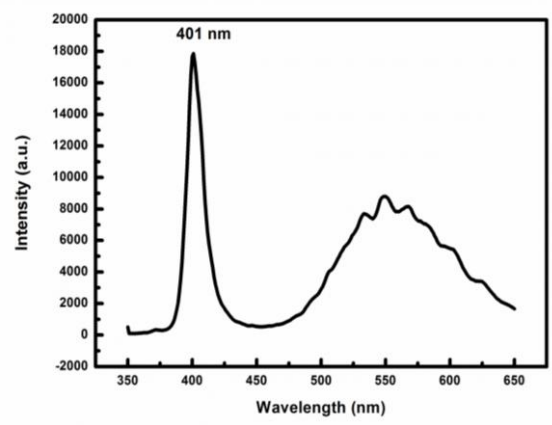

Figure 6. 8 PL spectrum of monolithic white LED structures with blue MQW and nanodisks.

The EL measurement was performed for the fabricated LED at room temperature. Figure 6.9 shows the EL characteristic of monolithic white LED with the combination of MQW and single nanodisk at room temperature. At a low injection current of 5 mA a broad spectrum was observed with a peak wavelength of 521 nm. On further increasing the injection current the intensity increased and the peak emission was at 520 nm. On comparing the EL result with PL result we observed that the shorter order wavelength was missing in EL. In order to investigate the reason for the missing shorter wavelength we performed experiments mentioned in the next section.

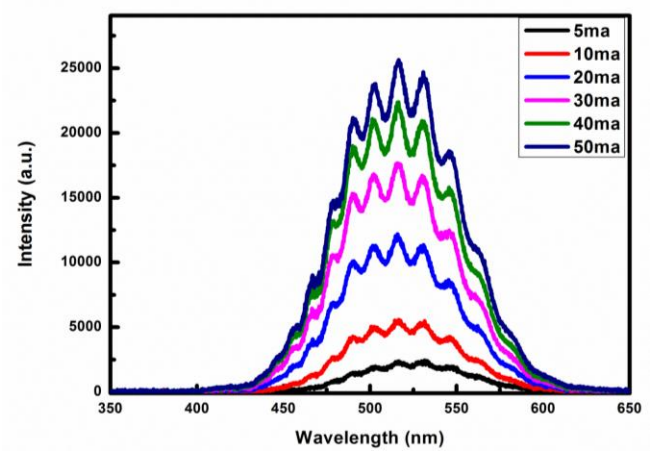

Figure 6. 8. EL spectrum of monolithic white LED structures with blue MQW and nanodisks.

6.3.1 Discussion

From the EL graph we can observe that in spite of having 5 MQWs there is no emission from them while PL intensity showed the presence of QWs. The reason for bimodal emission in PL is due to the electron hole pair generation in the MQW due to high power density of incident light. In case of EL no emission in the blue region is due to electron overflow. Electrons having higher mobility tend to move faster and most of the recombination's takes place inside the nanodisk. The thickness of InGaN in nanodisk is 4 times larger than that of MQWs and hence having large density of states (DOS). Therefore most of the holes coming from p-GaN recombine at nanodisk due to their less mobility and large DOS available there. Nanodisk has an InGaN composition fluctuation which results in broad spectrum. Figure 6.9 shows the schematic representation of emission mechanism in 5 MQW + single nanodisk structure.

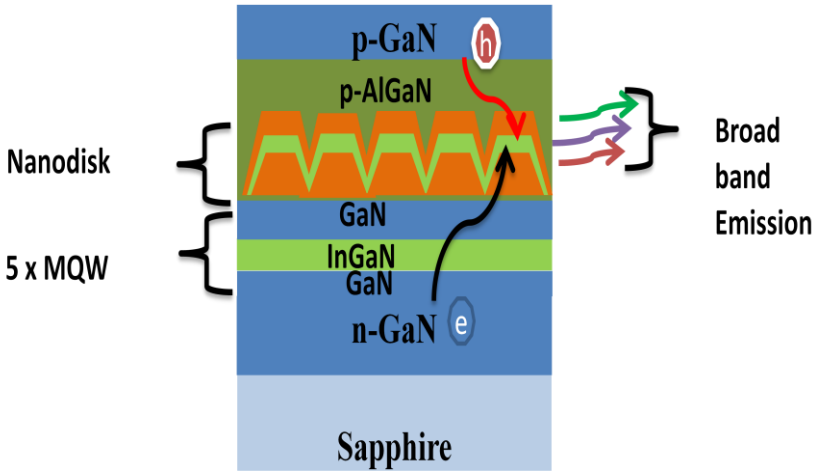

Figure 6.9 Schematic representation of emission mechanism in 5 MQW + single nanodisk structure

6.4 Impact of number of MQWs on monolithic white LEDs

In order to investigate the missing shorter wavelength we grew three samples. A 25-nm thick low temperature GaN nucleation layer was grown at 550°C followed by a 3.4-µm-thick Si-doped n-type GaN on (0001) c plane sapphire substrate. This served as a template for three samples. On the first template single InGaN/AlN nanodisk were grown. Second template consisted of 2 $In_{.13}Ga_{.87}N$/GaN MQWs and a single InGaN/AlN nanodisk while for the third template the number of $In_{.13}Ga_{.87}N$/GaN MQWs were increased from 2 to 8 and rest of the structure remained same as second sample. The MQW and nanodisk growth conditions were same as mentioned in section 6.3. Finally 40-nm thick Mg-doped $Al_{0.15}Ga_{0.85}N$ layer followed by 125-nm thick Mg-doped p-GaN were grown on all the three samples. LEDs were fabricated using Ni (20 nm)/Au (80 nm) ohmic contacts for p-GaN and indium contact for n-GaN for all the samples. The diameter of Ni/Au contact was 300 µm.

PL measurements were performed on all the three samples using 325 nm He-Cd laser at room temperature. Figure 6.10 shows PL spectrum for samples with single nanodisk, 2 MQW + 1 nanodisk and 8 MQWs + 1 nanodisk. From the spectrum it is observed that single nanodisk LED had a broad spectrum in the longer wavelength while the other two samples had bi modal emission in both shorter and longer wavelength. The intensity at shorter wavelength of second sample is less compared to third sample due to less number of QWs.

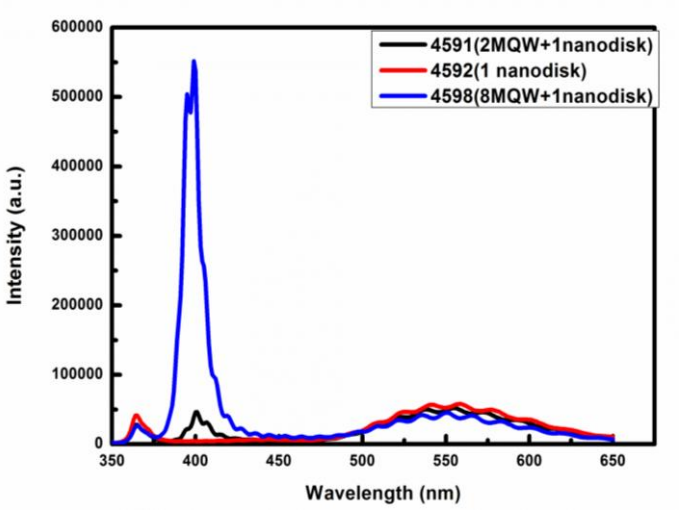

Figure 6.10 Room temperature PL spectrum for samples with single nanodisk, 2 MQW + 1 nanodisk and 8 MQWs + 1 nanodisk.

The EL measurements were performed for the fabricated LEDs at room temperature Figure 6.11 shows EL spectrum for samples with single nanodisk, 2 MQW + 1 nano disk and 8 MQWs + 1 nanodisk at 20 mA current. Measurement for all the samples was done under the same conditions. For a single nanodisk there was a broad emission in the longer wavelength region. When we had inserted 2 MQWs beneath nanodisk the intensity in the yellow region increased but still there was no emission in the shorter wavelength region. On further increasing the number of MQWs to 8 there were two peaks at longer and shorter wavelength. From the EL spectrum it is evident that for the first sample the emission is coming from nanodisk. For the second sample there is no emission in the shorter wavelength in spite of having 2 MQWs but there is an increase in intensity at longer wavelength. The third sample had bimodal emission coming from both MQW and nano disks.

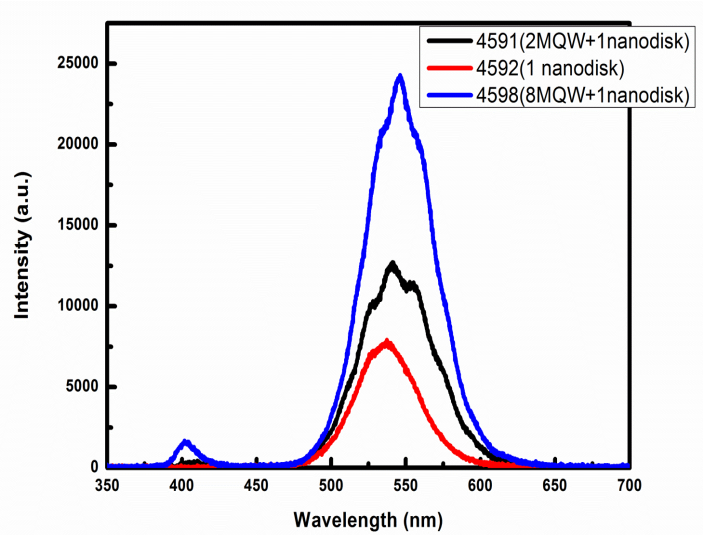

Figure 6.11 Room temperature EL spectrum for samples with single nanodisk, 2 MQW + 1 nanodisk and 8 MQWs + 1 nanodisk at 20 mA current.

In summary, dual wavelength was achieved when the number of MQWs were increased to 8 but the intensity of shorter wavelength was still less. The detail explanation of this behavior will be discussed in the next section. To solve this problem modification has to be done on the designing of monolithic structure.

6.4.1 Discussion

From the PL intensity for all the three structures it can be observed that on increasing the number of QWs the intensity in blue region increases on the other hand yellow luminous intensity is lower than single nanodisk. Due to high pumping intensity of the laser source and non availability of QWs in single nanodisk structure all the recombination is taking in nanodisk while for other structures with QWs and nanodisk recombination takes place in both nanodisk and QWs thus reducing the emission in yellow region.

From the EL graph we observe that the intensity of LEDs increased in yellow region in spite of having MQWs. The EL emission from the 2 MQW and nanodisk structure did not show any emission from the blue region due to electron overflow. Vampola *et al* had experimentally demonstrated the presence of electron overflow in LEDs [24]. For single nanodisk LEDs without any quantum wells most of the recombination was taking place at

the upper interface of the InGaN/AlN. Since the thickness of InGaN was 4 times that of standard blue LED MQW structure and mobility of electron is 60 times that of holes, hence most of the recombination in nanodisk was taking place on the top region of nanodisk. When two MQWs were inserted below the nanodisk structure then there was an increase in intensity in the green region but no intensity in the blue region. The reason for having no emission in blue region is due to the reduced number of electron reaching the nanodisk. MQWs help in traping some of the electrons in form of recombination which enhances movement of holes towards nanodisk enabling larger recombination. Holes are still not able to reach MQWs due to large DOS present in nanodisks. Figure 6.12 shows schematic band gap structure of MQW and nanodisk LED.

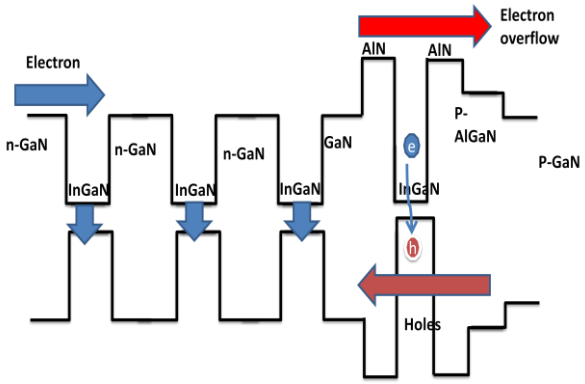

Figure 6.12 Schematic band gap structure of MQW and nanodisk LED.

When the number of MQWs was increased from 2 to 8 then the emission from the blue region was observed. Increasing the number of QWs increases the trapping of electron inside the well prohibiting them to reach nanodisk. This helps holes from p-GaN to arrive at the top QWs resulting in emission from QWs. The small blue emission peak observed in 8 MQW and nanodisk is due to carrier trapping in MQWs. Figure 6.13 shows radiative recombination places for all the three LEDs.

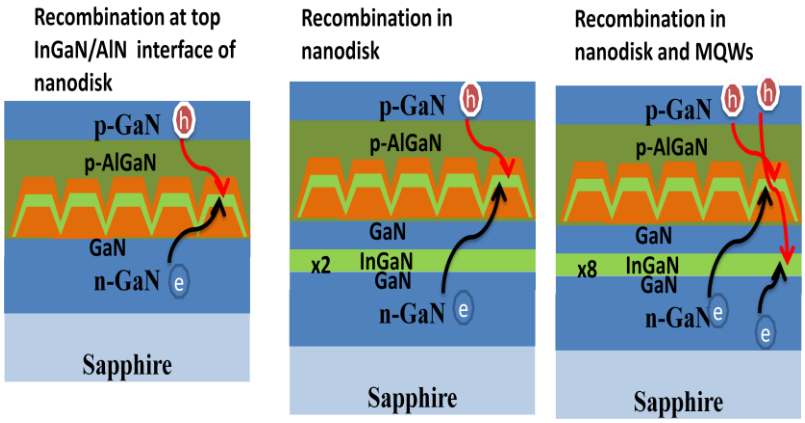

Figure 6.13 Radiative recombination places for nanodisk, 2 MQW + 1 nanodisk and 8 MQWs + 1 nanodisk at 20 mA current

6.5 Monolithic white LEDs using combination of MQW, nanodisk and SQW

In the previous section the monolithic white LEDs had lower intensity in the shorter wavelength region compared to longer wavelength. To solve this issue we modified the device structure. The new structure consisted of combination of 6 MQW, nanodisk and SQW.

After annealing the substrate, a 30 nm thin low temperature GaN nucleation layer was grown at 550°C on sapphire substrate, then the temperature was ramped up to 1130°C to grow a 4 µm thick Si doped GaN cladding layer. Temperature was then ramped down to 780°C to grow active layers at 200 mbar pressure. The active layers consisted of 6 InGaN/GaN MQWs followed by single InGaN/AlN nanodisk and InGaN/GaN quantum wells. There was no temperature swing between InGaN and AlN during growth. The partial pressure for TMIn for first 6 MQW and nanodisk was 11 x 10^{-3}mbar and the partial pressure for the top SQW was 47.2 x 10^{-3}mbar. Finally 40-nm thick Mg-doped $Al_{0.15}Ga_{0.85}N$ layer followed by 125-nm thick Mg-doped p-GaN were grown on the sample. The schematic cross sectional diagram of sample B is shown in Figure 6.14.

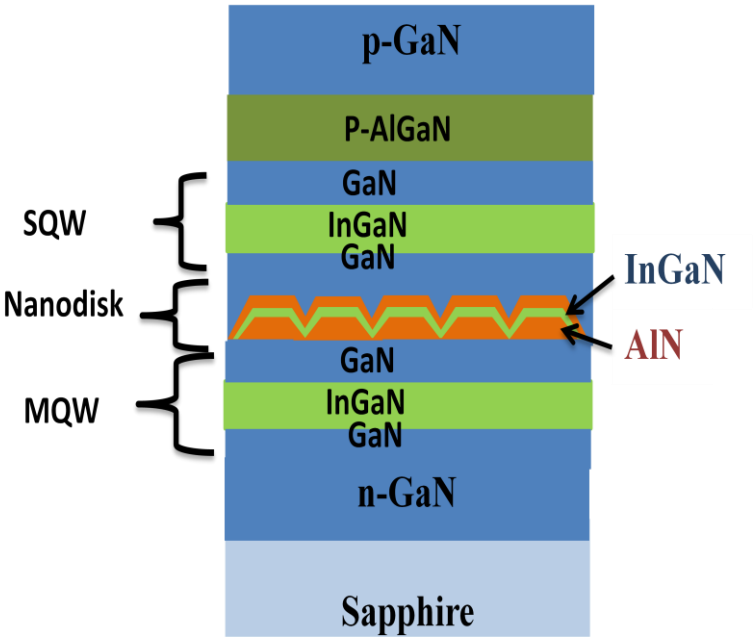

Figure 6. 14. schematic cross sectional structure of monolithic white LED structures with 6 blue MQW, nanodisks and SQW.

Monolithic white LED sample was characterized by HAADF-STEM shown in figure 6.15(a,b). White region represents InGaN, while black region represents AlN. Gray portions in HAADF image represent GaN. There was no contrast in the InGaN region indicating uniform indium composition inside the nanodisks. We had discussed earlier in chapter 3 that it is difficult to obtain nanoscale fluctuation in InGaN from TEM images. There can be possibility of indium fluctuation in InGaN at the vicinity of AlN. Figure 6.15 (b) shows nanodisk like structure at the bottom while the top AlN is flat. It may be due to low partial pressure of TMIn resulting in less indium composition and hence less compressive strain.

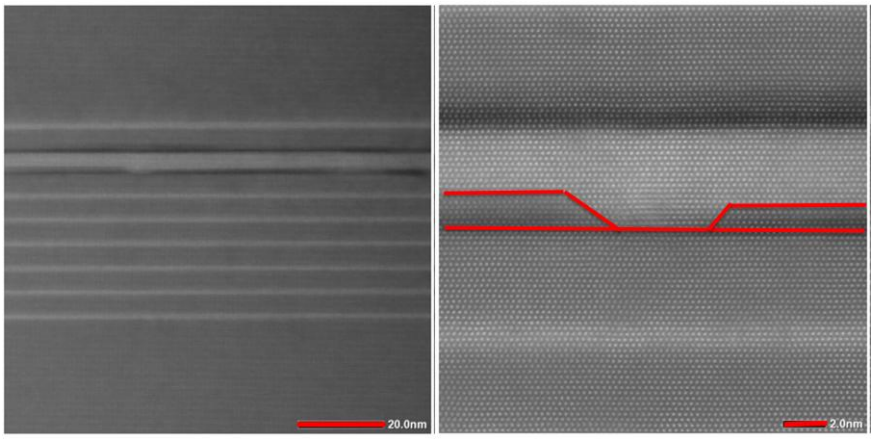

b

Figure 6. 15 (a) HAADF-TEM image of monolithic white LED structures with 6 blue MQW, nanodisks and SQW (b) close view of nanodisk

PL measurements were performed on the sample using 325 nm He-Cd laser at room temperature. Figure 6.16 shows PL spectrum for samples with 6 MQW + 1 nanodisk and SQW. PL spectrum had bimodal emission. The shorter wavelength had a peak emission at 419 nm which came from bottom 6 MQW. The long wavelength emission came from nanodisks. There was no emission from the top SQW.

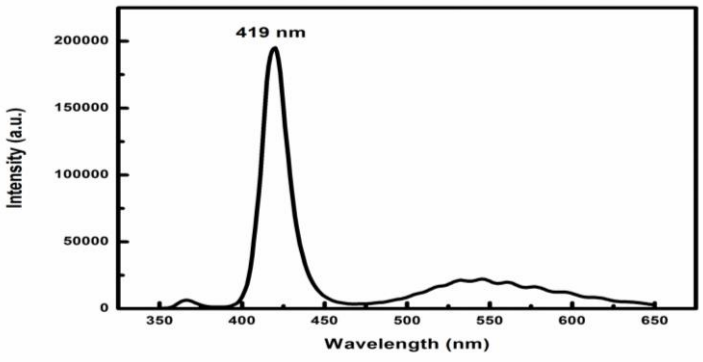

Figure 6.16 Room temperature PL spectrum for monolithic white LED structures with 6 blue MQW, nanodisks and SQW.

LEDs were fabricated using Ni (20 nm)/Au (80 nm) ohmic contacts for p-GaN and indium contact for n-GaN for all the samples. The diameter of Ni/Au contact was 300 μm. EL measurements were performed at room temperature under dc biased conditions. LED

were driven from 10 mA to 60 mA with interval of 10 mA. At 10 mA dual peaks at 448 and 527 nm were observed. The intensities of both the peaks were same. On increasing the injection current to 20 mA, the intensity at shorter wavelength became higher compared to longer wavelength. This tendency was consisted with further increase in current. At 60 mA bimodal emission at 448 nm and 527 nm were observed. Figure 6.17 shows EL spectrum of monolithic white LED and inset shows the picture of monolithic cool white LED.

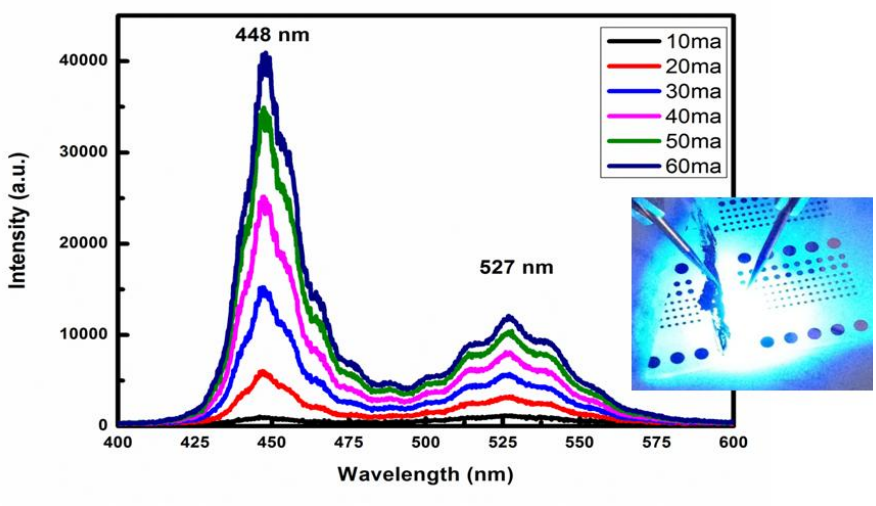

Figure 6.17 Room temperature EL spectrum of monolithic white LED and inset shows the picture of monolithic cool white LED.

On comparing the EL and the PL spectrum we observed disparities in the shorter order wavelength. The peak wavelength for shorter order wavelength for PL was 419 nm while the peak wavelength for EL was 448 nm. The difference of 29 nm between EL and PL was observed. This difference is due to the emission from different regions. In PL, the major emission is coming from bottom MQW while the emission for SQW is negligible. For EL shorter wavelength emission is coming from to SQW due to low mobility of holes. Partial pressure for TMIn was 4 times higher than MQW this resulted in longer wavelength than MQWs.

6.5.1 Discussion

The white LED structure discussed above had higher indium composition on the top SQW while low indium composition in MQWs. When the sample was excited by He-Cd laser emitting at 325 nm there was no emission from the upper SQW while high intensity was observed from MQWs. The disappearance of peak from SQW might be due to high optical pumping power intensity of the laser. When we look at the EL spectrum there was

only emission from the top SQW and nanodisk but not from the bottom MQWs. The reason for this is again related to mobility of electron and holes as most of the radiative recombination is taking place on nanodisk and upper SQW.

6.6 Comparison of monolithic white LEDs with other LEDs

Different research groups used different methods to achieve monolithic white LEDs. The first method is to use of light converter. Damilano et al replaced the phosphor from white LEDs with a light converter having InGaN/GaN MQW grown at lower temperature [25]. Over this light converter layers a blue MQW LED structure was grown. LEDs were fabricated using a standard fabrication procedure. These LEDs had a bimodal emission from blue MQWs and bottom light converters, but the intensity of these LEDs were not high. The second approach for making monolithic white LEDs is using InGaN/GaN quantum dot structure. Quantum dots can be grown by reducing the growth temperature of InGaN resulting in 3D S-K growth. Li et al used this technique to realize monolithic white LEDs [26]. Though bimodal emission was observed with a broad emission in the green gap region but the quality of these device were not good due to low temperature InGaN growth. Low temperature InGaN hampers defect free epitaxial growth of materials.

Table 6.1 shows the comparison of our monolithic white LEDs using nanoislands and MQW+ nanodisks with other LEDs. All the LEDs were grown my MOVPE. Our monolithic white LED used AlN nanoisland and AlN nanodisk techniques to achieve white LEDs while Damilano et al used light converter technique while Li et al used self assembled quantum dot technique to fabricate the LEDs. Nanoisland LEDs had a very thin AlN at the first interface of GaN and InGaN in each MQWs which resulted in the bimodal emission at high current injection. Shorter wavelength came from InGaN/GaN interface while broad emission in the long wavelength came from the AlN nanoislands. In case of MQW + nanodisk the bimodal emission with shorter wavelength came from InGaN/GaN MQWs and broad long wavelength emission was from nanodisks. The combination of these two resulted in monolithic white emission. Li et al and Damilano et al both used InGaN/GaN material to obtain monolithic white LED. Growth temperature of InGaN has a crucial role in the quality of material. High temperature InGaN growth leads to better crustal quality. For both of our monolithic white LED structure we grew InGaN at 780°C which is same as that of blue LED as discussed in chapter 2. Damilano et al grew light converter at temperature of 550°C and barrier at 800°C. Due to this low temperature growth the output intensity of their monolithic white LED was not good. Similarly Li et al also grew InGaN at lower

temperature to achieve quantum dot structure which resulted in deteriorated white light emission. On comparing our result with other groups the quality of our monolithic white LED is better since we had grown InGaN at relatively higher growth temperature.

Table 6.1 Comparison of monolithic white LEDs using nanoislands and nanodisks with light converter and quantum dot techniques.

	Nanoisland	**MQW+ Nanodisk**	**Light converter, Damilano et al**	**Quantum dot, Li et al**
Year	2013	2014	2008	2013
Equipment	MOVPE	MOVPE	MOVPE	MOVPE
Technique	**AlN nanoisland**	**AlN nanodisk**	Light converter	Self assemble
Material	**AlN/InGaN/GaN**	**MQW+ 1ND(InGaN/AlN)**	InGaN/GaN	InGaN/GaN
Growth temperature	**780° High temp -> better crystal quality**	**780°C High temp -> better crystal quality**	550°C-InGaN, 800 °C GaN **Low temp -> bad crystal quality**	InGaN-735°C **Low temp -> bad crystal quality**

6.7 References

[1] E. F. Schubert and J. K. Kim, Science, 308, 1274 (2005).

[2] M. R. Krames, O. B. Shchekin, R. Mueller-Mach, G. O. Muller, L. Zhou, G. Harbers, and M. G. Craford, J. Display Technology, 3, 160 (2007).

[3] J. Baur, F. Baumann, M. Peter, K. Engl, U. Zehnder, J. Off, V. Kuemmler, M. Kirsch, J. Strauss, R. Wirth, K. Streubel, and B. Hahn, Phys. Status Solidi C, vol. 6, 905 (2009).

[4] Y. Narukawa, M. Ichikawa, D. Sanga, M. Sano, and T. Mukai, J. Phys. D: Appl. Phys., vol. 43, 354002 (2010).

[5] B. Hahn, K. Engl, and M. Klein, Compound Semicond., vol. 15, no. 5, 25 (2009).

[6] R. Mueller-Mach, G. Meuller, M.Krames and T. Trottier, IEEE J. Sel. Top. Quantum Electronics, 8, 339 (2002).

[7]M. Meneghini, A. Tazzoli, G. Mura, G. Meneghesso, and E. Zanoni, IEEE Trans.Electron Devices, 57, 108 (2010).

[8] M. Yamada, Y. Narukawa, and T. Mukai, Jpn. J. Appl. Phys, 41, L246 (2002).

[9] S. Dalmasso, B. Damilano, C. Pernot, A. Dussaigne, D. Byrne, N. Grandjean, M. Leroux, and J. Massies, Phys. Status Solidi A, 192, 139 (2002).

[10] S. J. Chang, L. W. Wu, Y. K. Su, C. H. Kuo, W. C. Lai, Y. P. Hsu, J. K. Sheu, J. F. Chen, and J. M. Tsai, IEEE Trans. Electron Devices, 50, 519 (2003).

[11] A. Dussaigne, J. Brault, B. Damilano, and J. Massies,Phys. Status Solidi C, 4, 57 (2007).

[12] C.-F. Huang, C. F. Lu, T.-Y. Tang, J.-J. Huang, and C. C. Yang, Appl. Phys. Lett., 90, 151122 (2007).

[13] S. N. Lee, H. S. Paek, H. Kim, T. Jang, and Y. Park, Appl. Phys. Lett., 92, 081107 (2008).

[14] C. F. Lu, C. F. Huang, Y. S. Chen, W. Y. Shiao, C. Y. Chen, Y. C. Lu, and C. C. Yang, IEEE J. Sel. Top. Quantum Electron., 15, 1210 (2009).

[15] A. F. Tsatsulnikov, W. V. Lundin, A. V. Sakharov, E. E. Zavarin, S. O. Usov, A. E. Nikolaev, N. V. Kryzhanovskaya, M. A. Synitsin, V. S. Sizov, A. L. Zakgeim, and M. N. Mizerov, Phys of Semi Devi, 44, 808 (2010).

[16] S. N. Lee, H. S. Paek, H. Kim, T. Jang, and Y. Park, Appl. Phys. Lett. 92, 081107 (2008).

[17] C. F. Huang, C. F. Lu, T. Y. Tang, J. J. Huang, and C. C. Yang, Appl. Phys. Lett. 90, 151122 (2007).

[18] M. Funato, T. Kondou, K. Hayashi, S. Nishiura, M. Ueda, Y. Kawakami,Y. Narukawa, and T. Mukai, Appl. Phys. Express, 1, 011106 (2008).

[19] H. W. Lin, Y. J. Lu, H. Y. Chen, H. M. Lee, and S. Gwo, Appl. Phys. Lett., 97, 073101 (2010).

[20] W. Guo, A. Banerjee, P. Bhattacharya, and B. S. Ooi, Appl. Phys. Lett., 98, 193102 (2011).

[21] T. Mukai, M. Yamada, and S. Nakamura, Jpn. J. Appl. Phys, 38, 3976 (1999).

[22] B. Damilano, A. Dussaigne, J. Brault, F. Natali, P. Demolon, P. De Mierry, S. Chenot, and J. Massies, Appl. Phys. Lett, 93, 102227 (2008).

[23] M. Mathew, H. Sodabanalu, M. Sugiyama, and Y Nakano, Phys. Status Solidi C, 10, No. 11, 1525–1528 (2013).

[24] K. J. Vampola, M. Iza, S. Keller, S. P. DenBars, and S. Nakamura, Appl. Phys. Lett. 94, 061116 (2009)

[25] B. Damilano, A. Dussaigne, J. Brault, T. Huault, F. Natali, P. Demolon, P. De Mierry, S. Chenot and J. Massies, Appl. Phys. Lett. 93 , 101117 (2008)

[26] Hongjian Li, Panpan Li, Junjie Kang, Zhi Li, Zhicong Li, Jing Li, Xiaoyan Yi, and Guohong Wang, Appl. Phys. Express 6 ,102103 (2013)

7 Conclusions and future scope

This work focused on the broad band emission in the green gap region for developing monolithic white LEDs. We were the first to use the concept of InGaN/AlN nanodisk LEDs rather than conventional structure of InGaN/GaN for getting a broad band emission in the green gap region. The use of AlN served two purposes first it helped in getting more indium into InGaN secondly it prevented the diffusion of indium to overlying layer.

The experiments in this thesis have been carried out step-by-step from the investigation of thick InGaN on InGaN/GaN MQW, effect of AlN nanoisland on InGaN/GaN MQWs to InGaN/AlN nanodisks. Since both nanodisks and nanoisland emitted broad emission in green gap region so they were used to make monolithic white LEDs.

In chapter 1, we introduced to basics of III- Nitride materials and their properties followed by different industrial fabrication process for making the standard white LEDs for solid state lighting. The motivation of doing this work is also included in this chapter.

Chapter 2 is related to the growth, characterization and fabrication of conventional blue LED used in SSL. Since blue LEDs along with yellow phosphor emits white light so we grew InGaN/GaN MQW blue LED structure in our MOCVD system and characterized the samples with different characterization techniques. Later LEDs were fabricated on these wafers. These LEDs had a narrow band emission in the blue region. The EL from fabricated LEDs was later used for comparison with nanodisk and nanoisland LEDs.

The effect of insertion of AlN layer on InGaN/GaN MQW was analyzed in chapter 3. Our main aim in this work was to get a broad emission in the green gap region without compromising on the quality of material growth. In order to have a broad band emission in InGaN more indium composition in InGaN is required. To increase the indium composition, InGaN thickness in standard InGaN/GaN MQW was increased and it was found that on increasing the InGaN thickness the indium composition increases but after reaching a critical thickness strain relaxation of indium starts, resulting in indium segregation. To solve this issue we introduced tensile strained, very thin AlN layer between first interface of each InGaN/GaN MQW and found that tensile strain of AlN helped in getting more indium in InGaN due to their compressive strain and hence more indium. The growth conditions of InGaN/GaN MQW were same as that of blue LED but the insertion of thin AlN layers

helped in red shift in wavelength. The AlN layer was grown at the same temperature of that of MQW which resulted in rough island type surfaces which caused compositional fluctuation of indium in InGaN. Since lower temperature AlN had a nanoisland structure so these types of LEDs were referred as nanoisland LEDs.

Since AlN had a crucial role in getting more indium in InGaN, so AlN structure was further investigated by replacing GaN barrier with AlN in standard MQW LEDs. This device structure was investigated in chapter 4. AlN was grown at the same temperature of 780°C it formed 3D structure which in turn resulted in the formation of nanodisks. Five stacks of InGaN/AlN LED structure was grown on sapphire substrate and the EL emission from these LEDs had a peak wavelength of 586 nm and broad linewidth of 100 nm. The IQE of these LEDs were 23 times higher compared to conventional QW LEDs. To further improve the crystal quality of these nanodisks a monolayer of GaN was introduced at each interface of GaN and AlN. Insertion of GaN layer improved the IQE of nanodisk LED 38 times to that of standard blue LEDs. Tensile behavior of AlN helped in getting more indium in InGaN compared to conventional method. High atomic bond energy of AlN was helpful in preventing the diffusion of indium in the overlying layer and hence maintaining high indium in InGaN. The broad band emissions in these LEDs were due to indium rich portions at the InGaN/GaN interface and indium relaxation on the relaxed AlN. These nanodisk LEDs also exhibited blue shift in wavelength with increasing driving current due to QCSE. Hence, in this chapter, the InGaN/AlN nanodisk showed a broad band emission in the green gap region which would be helpful in making monolithic white LEDs.

On comparing our broad band emitter with other researchers, we found that we were able to achieve high indium composition in InGaN at relatively higher temperature. Lower temperature InGaN often lead to crystal quality degradation due to indium segregation. Nanodisk LEDs had a peak wavelength emission and FWHM of 586 nm and 100 nm respectively. These values are higher compared to values reported by other research groups.

On comparing nanoisland and nanodisk broad band emission LEDs, its observed that nanodisk LEDs are much better then nanoislands because in nanodisk LEDs the strain is already released due to its 3D structure while in case of nanoisland LEDs the high indium composition in QWs leads to stress relaxation between QW number two and three. This type of stress relaxation produce V defect in the crystal and reduces the efficiency of LEDs.

In chapter 5 the impact of AlN and InGaN growth conditions on nanodisk were investigated. First the effect of InGaN growth time on single nanodisk was studied and it was found that increasing the InGaN thickness on AlN leads to red shift in wavelength. The higher compressive stress of InGaN on 3D tensile AlN helped in accommodating more indium in InGaN. Increasing the TMIn flow rate in nanodisk lead to indium composition increases but it got saturated later on. This phenomenon was consistent with standard InGaN/GaN LED with the only difference that more indium in InGaN was achieved compared to conventional LEDs. After changing indium parameters, then the focus shifted to AlN. First the AlN cap temperature was changed. Temperature was varied from 700°C to 800°C with interval of 50°C.Higher temp capped AlN had shorter wavelength compared to low temperature AlN due to evaporation of indium during ramping of temperature. Later changing of cap AlN thickness was investigated while keeping the bottom AlN. Thicker AlN cap helped in getting more indium in InGaN by preventing diffusion but it also resulted in increase in resistance. AlN cap with 2 min growth time was better compared to 1 and 3 min AlN growth time. In the next part of this chapter the effect AlN temperature on 5 stacks of InGaN/AlN nanodisk was investigated. AlN grown at lower temperature exhibited 3D structure, which enabled the formation of nanodisk. These LEDs had low resistance due to current injection to InGaN nanodisks via the gap in AlN. High temperature AlN had more flat surface so it exhibited high resistance due to current injection in vertical direction. Less indium composition in InGaN for high temperature AlN was due to evaporation of indium during the ramping up of temperature for AlN growth. Thus 3D AlN surface is important for having LEDs with broad band emission in green gap region with less resistance. In the entire nanodisk LEDs mentioned so far, AlN was either n-doped or undoped so in the final step we studied the effect of doping on AlN. We grew three single nanodisk samples with first sample with undoped AlN, second sample with p doped AlN and third sample with bottom undoped and top p-doped AlN. For first sample intensity was less because high resistance of AlN prevented the flow of carriers. In second sample p-doping helped in injecting more holes in the wells and it also helped in reducing device resistance. For the third sample electrons from bottom can reach the well faster and most of the recombination will take at the top layer of InGaN well and since indium composition is larger at the InGaN/AlN interface thus longer wavelength is achieved. In summary different growth parameters of InGaN and AlN growth conditions effects broadband emission.

After having a broad band emission our final aim was to have a monolithic white LED which was investigated in chapter 6. As discussed earlier we mainly used two different

methods to get a broad band emission. The first method was the use of AlN nanoisland. On increasing the InGaN growth time on AlN nanoisland resulted in more indium in InGaN and also micro level fluctuation in the well region. The second method was the use of AlN/InGaN nanodisk LEDs. These LEDs had a very broad spectrum and high IQE than our conventional blue LEDs. By taking into this advantage of nanostructure we fabricated monolithic white LEDs by three different methods. The first method was the use of nanoislands. These LEDs had very thin AlN nanoislands between first interface of InGaN/GaN layers. The bimodal emissions in these LEDs were coming from InGaN/GaN interface and InGaN/AlN/GaN interface. Narrow wavelength emission was from InGaN/GaN interface while broad emission in green gap region was from InGaN/AlN/GaN interface. Color temperature of this monolithic white LED was 4500 K at 70 mA driving current. The problem with this LEDs is that it requires high injection current for driving, due to the defects origination from the stress field. To solve this issue we used the second concept of combination of nanodisk and blue MQW LEDs. By using this technique we should get bimodal emission from quantum wells and nanodisks. But these LEDs did not emit light at shorter wavelength when the number of MQWs were less. Since the active region in nanodisk was thicker compared to MQWs, hence it provided more DOS for radiative recombination's and all the recombination's were taking place inside the disk. If the number of MQWs were increased it helped in trapping some of the electrons in the well and prevented electron overflow. In this case bimodal emission from both MQW and nanodisk was observed but the emission intensity from MQW was still less. In order to increase the intensity in blue region we finally fabricated monolithic white LEDs using the combination of MQW, nanodisk and SQW with higher indium fraction. The upper SQW is thinner compared to nanodisk so holes can easily reach nanodisk emitting bimodal emission. The bimodal emission was from SQW and bottom nanodisks.

On comparing our research in monolithic white LED with other research group, we were able to achieve monolithic white light emission with nanodisk and nanoislands at the same InGaN growth temperature of standard blue LEDs. Other group used light converts nad quantum dots to make monolithic white LEDs which results in poor crystal quality.

In summary the salient points of our work are

- InGaN/AlN nanodisk structure was successfully grown on sapphire substrate. LEDs emitted broad band spectrum in the green gap region.

- Monolithic white LED structure was grown and fabricated using AlN nanoislands. Longer wavelength originated from nanoisland region while shorter wavelength came from InGaN/GaN MQWs region.
- Monolithic white LED was also achieved by the combination of blue MQWs and a nanodisk.
- Two broad wavelengths emission in blue and green regions were observed for nanoisland and (MQW+ND+SQW) LEDs.
- White LED had a color temperature of 4500 K at 70 mA for AlN nanoislands based LEDs.
- High indium composition in InGaN is achieved due to strain effect on InGaN and AlN layers.

Future Scope

We were successfully able to fabricate monolithic white LEDs using different methods but these LEDs lacked emission in the red region. Roughened AlN is very much important to achieve high indium composition in InGaN because, rough AlN will help in increasing the surface area of AlN and hence more indium can be accommodated in InGaN. AlN on GaN had rough surface but AlN on MQW has more 2D structure due to compressive stress developed from MQWs. Efforts have to be made to get rougher AlN on MQWs. The partial pressure of AlN was kept constant for all of our experiments. In future the effect of TMA partial pressure and rector pressure has to be studied to get roughened AlN.

For the monolithic white LEDs there is still a room to increase the partial pressure of indium to get high indium in InGaN. But this might also be a trade-off as high indium will put more stress on the material and thus deteriorate the crystal quality. So this parameter has to be carefully optimized. The other method of getting more indium is by grading of temperature during InGaN growth in nanodisk. This will help in compositional fluctuation in InGaN and thus help in broad emission.

Since the output power of our conventional blue MQW LED is not good so improvement is needed to increase the intensity and power of our blue LED. The commercial blue LED available in the market has a peak wavelength of 450 nm and for our

blue LED it is in the range of 420-430 nm, so we need to red shift this wavelength to 450 nm to better mimic the phosphor based LEDs. The one way to increase the crystal quality is to insert a strain release layer before MQW this will help in increasing the power of LEDs.

Finally I would like to propose that the best structure for making monolithic white LED on sapphire substrate. The structure will consists of a good GaN template on sapphire followed by stacks of InGaN/GaN superlattice with less indium composition in InGaN which will act as a strain release layer. Over this strain release layer blue MQW should be grown with the peak wavelength emission of 450 nm. The number of MQW should be increased to 8 or 9 so that it can trap some electron to prevent carrier overflow. Nanodisk structure should be grown on these MQW with rough AlN so that it can trap more indium in InGaN. Both the AlN should be p-doped so that holes can injected more into MQWs and nanodisks. Finally device should be capped with p-AlGaN and P-GaN. Figure 7.1 shows the schematic of future device structure for monolithic white LED.

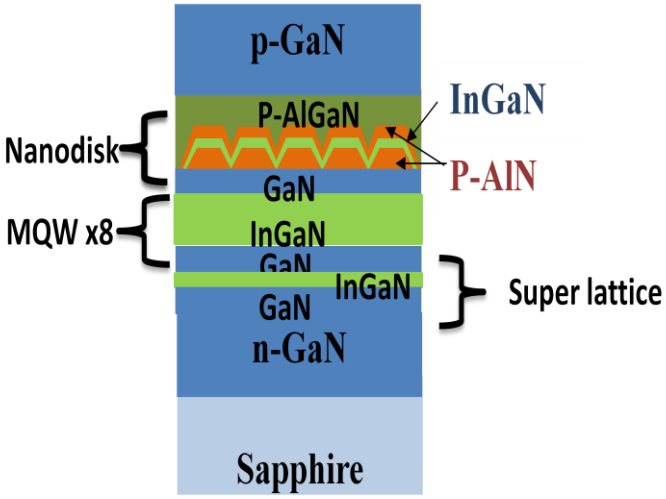

Figure 7.1 Schematic device structure of future monolithic white LED.

Publication List

Patent

- LED device and its fabrication method ,M. Sugiyama, M. Mathew, Y. Nakano, H. Sodabanlu, JP2013-99378

Journals

- Orange/yellow InGaN/AlN nanodisk light emitting diodes, M. Mathew, H. Sodabanlu, M. Sugiyama ,Y. Nakano, physica status solidi (c), vol 10, issue 11,pp 1525–1528,(2013).
- Monolithic white light emitting diodes based on AlN nanoislands, M. Mathew, H. Sodabanlu, M. Sugiyama ,Y. Nakano, [To be submitted]

Conferences

- Orange/yellow InGaN/AlN nanodisk light emitting diodes, M. Mathew, H. Sodabanlu, M. Sugiyama ,Y. Nakano,ISCS-2013, (May 19 – 23, 2013 Kobe, Japan.
- Long wavelength InGaN/AlN nanodisk light emitting diode , M. Mathew, H. Sodabanlu, M. Sugiyama ,Y. Nakano, E-MRS Spring Meeting May 27 - 31, 2013 Strasbourg, France.
- Monolithic Cool White Light Emitting Diodes Based on AlN Islands, M. Mathew, H. Sodabanlu, M. Sugiyama ,Y. Nakano, 10th International Conference on Nitride Semiconductors 2013 (ICNS-10), August 25-30, 2013Washington DC, U.S.A.
- Monolithic cool white light emitting diodes based on InGaN/AlN nanodisk, M. Mathew, H. Sodabanlu, M. Sugiyama ,Y. Nakano, JSAP-MRS Joint Symposia ,September 16-19, 2013 Kyoto, Japan
- Effect of AlN beneath InGaN for red shift of the electroluminescence, M. Mathew, M. Sugiyama, Y. Nakano, ISGN-5 May 18-22 2014, Atlanta, U.S.A.
- Effect of AlN temperature on broadband visible elctroluminesence from InGaN/AlN nanodisks, M. Mathew, M. Sugiyama, Y. Nakano, ICMOVPE- XVII July 13-18 2014, Lausanne, Switzerland.